CONE WAKE VELOCITY PROFILES MEASURED BY MEANS OF THE SEQUENTIAL SPARK TECHNIQUE

C. Lahaye

Defence Research Establishment

Prepared for:

Advanced Research Projects Agency

December 1972

DISCLAIMER NOTICE

THIS DOCUMENT IS THE BEST QUALITY AVAILABLE.

COPY FURNISHED CONTAINED A SIGNIFICANT NUMBER OF PAGES WHICH DO NOT REPRODUCE LEGIBLY.

DREV TN-2029/72
PROJ: 95-51-10

NON CLASSIFIÉ
UNCLASSIFIED

CONE WAKE VELOCITY PROFILES MEASURED BY MEANS OF THE SEQUENTIAL SPARK TECHNIQUE

C. Lahaye

CENTRE DE RECHERCHES POUR LA DEFENSE

DEFENCE RESEARCH ESTABLISHMENT

VALCARTIER

DEFENCE RESEARCH BOARD

CONSEIL DE RECHERCHES POUR LA DÉFENSE

Québec, Canada

December/décembre 1972

CONE WAKE VELOCITY PROFILES MEASURED BY MEANS OF THE SEQUENTIAL SPARK TECHNIQUE

by

C. Lahaye

This research was sponsored jointly by

The Defence Research Establishment
Valcartier
P.O. Box 880
Courcelette, Quebec, Canada
Under Project D-95-51-10

The Advanced Research Projects Agency
ARPA Order 133
Monitored by the U.S. Army Missile Command,
Redstone Arsenal, Alabama 35809
Contract DA-H[illegible]-69-C-0921

CENTRE DE RECHERCHES POUR LA DEFENSE
DEFENCE RESEARCH ESTABLISHMENT
VALCARTIER
Tel: (418) 844-4271

Québec, Canada

December/décembre 1972

RESUME

Dans cette Note technique, on publie les profils de vitesse mesurés à l'aide de la technique des étincelles consécutives au cours du programme d'étude du sillage des cônes hypersoniques. A cause de la présence d'angles d'incidence d'amplitude et d'orientation différentes lors de la plupart des tirs de cônes, il n'a pas été possible de déterminer la distribution transverse de la vitesse axiale moyenne comme dans le cas des sphères. L'utilisation de ces profils a été limitée à la détermination de caractéristiques de vitesse axiale au centre et à la frontière du sillage turbulent et à la visualisation de l'asymétrie du profil de vitesse axiale. Cependant, ces mesures contiennent de l'information additionnelle sur la structure du sillage, information qui ne peut être extraite à cause du manque de données statistiques mais qui pourrait intéresser les spécialistes dans le domaine.

ABSTRACT

The purpose of this Note is to document on the velocity profiles measured with the sequential spark technique during the program of study of cone wakes. Due to the presence of angles of attack of different amplitude and orientation with respect to the spark traces, it has not been possible to determine the transverse distribution of the mean axial velocity as was done in the case of spheres. The use of these profiles has been limited to the determination of characteristics of wake axis and wake front velocities and to the visualization of the skewness of the transverse profile of axial velocity. The results, however, contain additional information on the wake structure which cannot be extracted presently because of lack of statistical data but which could be of interest to specialists in the field.

TABLE OF CONTENTS

1.0 INTRODUCTION

An experimental study has been carried out on the wakes produced by hypersonic cones flying at a velocity of 15,000 feet/second in Range 3 at the Defence Research Establishment Valcartier (DREV). Two basic cone shapes have been flown: 0.7 inch base diameter, 20° included angle cones with either sharp or blunted noses and a 1.0 inch diameter, 44° included angle, sharp nose cone. Because of the complexity of the flow field generated by these cones which usually fly at some angle of attack, the experimental study was limited to one set of ambient conditions, namely, cone velocity of 15,000 feet/second and ambient pressure of 100 torr of air.

The sequential spark technique used for the measurement of the wake velocity distribution was the main diagnostic tool of this experimental study of cones wakes. The technique, which has been described in length (1), is based on the formation of an ionized luminous path in the wake by a first spark and on the periodic re-illumination of the displaced ionized path by successive sparks. Additional diagnostic tools included the photo-attitude and velocity measurement system of the range which were used to determine the flight history and to measure the drag coefficient, and also the schlieren technique used to measure the growth and deflection of the wake behind cones flying at angles of attack.

Over one hundred profiles of velocity were measured behind the cone shapes. The measurements have revealed the presence of an asymmetry in the transverse profile of axial velocity and the presence of a lateral velocity component in the wake of high lift to drag ratio cones flying at angle of attack. Characteristics of the wake axis and the wake front velocities have been derived and show good agreement with other available results. The results of this experimental study of cone wakes have been published in Reference 2.

The purpose of the present note is to document the velocity profiles measured with the sequential spark technique during the program of study of cone wakes. Due to the presence of angles of attack of different amplitude and orientation with respect to the spark traces, it has not been possible to determine the transverse distribution of the mean axial velocity as was done in the case of spheres (3). The use of the profiles of axial velocity in Reference 2 has been limited to the determination of characteristics of wake axis and wake front velocities and to the visualization of the skewness of the transverse profile of axial velocity. These profiles contain additional information on the wake structure which cannot be extracted presently because of lack of statistical data but which could be of interest to specialists in the field. The method of analysis of the spark data is described and results collected by the other diagnostic tools which are required for the analysis of the spark data are included.

2.0 PREREQUISITES TO THE ANALYSIS

The presence of an angle of attack on most cone firings has necessitated an extensive modification of the method used to analyse the spark data on spheres (1, 3). A number of effects of the angle of attack have been observed on cone wakes: these are increased wake diameter and axial velocity which are related to the drag coefficient; wake deflection and lateral velocity which are associated with the lift forces acting on the cones; asymmetry in the form of a skewness of the transverse profile of axial velocity in planes parallel to the one defined by the cone axis of symmetry and the angle of attack. The presence of these effects has set a number of prerequisites for the analysis of the spark data: an accurate determination of the attitude of the cone in flight; a good knowledge of the drag and lift coefficients as a function of the angle of attack for the normalization of the data; a knowledge of the wake deflection.

2.1 Flight History and Drag Coefficient

The flight history of the cone is determined by a series of stereo flash X-ray photoattitude stations located at various points along Range 3 (4). From the analysis of the stereo X-ray films, the pitch and yaw angles and the coordinates of the position of the cone center of gravity are obtained at discrete locations down the range. A series of chronographs operated in conjunction with the X-ray stations are used to record the time of passage of the cone at each station and the velocity of the cone is calculated from this record using the distance between the stations.

Because the cone attitude is known only at discrete positions in the range and knowledge of the attitude is required at intermediate positions for the interpretation of the data measured by the spark and schlieren technique, it is necessary to interpolate the data between the discrete points. Interpolation of the position of the center of gravity is easy because the amplitude of its oscillation is relatively small and this interpolation is made graphically. As for the pitch and yaw angles, the oscillation of the angles with respect to the distance down range is usually large and graphical interpolation cannot give the required accuracy. Consequently the interpolation is made through the least mean square fit of expressions of the form:

$$\theta(x) = \theta_o + \theta_1 \sin\left(\frac{2\pi}{\lambda_\theta} x + \phi_\theta\right) \qquad 1$$

for the pitch angle and

$$\psi(x) = \psi_o + \psi_1 \sin\left(\frac{2\pi}{\lambda_\psi} x + \phi_\psi\right) \qquad 2$$

for the yaw angle where,

$\theta(x)$ and $\psi(x)$ are the pitch and yaw angles at any point down the range

Θ_o and ψ_o are trim angles
Θ_1 and ψ_1 are the amplitudes of the harmonic motion
λ_Θ and λ_ψ are the wavelengths in feet which are assumed to be equal
ϕ_Θ and ϕ_ψ are the phase angles in radians.

For both the pitch and yaw angles, four parameters have to be fitted to the data: the trim angle and the amplitude, wavelength and phase of the harmonic motion. The trim angles are caused by imperfections in the geometry of the cone due to its construction or to deformations resulting from gun launching under high acceleration. The analytical expression used to represent the variation of the pitch and yaw angles with distance down range is a first approximation of the expected behavior. The damping of the oscillation has been neglected because the measurement covers only one or two wavelengths and also the roll of the cone seems sufficiently small to be neglected. In Table I, the values of the parameters of the least mean square fits of equations 1 and 2 to the pitch and yaw data are listed for each firing on which a wake velocity measurement was obtained. For each velocity profile, the pitch and yaw angles were obtained by evaluating equations 1 and 2 at the location of the spark station in the range (X = 83 feet). The use of the pitch and yaw angles at the spark station leads to some error because the segment of the wake at the spark station has been produced at some distance upstream and has been convected to the spark station by the flow velocity. The knowledge of some 'average' velocity of the wake is required to determine the position in the range at which the wake has been generated for each axial distance. The data of Table I is given to allow correction for this error.

The flight history data measured by the X-ray photoattitude system have also been used to determine the drag coefficient as a function of the angle of attack for the three models used in the program. The total drag coefficient (C_D) can be determined from the relation:

$$\frac{-dV}{dx} = \frac{1}{2} \rho \frac{S}{M} V C_D, \qquad 3$$

where

V = velocity of the cone
$\frac{dV}{dx}$ = derivative of the cone velocity with respect to the distance in the range
ρ = ambient gas density
S = cone base area
M = mass of the cone.

The parameters ρ, S and M are constants which are determined from the flight ambient conditions or from measurements on the cone. The velocity V and the deceleration dV/dx are obtained from the flight history by fitting a straight line to the velocity data as a function of distance down range. The velocity V is an average velocity over the measured

interval and the deceleration dV/dx is the slope of the fitted line. From these values, a value of C_D averaged over the measured region is calculated from equation 3.

The next step is to determine an effective angle of attack for the drag from the fitted expressions for the pitch and yaw angles (equations 2 and 3). The RMS value of the angle of attack is given by the following expression:

$$\alpha_{RMS} = |\theta^2(x) + \psi^2(x)|^{\frac{1}{2}}. \qquad 4$$

The effective angle of attack from the point of view of the drag coefficient obtained from the cone velocity history is given by

$$\alpha_{eff.} = \frac{1}{x_2-x_1} \int_{x_1}^{x_2} |\theta^2(x) + \psi^2(x)|^{\frac{1}{2}} \, dx, \qquad 5$$

where x_1 and x_2 are the limits of the interval of the measurement.

Measurements of the total drag coefficient for the 20° vertex angle sharp nose cones are shown in Figure 1. The measurements were made on two model sizes: the 0.7 inch base diameter cones launched in Range 3 and the 2.0 inch base diameter cones launched in Range 5. The dashed curve represents a calculation of the pressure induced drag (C_{DP}) made by Laviolette (5) based on the modified Newtonean theory of Gray (6). The skin friction drag component was determined from the mean deviation of the experimental points with respect to the theoretical curve C_{DP}. The total drag curve (full curve) was then obtained by displacing the theoretical curve by an amount equal to C_{DF}.

Figures 2 and 3 show corresponding results for the 44° vertex angle sharp nose cone and for the 20° vertex angle blunted nose cone. The theoretical curve has been used to normalize the velocity data in the case of the 20° blunted cone because the small number of experimental points does not warrant the determination of the skin friction drag component.

Figure 4 shows the lift coefficient curves as a function of the angle of attack calculated by Laviolette and which have been used in the normalization of the wake deflection and the lateral velocity data.

2.2 Wake Deflection and Width

The lateral deflection of the wake on cones flying at angles of attack is produced by the vortex system generated by the cone. This deflection is in the direction of the windward side of the cone and is observed usually on bodies with high lift to drag ratio. The knowledge of the wake deflection is essential to the analysis of the velocity data measured with the spark technique in order to relate the velocity profile to the position of the turbulent core.

The schlieren technique was used to determine the lateral deflection and the growth of the turbulent wake. Measurements of the width and deflection were made on a large number of firings for each of the three cone models used in the program. The results for the 20° sharp and blunted cones are presented in Figures 5 and 6 respectively. The deflection in base diameter is normalized to the lift coefficient and the axial distance to the drag diameter $(C_DA)^{\frac{1}{2}}$. Normalization of the axial distance with respect to the base diameter results in approximately the same scatter of the data. The normalization to the drag diameter was selected for convenience in the analysis of the spark data. The full curves in Figures 5 and 6 represent the mean curves calculated from the data. These mean curves are used in the analysis of the spark data.

The 44° vertex angle sharp nose cone exibits no vortex induced wake deflection. This absence of deflection is explained by the small lift to drag ratio of this model.

Figures 7, 8 and 9 show wake growth characteristics for the 20° sharp and blunted cones and for the 44° sharp cone respectively. In each case, the cone data are compared with sphere data measured under almost identical test conditions (7). A value of C_D of 0.9 was used in the normalization of the sphere data. Cone and sphere data are in excellent agreement except in the case of 20° blunted cone (Figure 8). Part of the deviation in that case may be explained by the uncertainty of the drag coefficient for the blunted cone. The wake growth data given here may be of use in determining the position of the turbulent front on the velocity profiles.

A more detailed treatment of the results presented in this section is given in Reference 2.

3.0 METHOD OF ANALYSIS OF THE VELOCITY DATA

On sphere data, a fairly simple method is used to obtain the wake velocity from the spark traces (1, 3). The axial velocity of the wake is calculated from the projection of the sparks in the xoz plane, where x is the direction of the flight and z is the vertical axis of the range. The radial position of the measurement is calculated from the projection of the spark in the yoz plane where y is the horizontal axis perpendicular to the flight axis and o is the position of the projectile in the transverse plane of the range at the spark station. A lateral turbulent velocity of the wake is also calculated in the y direction from the projection of the spark traces in the yoz plane. The assumption is made in this method that the turbulent velocity in the z direction is equal to zero.

On cone wake velocity measurements, this rather simple method of reduction has to be extensively modified due to the presence of wake deflection, lateral wake velocity and axial velocity profile skewness.

In the presence of wake deflection, velocity profiles must be traced with respect to the wake position which is a function of axial distance. The assumption that the lateral velocity in the z direction is negligible is not valid in the presence of a pitch angle. The presentation of axial velocity profiles as a function or radial distance is not acceptable due to profile skewness. Finally, the velocity profile skewness prescribes the reorientation of the coordinate system in which the measurements were made in such a direction that the axes of symmetry of the velocity profiles are aligned.

Figure 10 illustrates the transformation of the coordinate system of the spark data required to align the axes of symmetry of the velocity profiles in the same direction and to take into account the deflection of the wake. This transformation consists in a rotation and a translation of the coordinate system. The angle of rotation is evaluated from the pitch and yaw angles at the spark station by the following expression:

$$\phi = \arctan \Theta/\psi \qquad 6$$

The coordinates Y and X in the rotated system of the point (x,y) in the original system are given by:

$$Y = z \sin \phi + x \cos \phi \qquad 7$$

$$Z = x \cos \phi - y \sin \phi \qquad 8$$

In the rotated system, the wake deflection due to vorticity is in the positive Y direction. At any axial distance behind the cone, the wake deflection is determined from the mean curve of Figure 5 or 6 and the axis is displaced to Z^1.

The Y axis is the symmetry axis of the axial velocity distribution. Velocity profiles measured along the Y axis or parallel to this axis should show a skewness toward the positive Y direction; velocity profiles measured perpendicular to this axis should be symmetric. Furthermore, the lateral velocity induced by vorticity will be in the positive Y direction.

The determination of the axial and lateral velocity of the wake is illustrated in Figure 11 which shows projections of the spark traces in the original xz and yz planes. The rotated and translated system of axes is also shown. S_1 and S_2 in both views represents segments of the first and second spark traces of the sequence. The points of these segments are the actual points measured on the projecting equipment. These points are measured at constant intervals along the z-axis. The lateral velocity is measured in the direction of positive Y from the measured point on S_1 to a point obtained by interpolation on S_2 (second degree interpolation on three points). The position of this interpolated point is then projected in the xoz view. The axial velocity (in the direction of positive x) is

then calculated from the corresponding point on S_1 to the interpolated value of x on S_2. In the case where the spark trace was parallel or nearly parallel to the y axis ($\psi \approx 0$), this method could not be used. The vertical displacement of S_1 with respect to S_2 was then determined from the wake deflection curves by evaluating the increase in deflection corresponding to the interval of time between S_1 and S_2. To avoid large errors in lateral velocity, all cases where the angle between the positive y axis and the spark trace was smaller than 45° have been rejected.

Figure 12 shows a typical result for one sequence of sparks. This figure also illustrates the format used for presenting individual measurements of velocity on cones. The firing number and the type of projectile are indicated at the top of the graph. In the upper left hand corner, the test conditions are indicated: cone velocity (V_∞), ambient pressure (ρ_∞), axial distance in base diameter (x/D) and drag diameters ($X/\sqrt{C_D A}$), the angles of pitch (Θ), yaw (ψ), attack (α) and rotation (ϕ) and the spark interval (τ). The graph on the lower left shows the position of the first spark (full line) in the rotated and translated system of axes. The origin of this system of axes is the position of the center of the turbulent core. The position of the projectile and the diameter of the turbulent core are indicated in this case. The dashed line is a straight line fitted on the spark trace. The axial and lateral velocity profiles shown on the upper and lower right side are plotted against this fitted line with the beginning of the velocity profile corresponding to the cross on the lower end of the spark trace on the left. These velocity profiles are calculated from the first and second sparks of the sequence. As mentioned earlier, no lateral velocity profile is obtained when the angle between the spark trace and the Y axis is smaller than 45°.

4.0 RESULTS

Figures 13 to 78 show the velocity profiles measured on the 20° vertex angle sharp nose cones. The profiles measured in the wake of 20° vertex angle blunted nose cones are presented in Figures 79 to 89 while profiles measured behind 44 vertex angle sharp nose cones are presented from Figures 90 to 121.

REFERENCES

1. Lahaye, C., Léger, E.G., Dufresne, M., Doyle, H. and Boucher, P., "The Sequential Spark Technique: A Tool for Wake Velocity Studies in Ballistic Ranges", ICIASF'71, 71-C-33 AES, pp. 33-44, June 1971.

2. Lahaye, C., "Experimental Study of Wakes Produced by Hypersonic Cones in Free Flight", DREV R-681 (Unclassified).

3. Lahaye, C., "Velocity Distributions of Sphere Wakes", DREV R-682 (Unclassified).

4. Léger, E.G. and Beaulieu, R., "Stereo Flash X-ray Photoattitude Station for Use on Ballistic Ranges", CARDE T.R. 563/67, April 1967 (Unclassified)

5. Laviolette, M., DREV Private communication, May 1969.

6. Gray, J.G., "Drag and Stability Derivatives of Missile Components According to the Modified Newtonian Theory", Arnold Engineering Development Center, AEDC-TN-60-191, November 1960 (Unclassified).

7. Lahaye, C, and Doyon, P., "Growth Characteristics of Turbulent Wakes", DREV R 687 (Unclassified).

TABLE 1

COEFFICIENTS FROM THE LEAST MEAN SQUARE FIT OF THE PHOTO ATTITUDE DATA USING EXPRESSIONS OF THE FORM:

$$\psi(x) = \psi_0 + \psi_1 \sin\left(\frac{2\pi}{\lambda_\psi} + \phi_\psi\right) \qquad \text{yaw}$$

and

$$\theta(x) = \theta_0 + \theta_1 \sin\left(\frac{2\pi}{\lambda_\theta} + \phi_\theta\right) \qquad \text{pitch}$$

No	ψ_0	ψ_1	λ_ψ	ϕ_ψ	θ_0	θ_1	λ_θ	ϕ_θ
68089	-.88	4.12	71.00	.34	.00	6.64	71.40	-2.92
68093	.00	8.43	82.65	.16	-.42	6.95	82.65	1.16
68094	-.17	5.56	82.40	1.58	-.20	11.07	82.40	1.18
68095	.00	7.39	84.80	-2.93	.09	5.04	84.80	-1.39
68096	-.95	4.10	74.50	.74	.31	3.81	74.50	-2.00
68113	.25	4.85	74.00	2.89	-.16	2.37	74.00	-1.00
68115	.00	5.29	77.30	2.66	1.82	1.61	77.30	-1.41
69001	-.04	2.46	77.00	.07	.42	.31	77.00	1.73
69002	2.39	7.25	69.50	-2.83	.31	5.76	69.50	-1.09
69004	3.73	2.99	70.00	-2.54	2.56	3.33	70.00	-1.17
69008	-1.50	3.74	69.00	2.18	-.30	2.63	69.00	-.63
69009	.15	3.56	71.00	-.01	.02	5.92	71.00	2.10
69010	.04	4.50	73.50	3.81	-.19	2.39	73.50	-1.41
69011	-.27	3.74	75.42	2.02	.11	1.62	75.42	1.90
69012	.10	1.67	72.50	-2.48	.25	4.62	72.50	-1.73
69014	.09	8.09	67.80	-.04	-.27	4.61	67.80	-3.89
69015	.79	6.66	75.36	1.53	-.32	2.60	76.09	1.13
69018	.18	2.41	70.00	2.30	.07	5.41	70.00	-.49
69019	.73	4.36	69.20	-2.15	1.26	2.77	69.50	2.95
69020	.51	1.85	79.00	-3.14	-.21	4.32	79.00	1.95
69038	.28	4.42	75.00	-2.11	.06	4.30	75.00	3.14
69040	-.41	4.42	70.24	-2.68	.04	6.58	73.50	-2.21
69041	-.07	5.25	70.41	2.02	-.45	3.61	70.41	.62
69042	-.62	6.25	70.00	2.14	.63	5.87	70.00	.14
69044	.00	3.96	73.10	-.48	.35	6.94	73.10	-1.47
69045	.32	4.94	71.40	.04	-.15	7.40	71.43	2.00
69046	-.05	2.53	66.60	2.53	.25	1.11	65.70	.68
69047	-.61	1.99	70.00	-3.14	-.13	5.12	70.00	.25
69051	.35	5.41	74.00	-1.74	.00	2.86	74.00	-2.23
69055	.73	4.75	75.50	3.06	-.73	4.15	75.50	3.95
69062	-.51	6.87	73.00	-3.86	-.23	7.59	73.00	1.84
69063	-.49	7.98	72.00	2.00	1.02	10.91	72.00	.24
69064	-.11	6.80	67.20	1.34	-.17	3.68	67.20	1.22
69065	-.45	1.70	76.88	1.62	-.02	1.88	76.88	2.65
69066	-.48	3.79	68.50	1.06	.94	3.32	68.52	3.00
69068	-.80	3.69	81.60	-1.33	1.30	4.36	81.59	-.68
69070	.01	5.39	67.09	.31	.09	6.82	67.00	1.76
69071	-1.18	7.31	70.80	.39	-.66	.35	70.80	1.33
69073	1.92	5.45	70.00	-1.56	.53	4.87	70.00	3.14
69076	-.09	4.15	71.60	.79	-.17	6.99	71.60	1.11
69077	-.15	2.91	71.70	-2.41	.60	5.98	71.70	-1.47
69078	-3.25	5.35	69.10	-.21	2.08	2.64	69.10	-2.30
69083	-.20	6.78	74.00	2.37	.01	4.32	74.00	1.87
69085	.31	1.31	76.20	-3.66	-.66	2.07	76.20	2.79
69086	-.42	6.00	59.20	.06	.27	5.26	59.20	2.20
69089	-.21	3.25	58.50	2.02	.05	3.88	58.50	-1.69
69091	.28	5.20	58.00	2.10	-.10	2.95	58.00	1.34
69092	-.41	5.89	60.00	2.67	-.10	2.63	60.00	-.82
69095	-.23	7.74	59.00	-.37	.15	3.51	59.00	2.13
69097	.12	8.94	63.50	.31	.09	6.28	63.50	.86
70002	.71	7.55	28.00	1.78	.27	2.30	28.00	1.14
70003	.05	2.04	32.00	-2.72	.03	3.11	32.00	-2.87
70004	.14	2.13	30.70	-1.93	.32	3.15	30.70	2.05
70006	-.25	6.90	30.70	-2.84	-.07	4.26	30.70	-2.81
70007	.18	1.80	30.70	-2.83	-.02	2.82	30.70	2.50
70008	-.01	2.51	33.80	-1.19	-.86	6.37	33.80	-1.40
70009	.58	2.10	31.00	-.30	.46	5.82	31.00	.60
70010	.97	3.44	29.00	-.42	.19	11.50	29.00	-.64
70011	.65	4.67	31.85	.35	.51	9.51	31.84	-.53
70012	.31	.64	31.50	1.09	.21	4.17	31.50	-.32
70014	.36	4.09	31.30	2.68	.09	2.18	31.30	-.21
70015	.26	5.79	31.00	3.14	-.04	6.54	31.00	2.62
70019	-.56	7.64	32.00	-2.74	.05	2.72	32.00	-2.31
70021	.47	1.95	31.00	2.93	-.05	5.27	31.00	2.27
70022	.62	10.68	32.00	.31	.48	2.89	32.00	.02
70023	-.36	11.24	32.40	3.11	.30	1.96	32.40	.03
70027	.44	2.46	33.20	1.70	.16	9.63	33.20	-.39

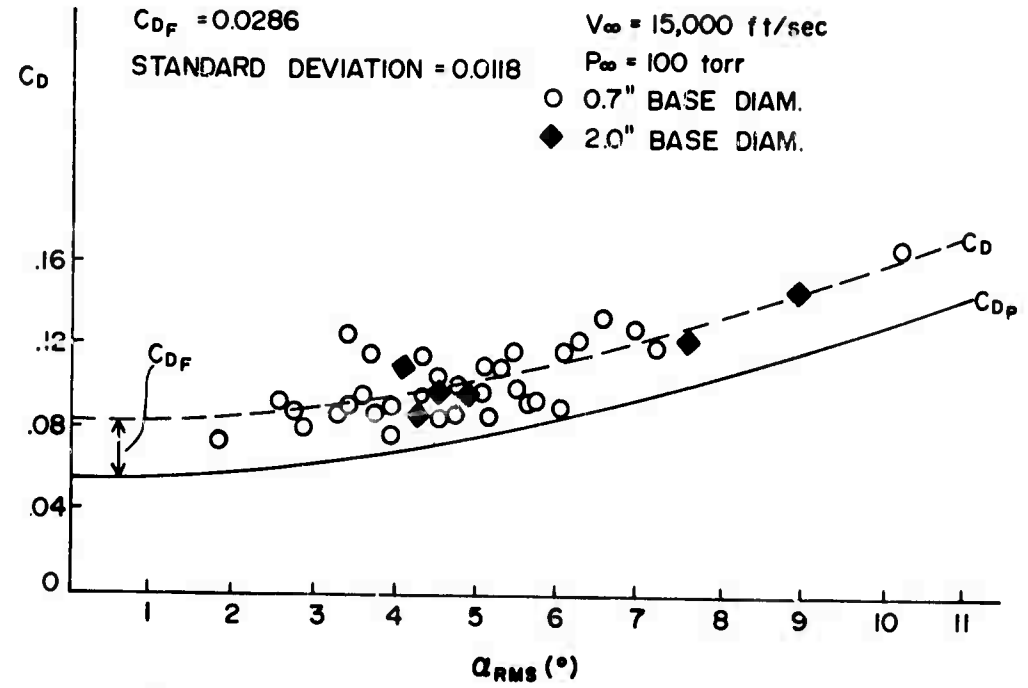

Figure 1. Measured drag coefficient of the 20° vertex angle sharp nose cone.

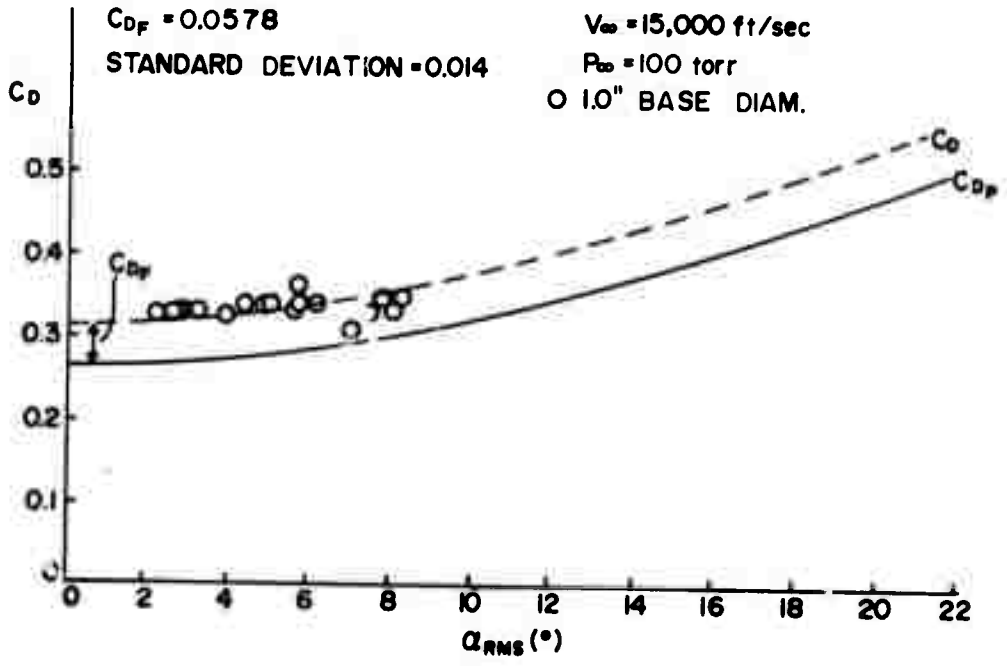

Figure 2. Measured drag coefficient of the 44° vertex angle sharp nose cone.

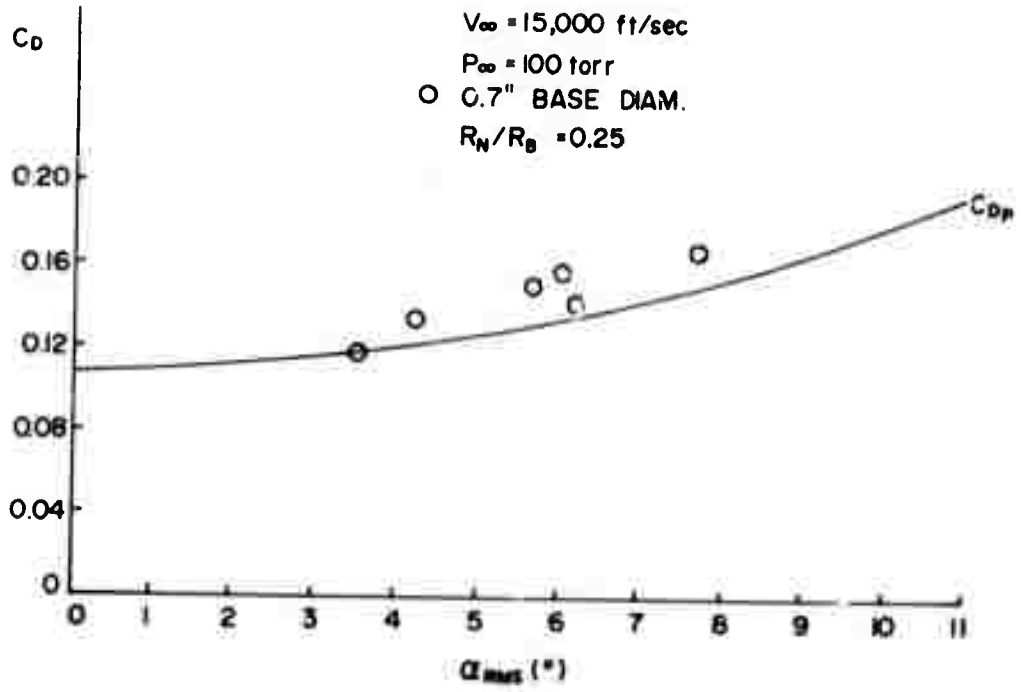

Figure 3. Measured drag coefficient of the 20° vertex angle blunted nose cone.

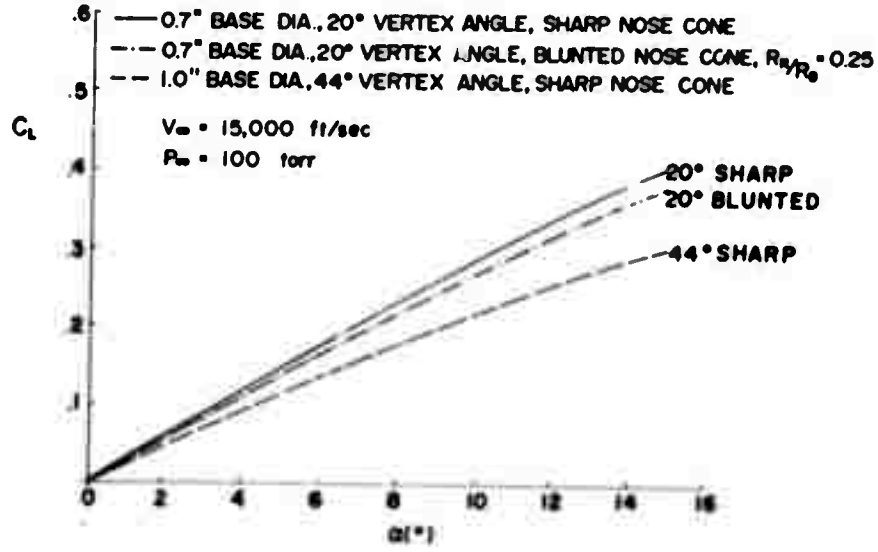

Figure 4. Theoretical curves of the lift coefficient as a function of the angle of attack.

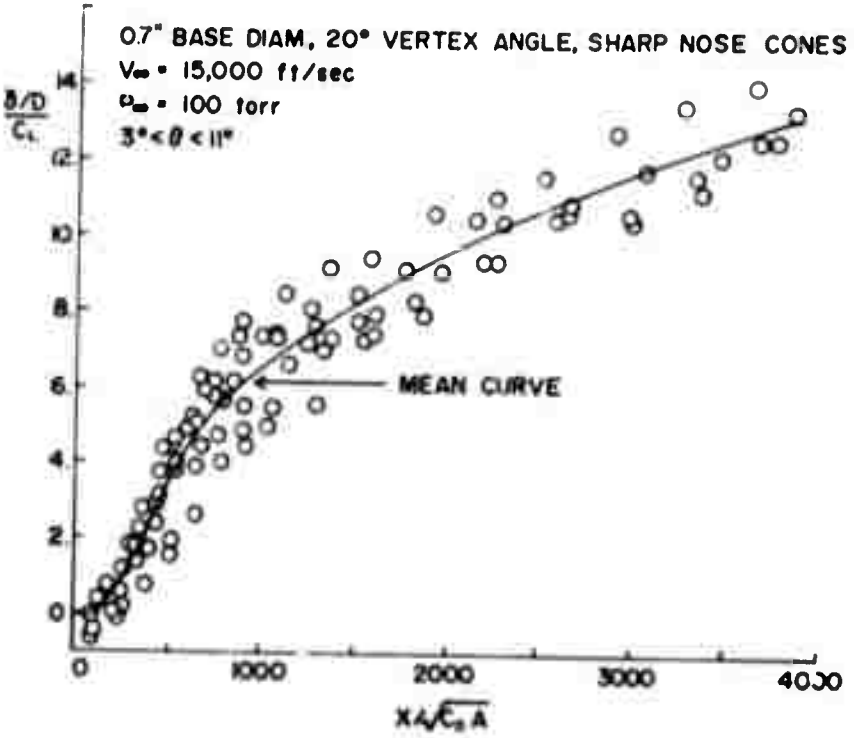

Figure 5. Normalized wake deflection as a function of axial distance for the 20° vertex angle sharp nose cone.

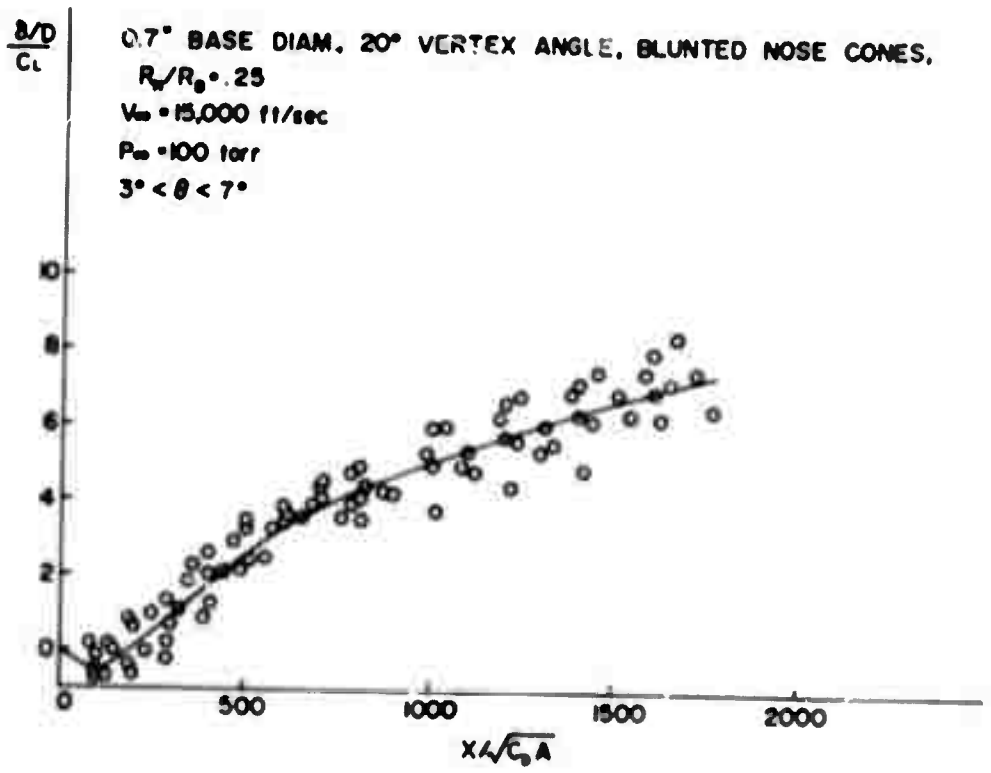

Figure 6. Normalized wake deflection as a function of axial distance for the 20° vertex blunted nose cone.

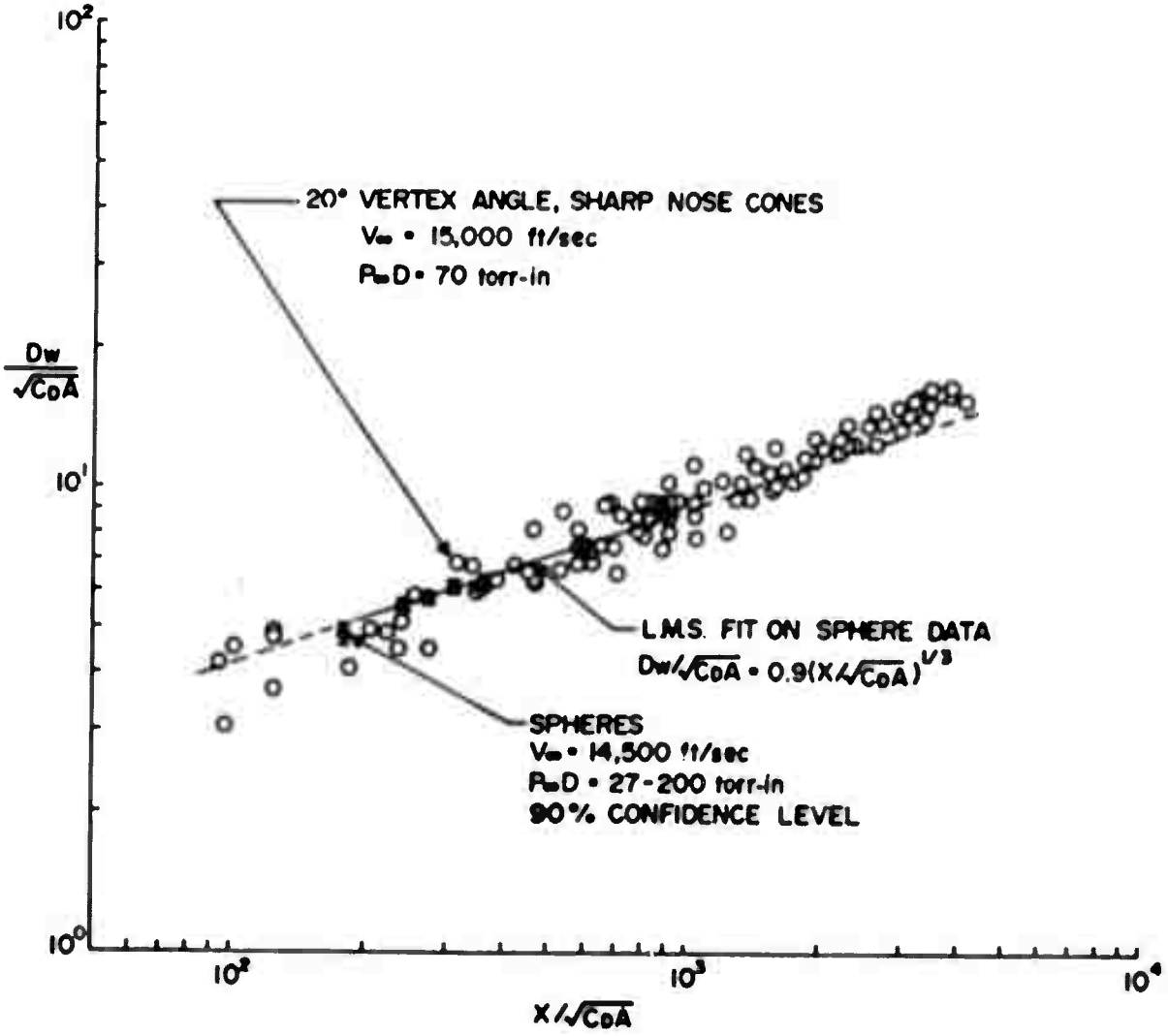

Figure 7. Wake growth of the 20° vertex angle sharp nose cone compared to sphere wake growth.

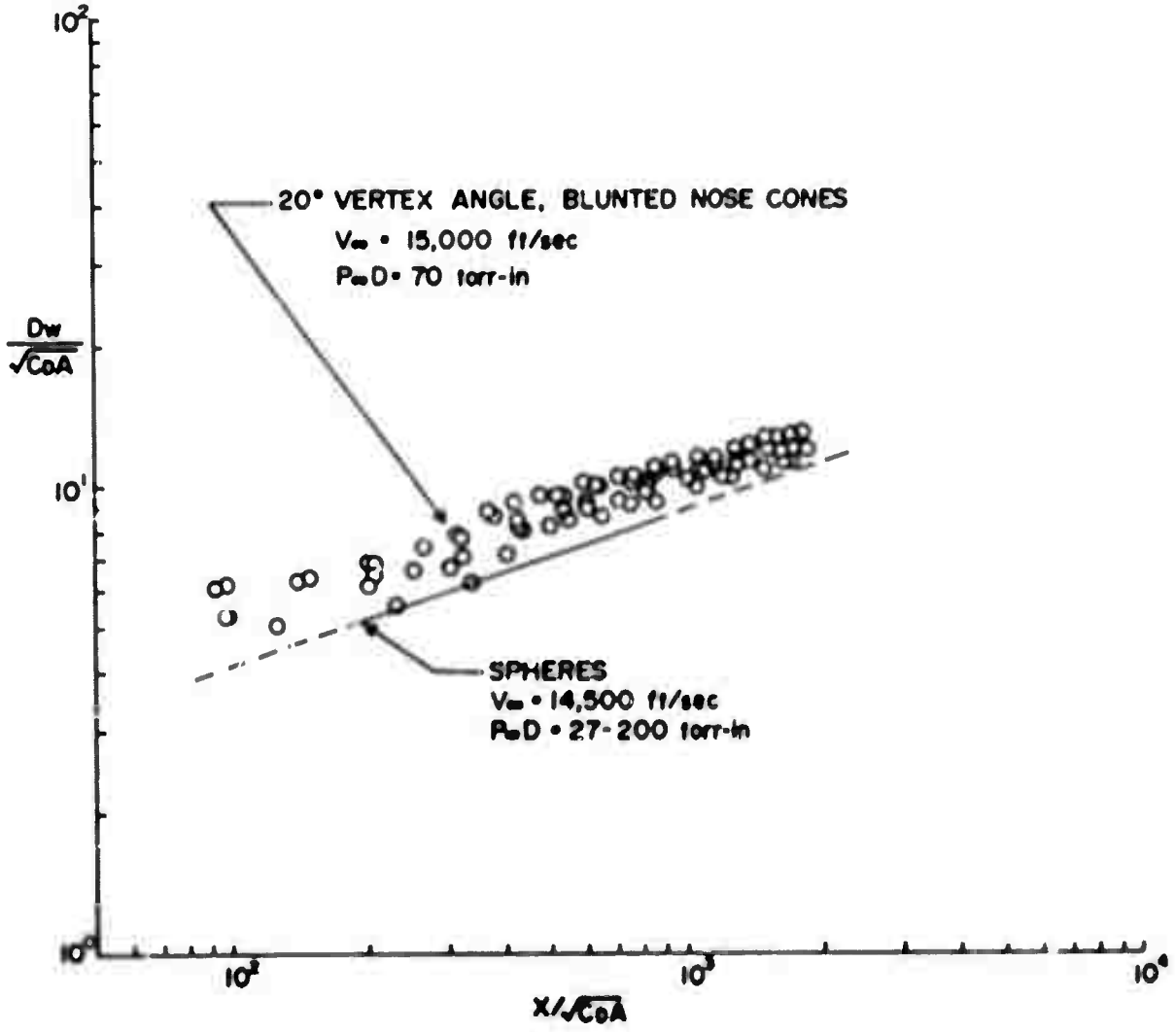

Figure 8. Wake growth of the 20° vertex angle blunted nose cone compared to sphere wake growth.

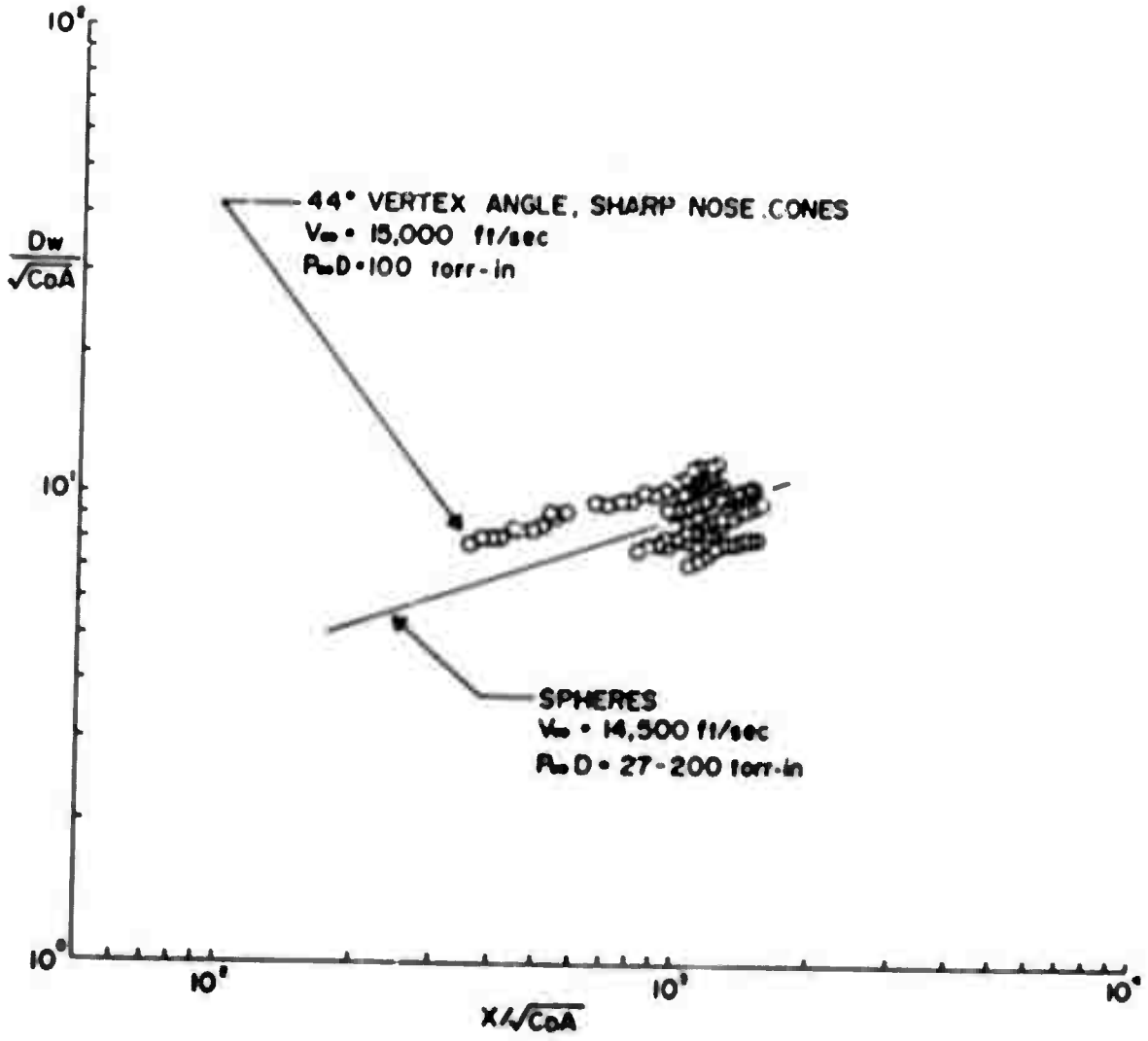

Figure 9. Wake growth of the 44° vertex angle sharp nose cone compared to sphere wake growth.

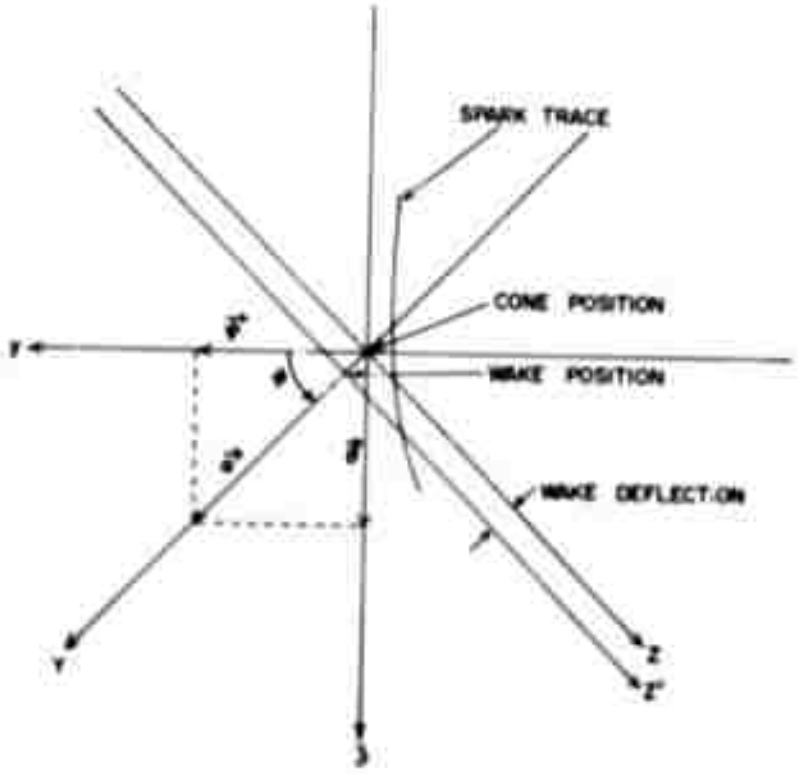

Figure 10. Transformation of the coordinate system of the spark data required to align the axis of symmetry of the velocity profiles and to take into account the deflection of the wake.

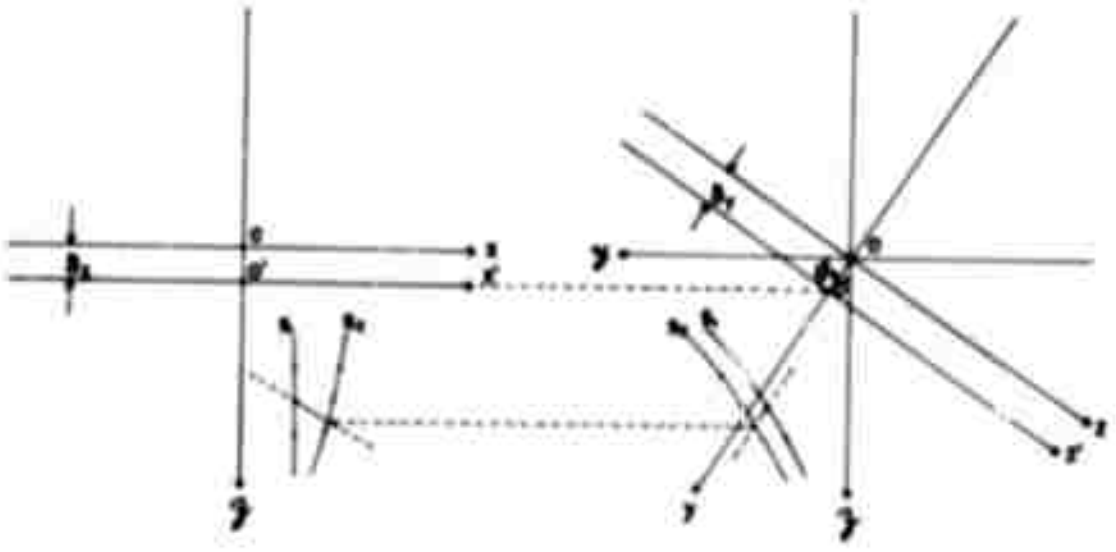

Figure 11. Determination of the axial and lateral velocities of the wake.

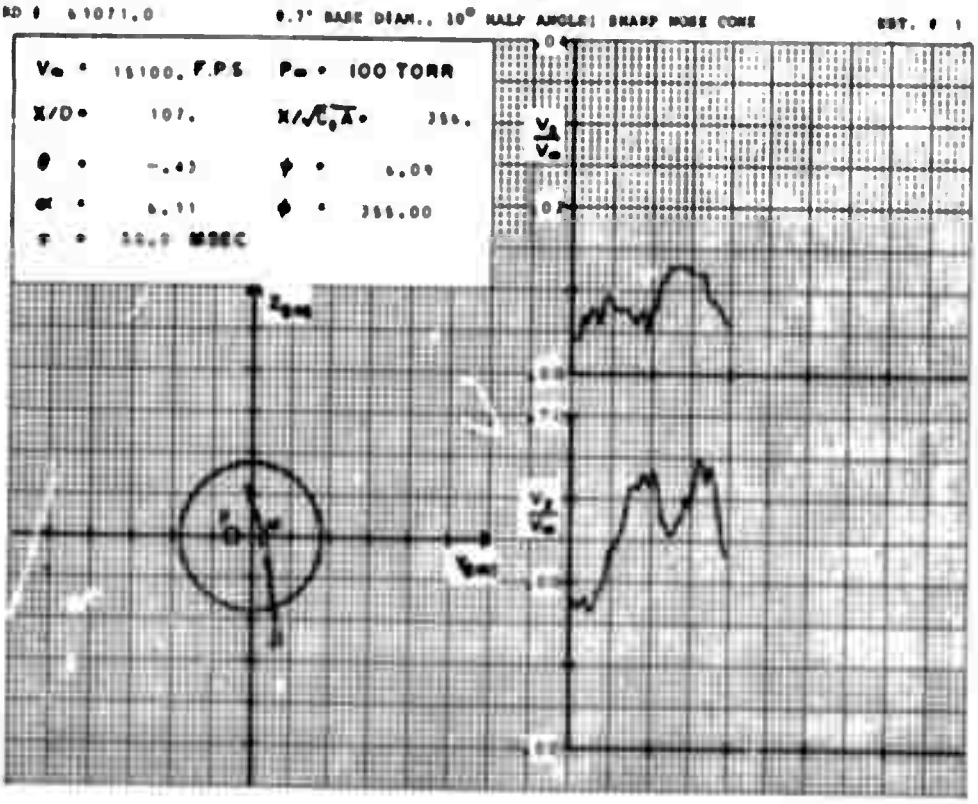

Figure 12. Typical results for the axial and lateral velocities obtained from one sequence of sparks.

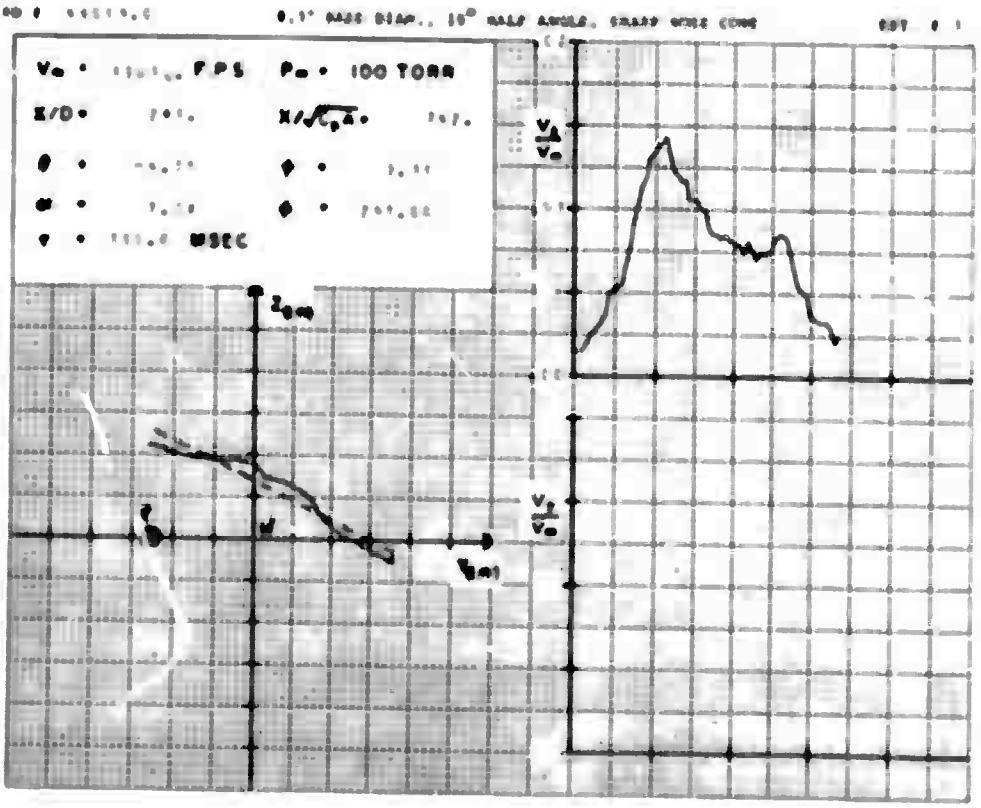

Figure 13

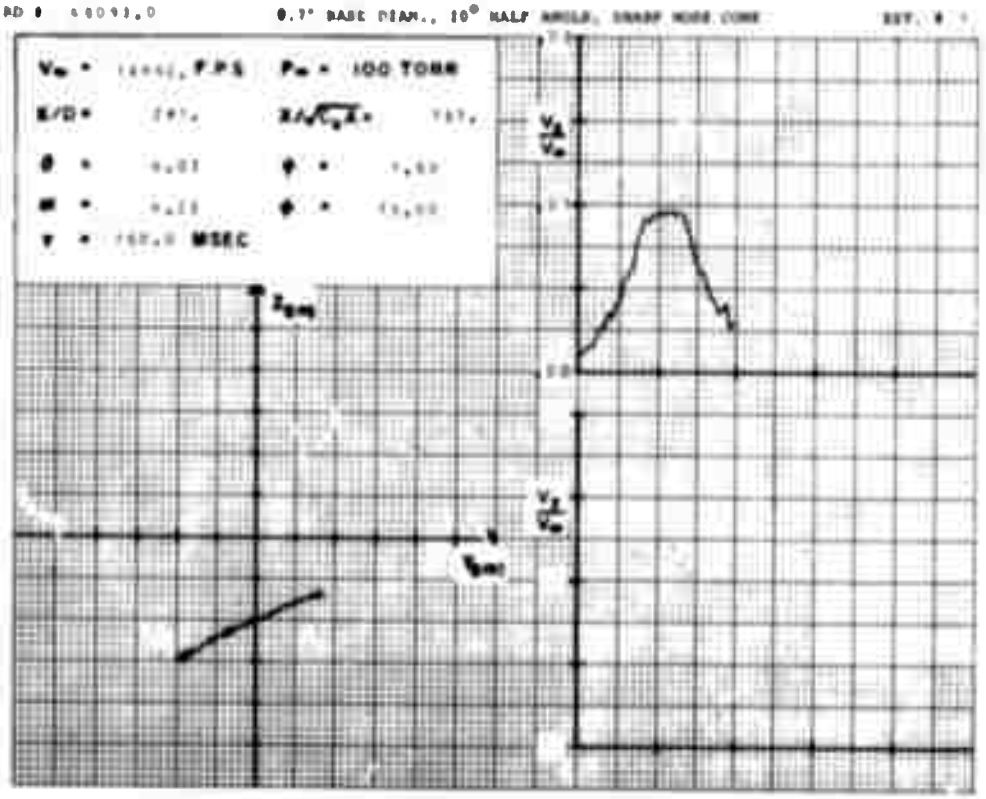

Figure 14

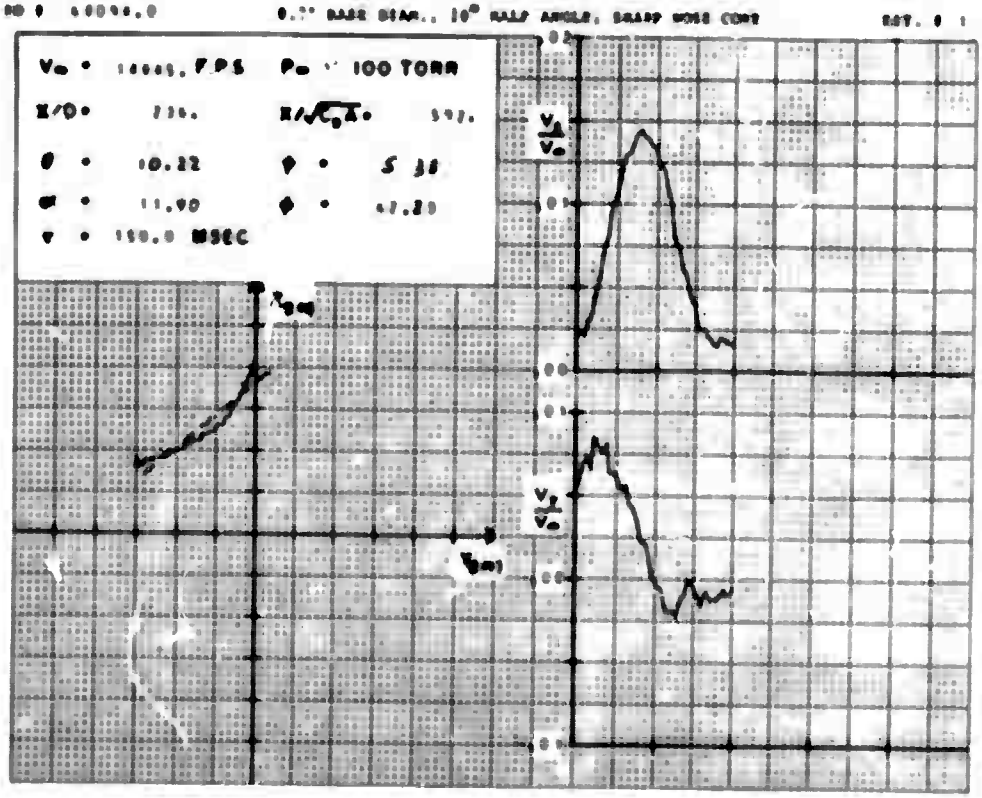

Figure 15

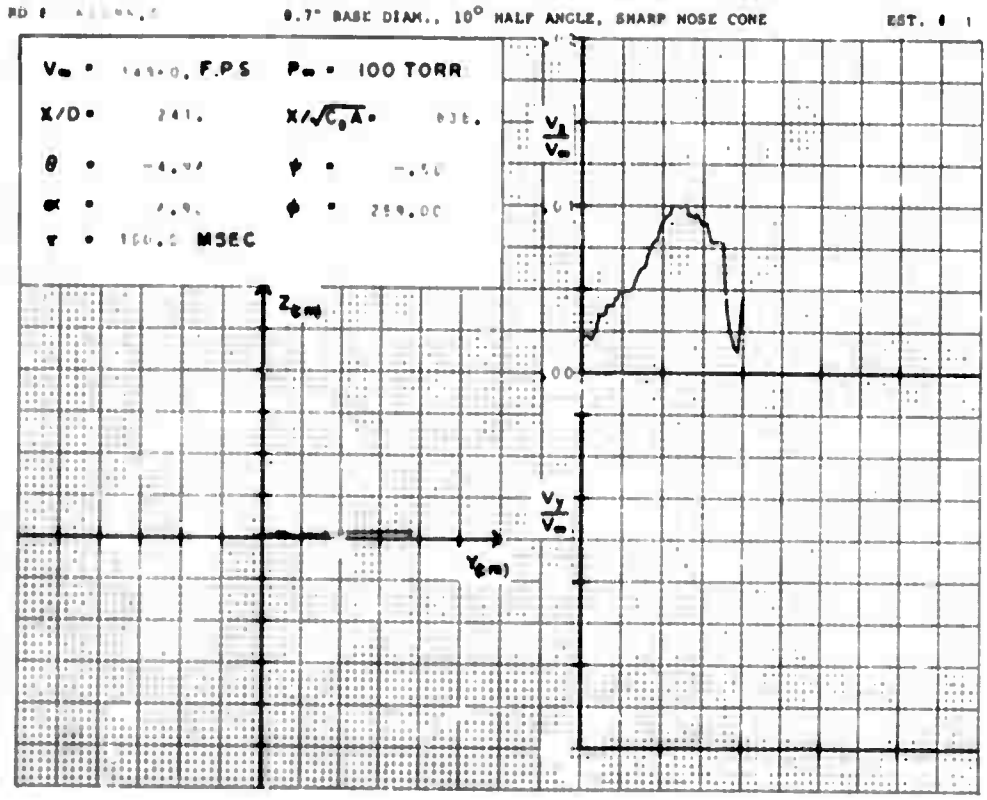

Figure 16

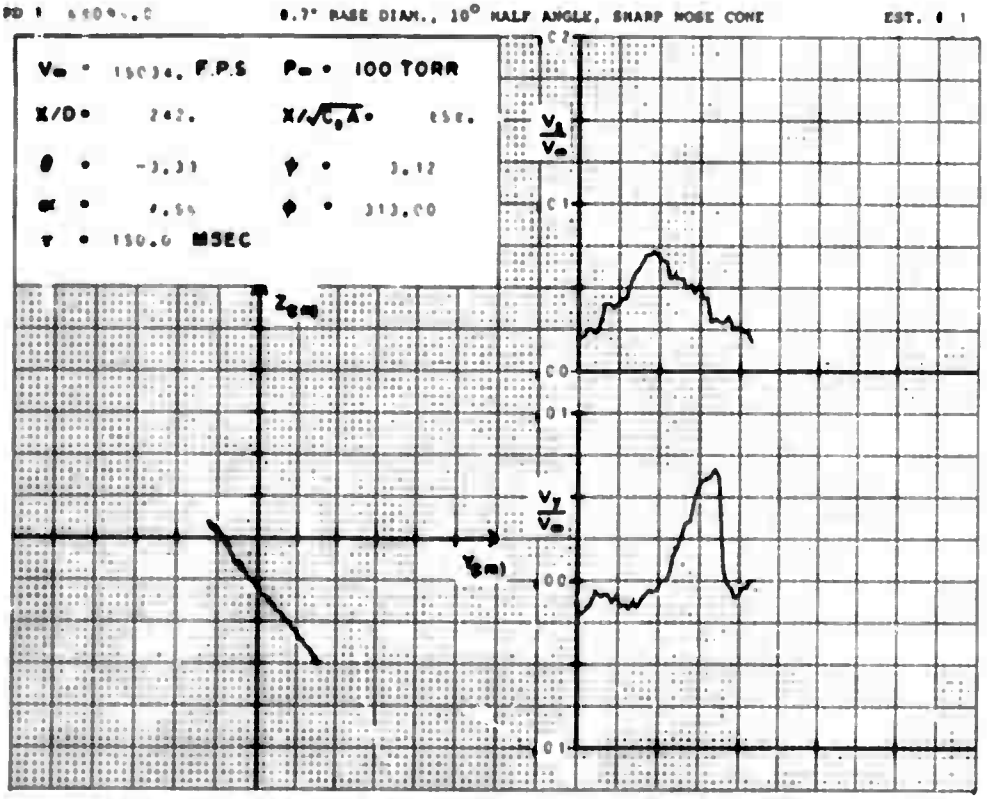

Figure 17

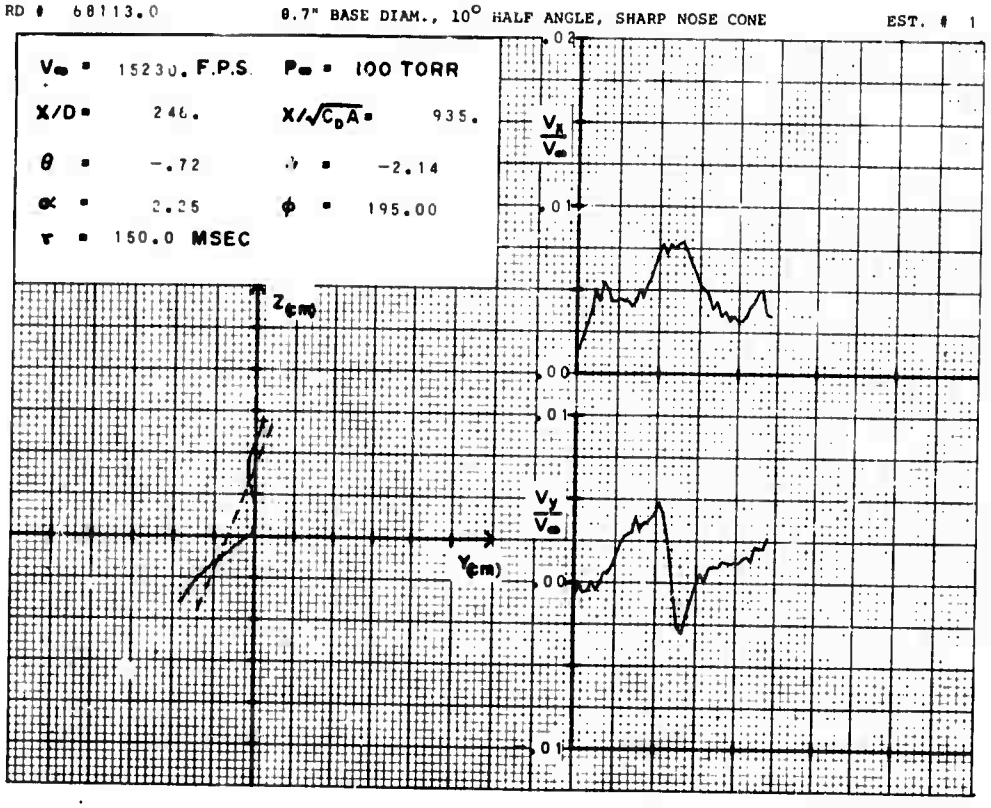

Figure 18

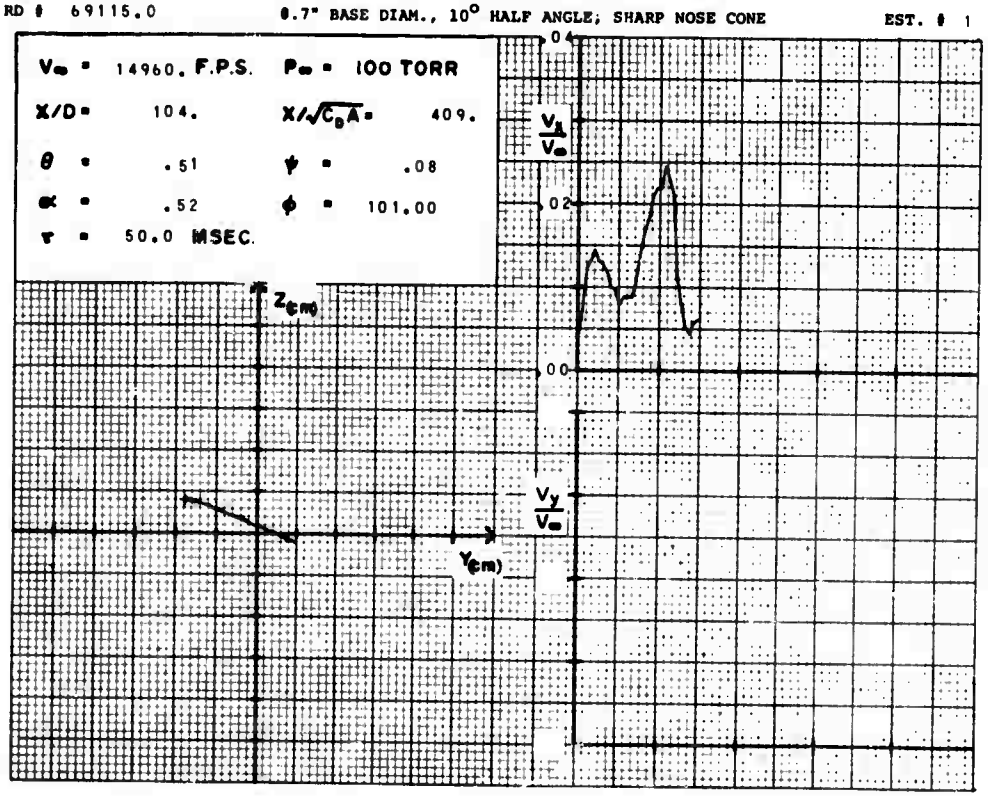

Figure 19

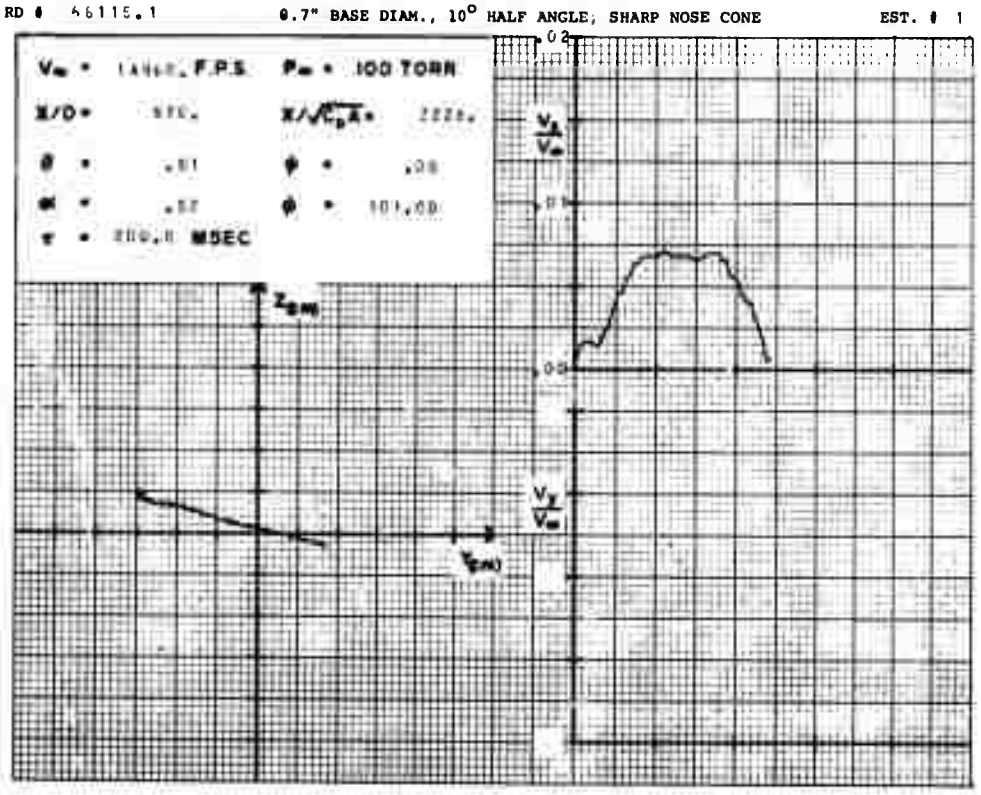

Figure 20

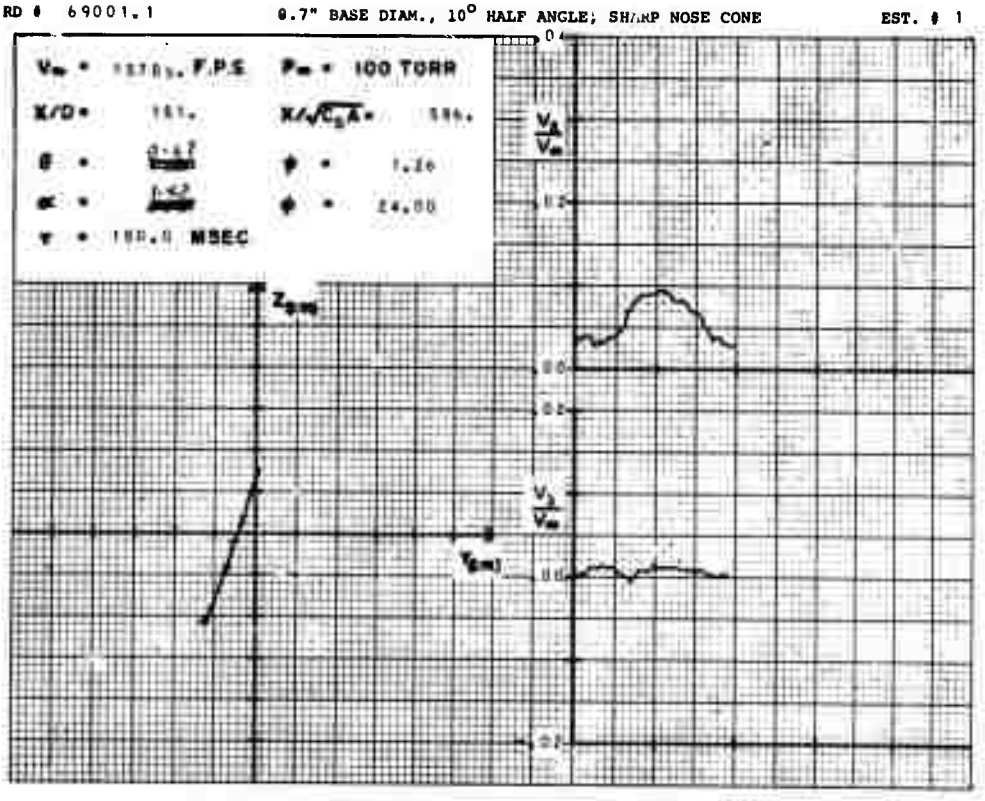

Figure 21

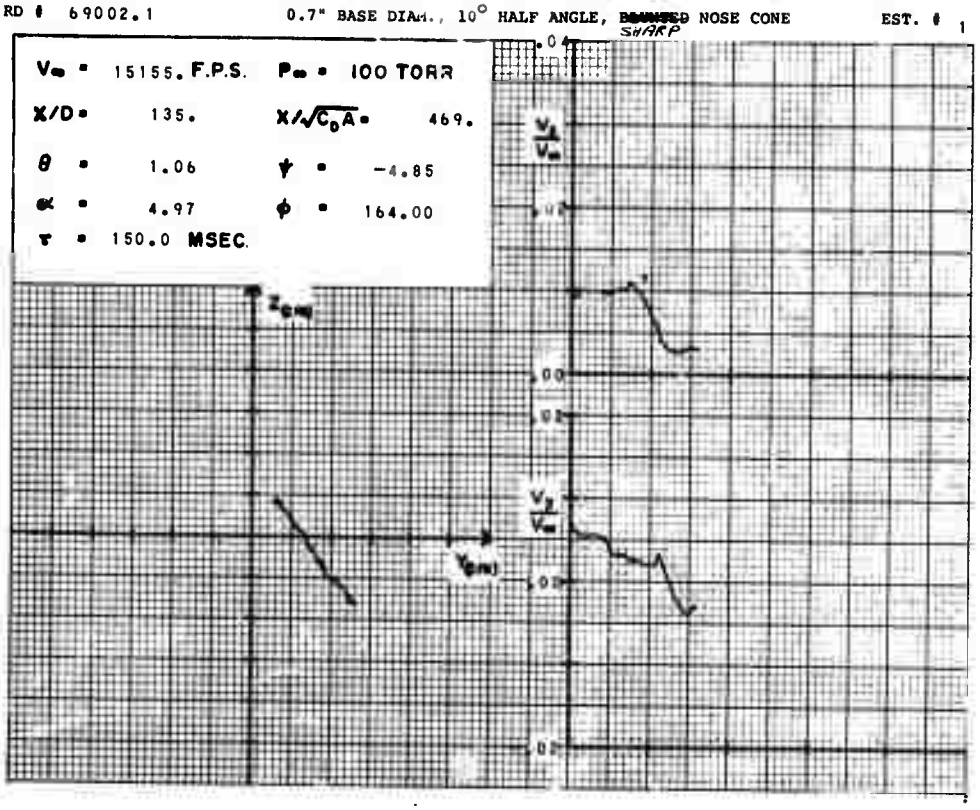

Figure 22

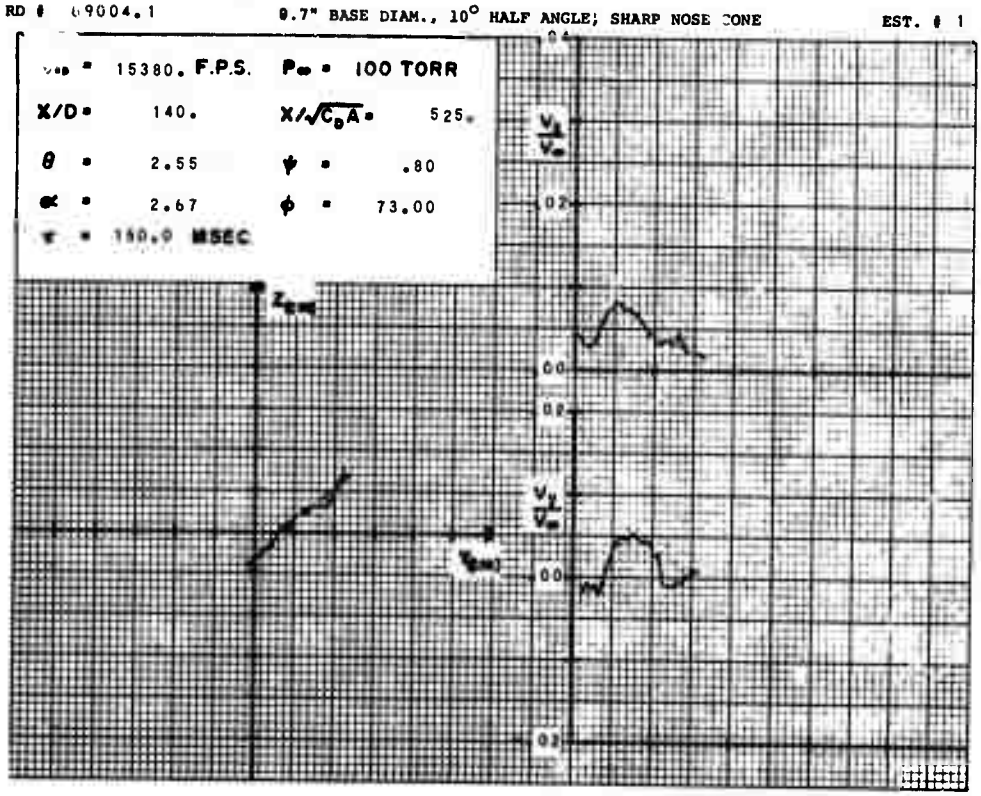

Figure 23

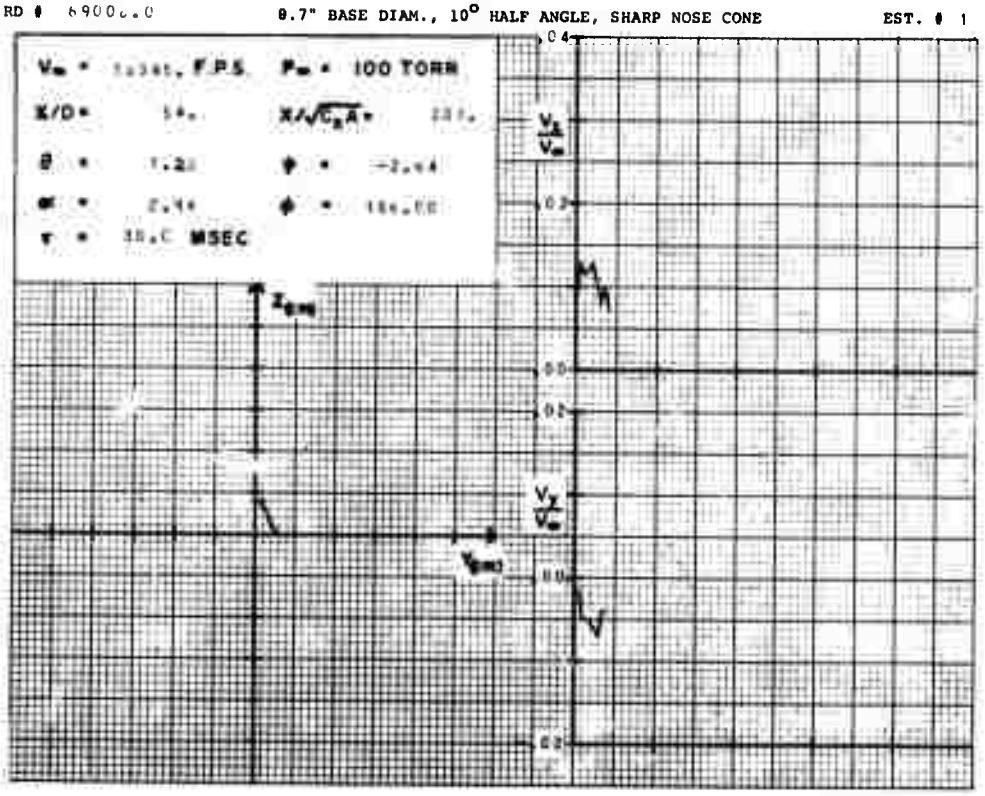

Figure 24

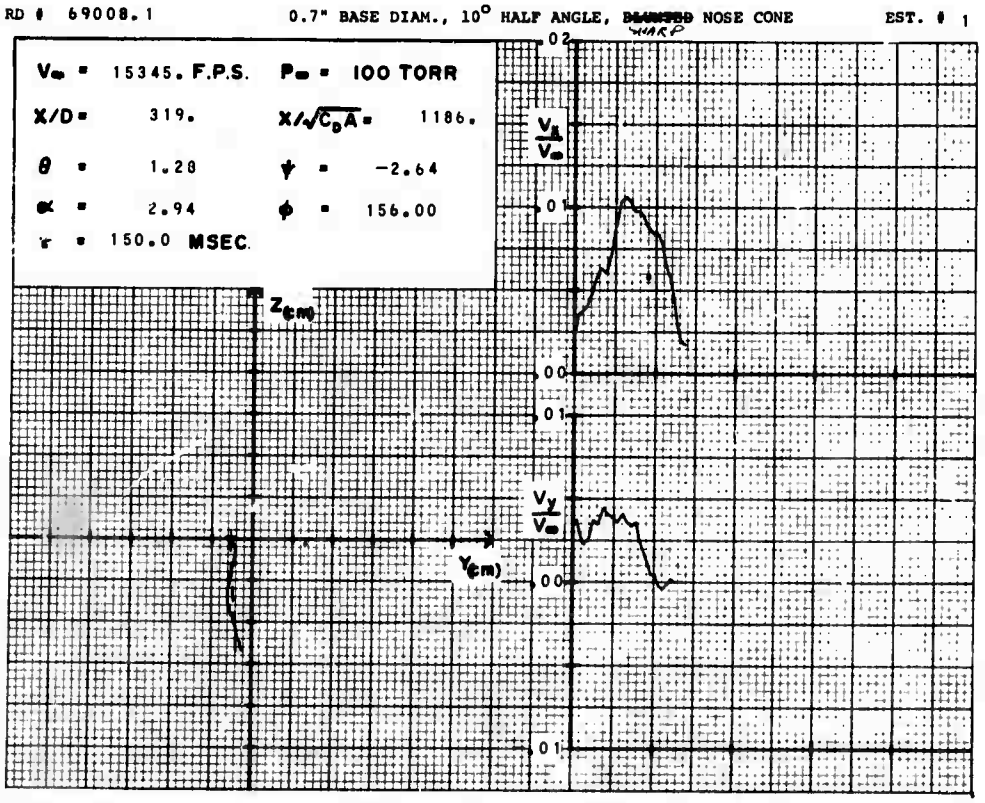

Figure 25

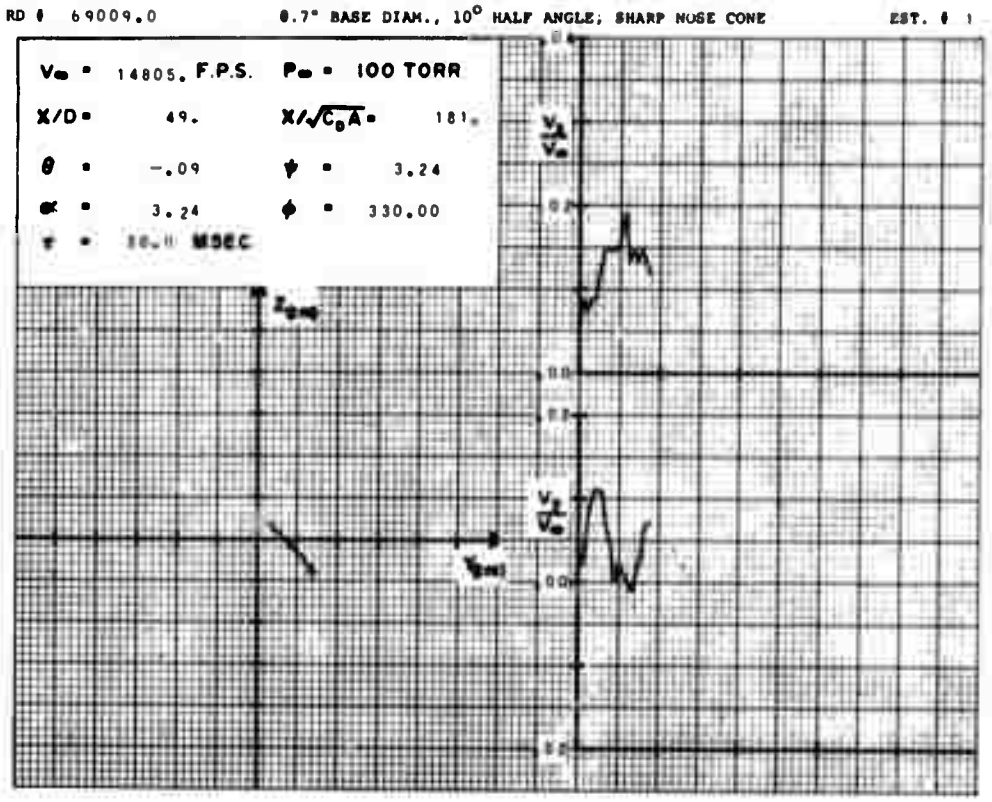

Figure 26

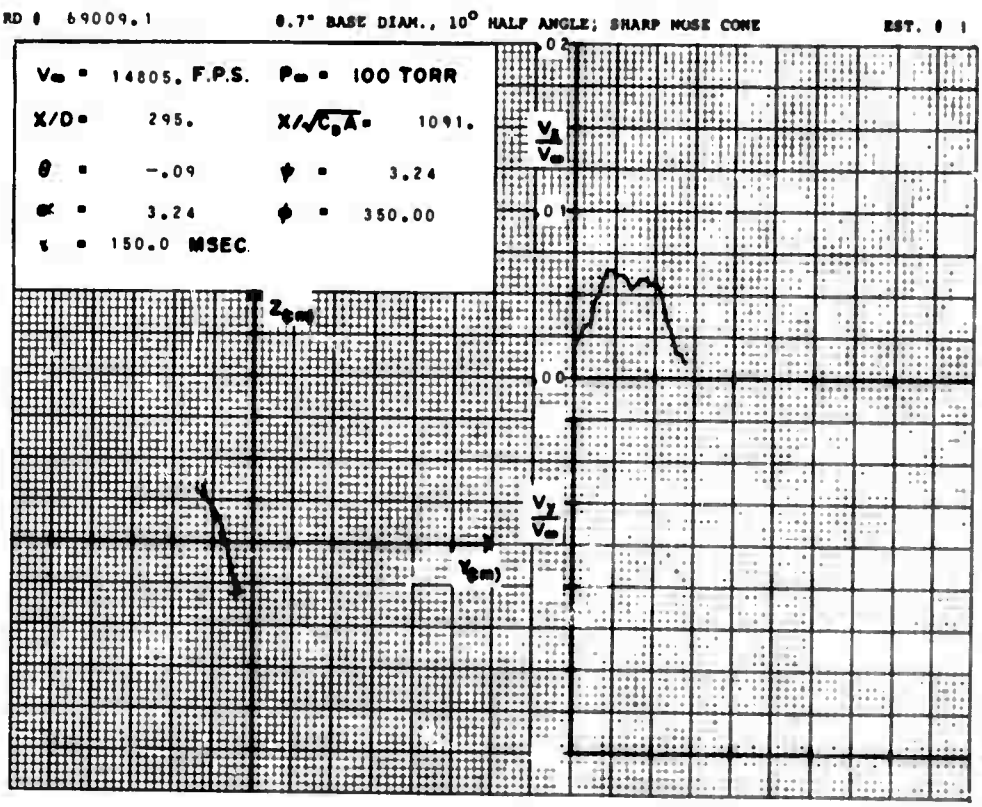

Figure 27

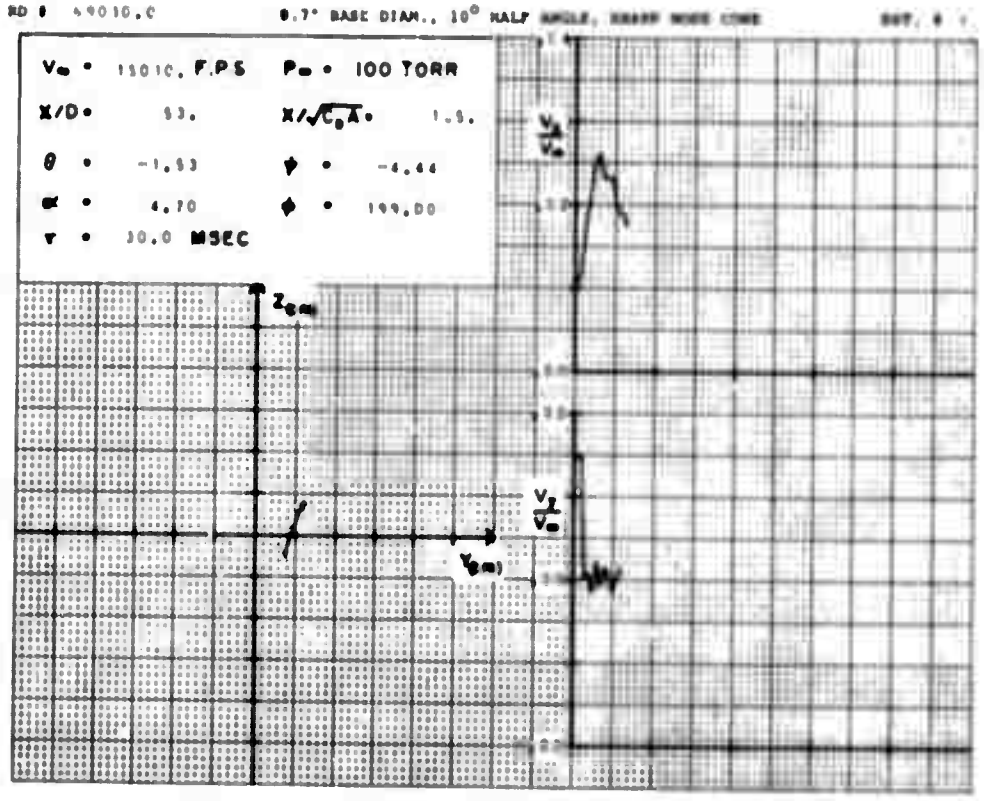

Figure 28

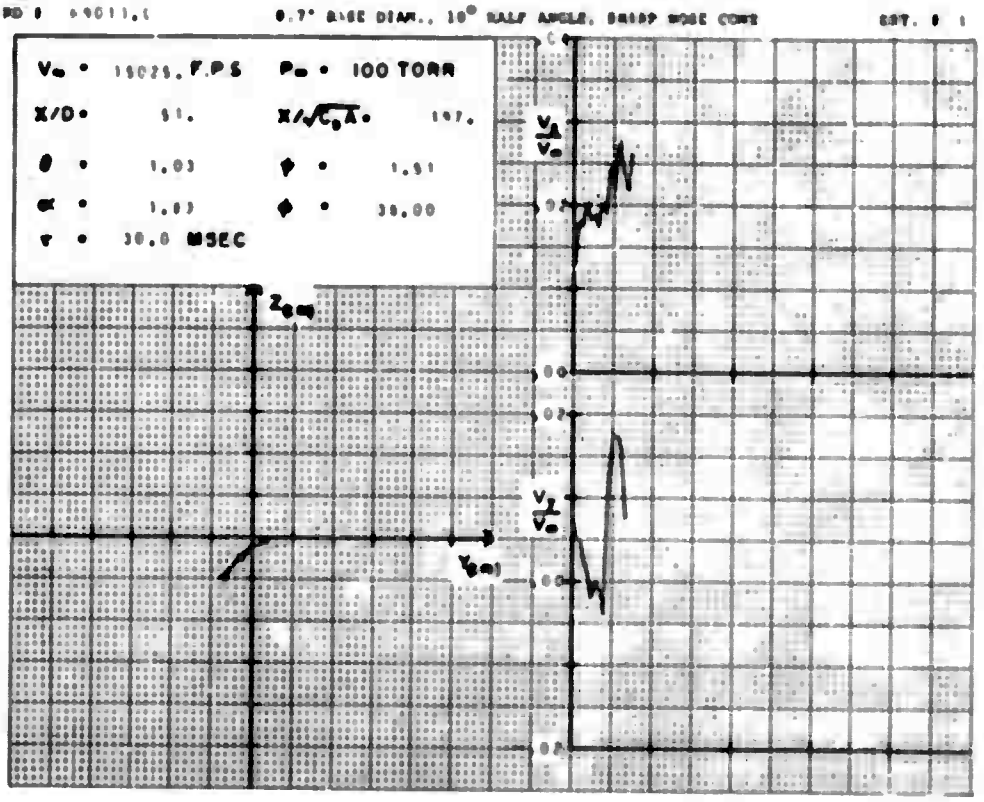

Figure 29

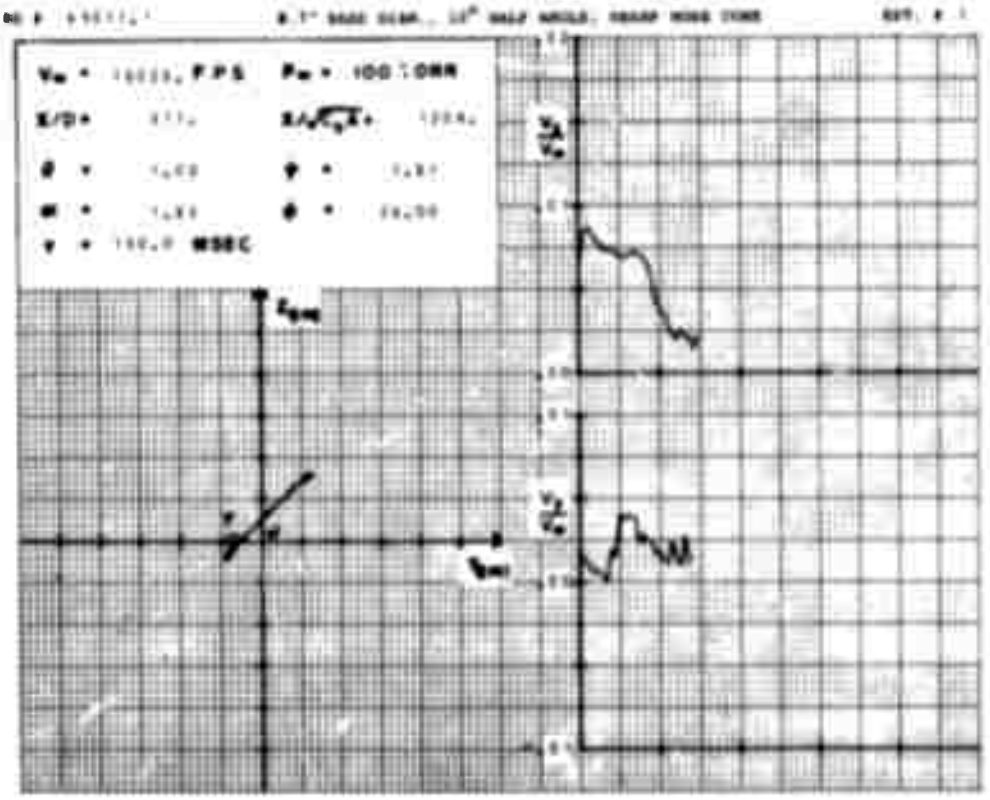

Figure 30

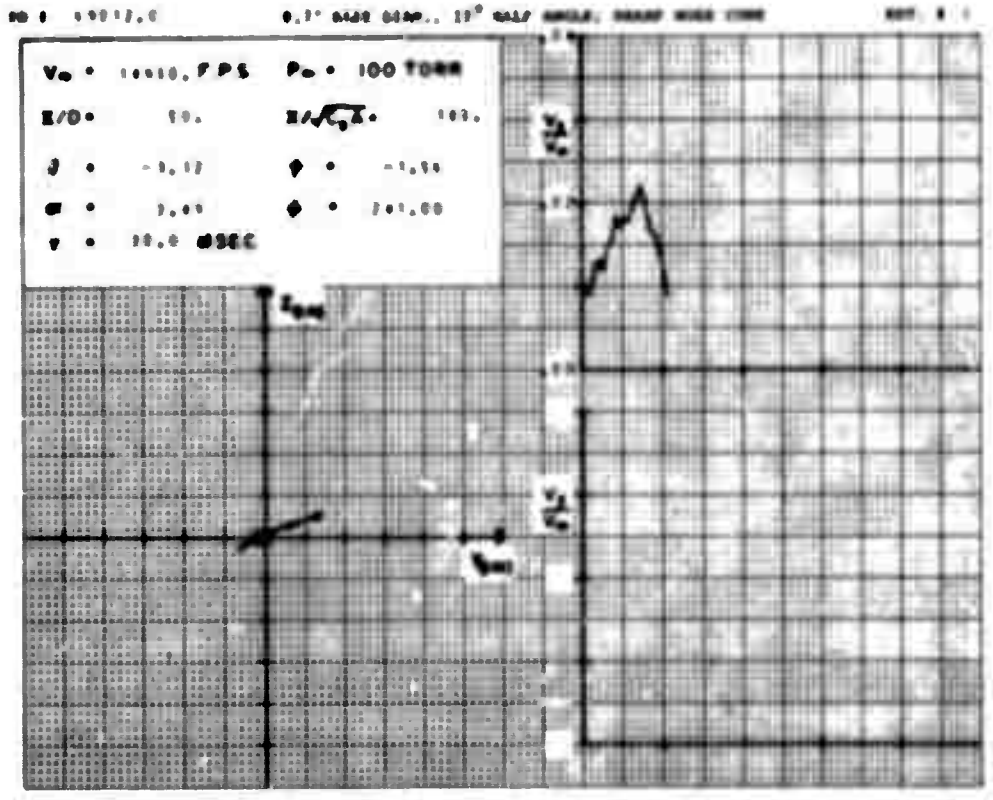

Figure 31

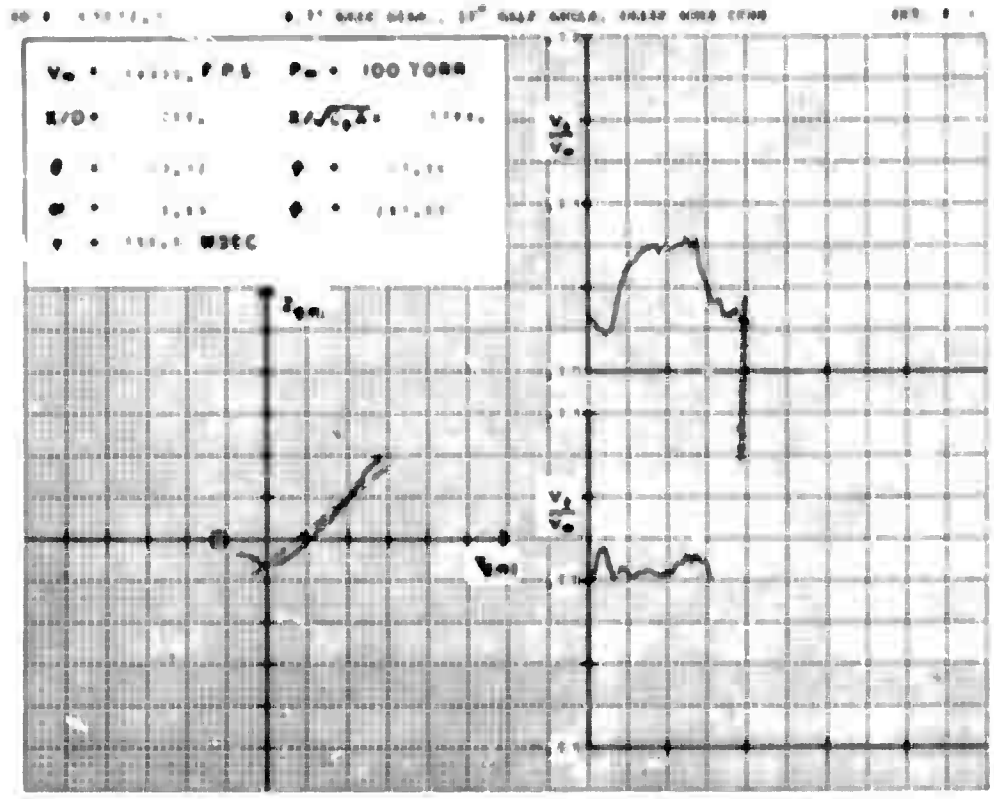

Figure 32

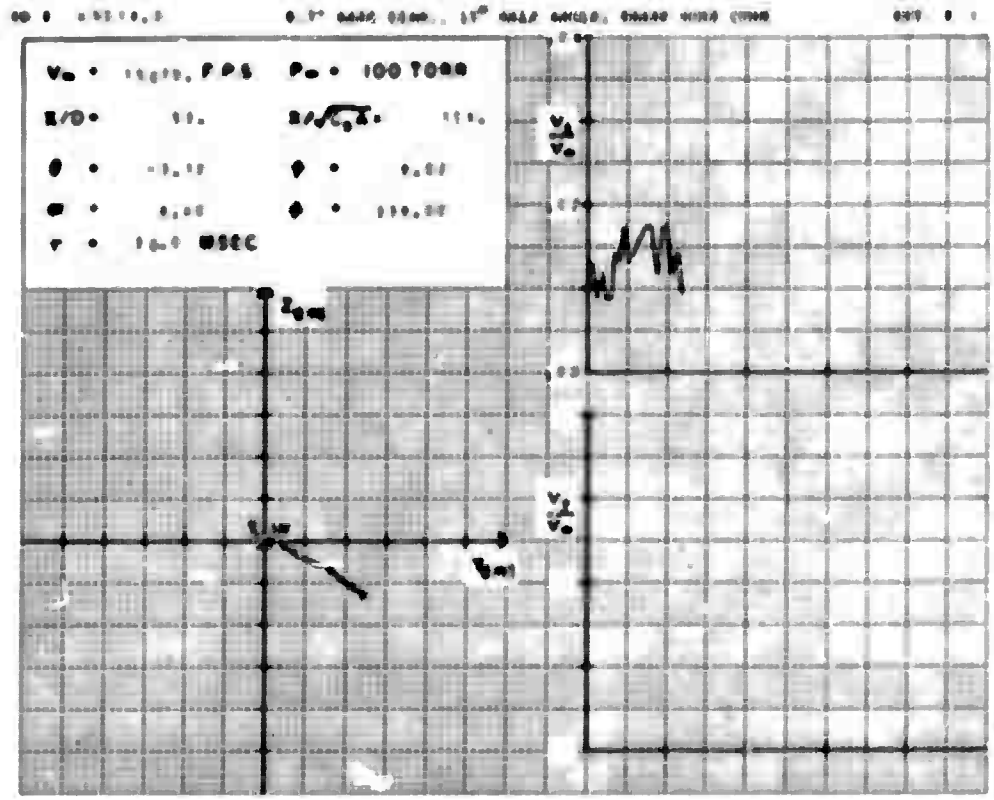

Figure 33

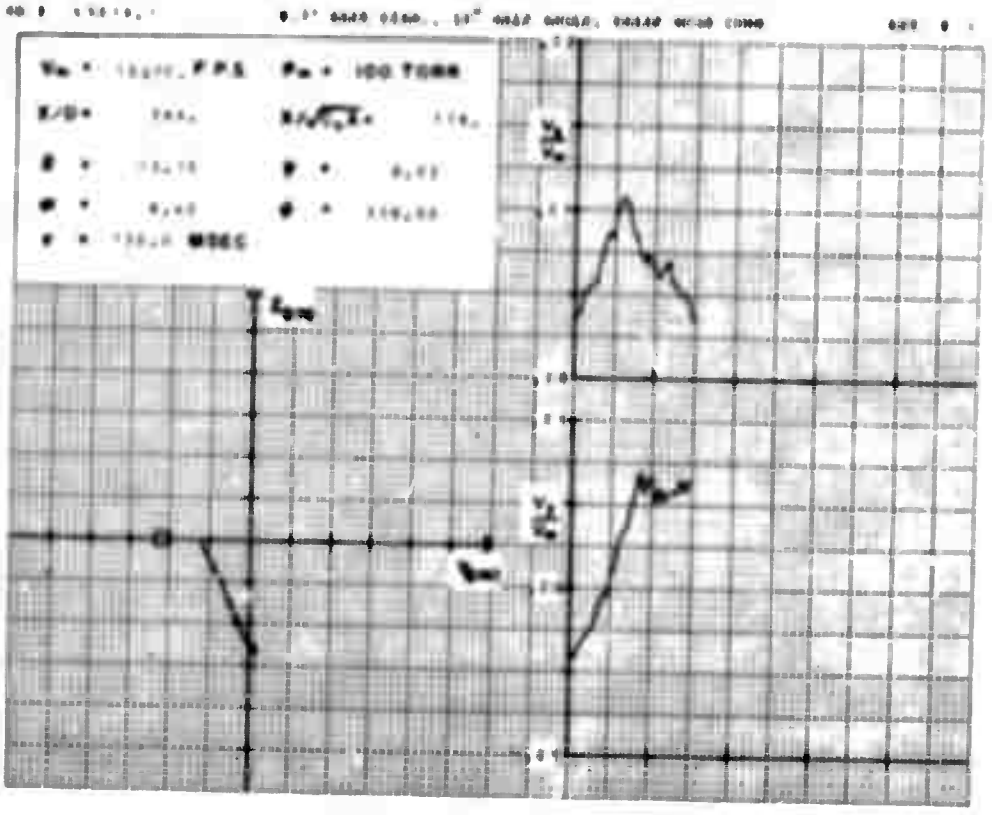

Figure 34

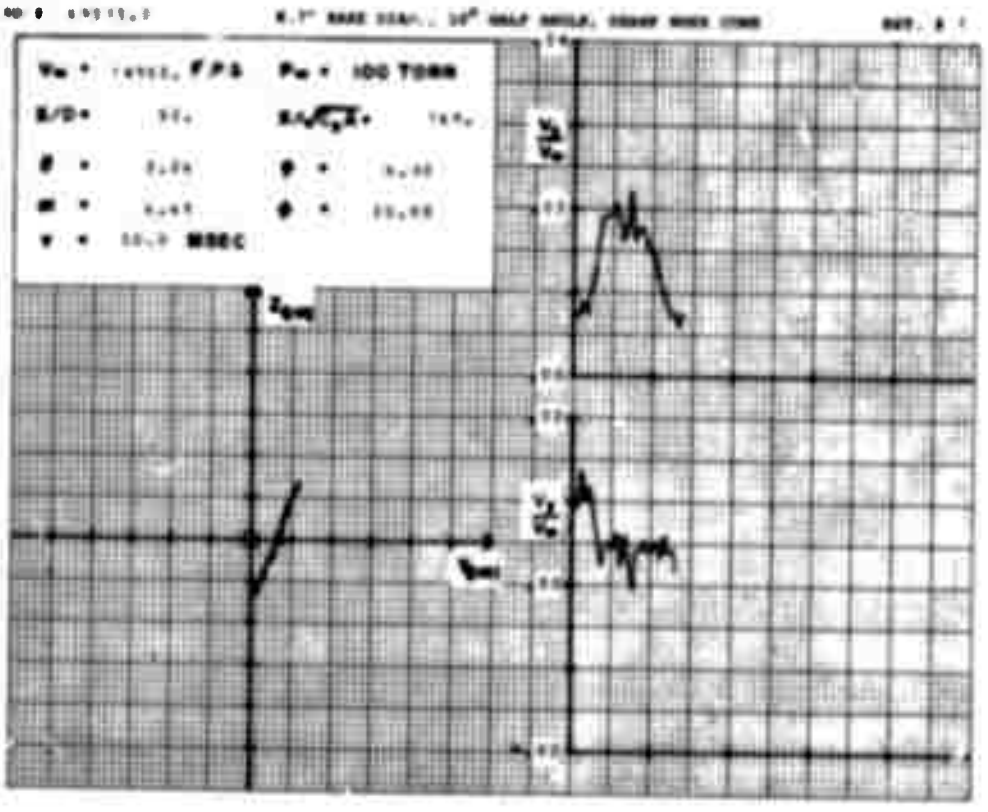

Figure 35

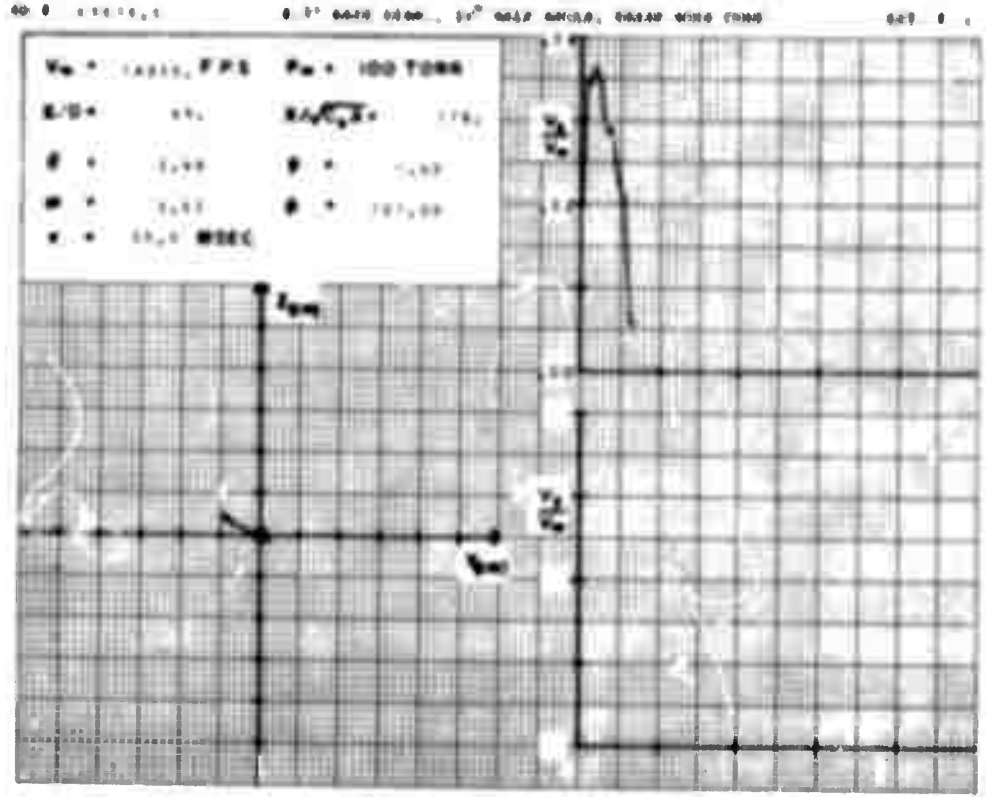

Figure 36

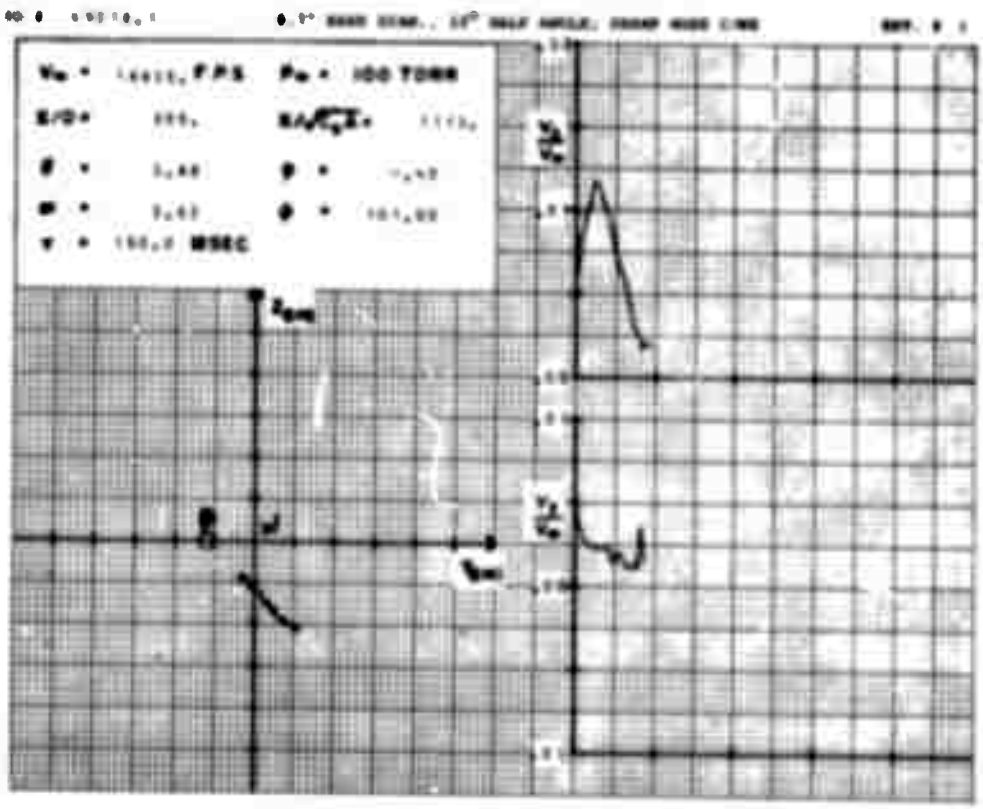

Figure 37

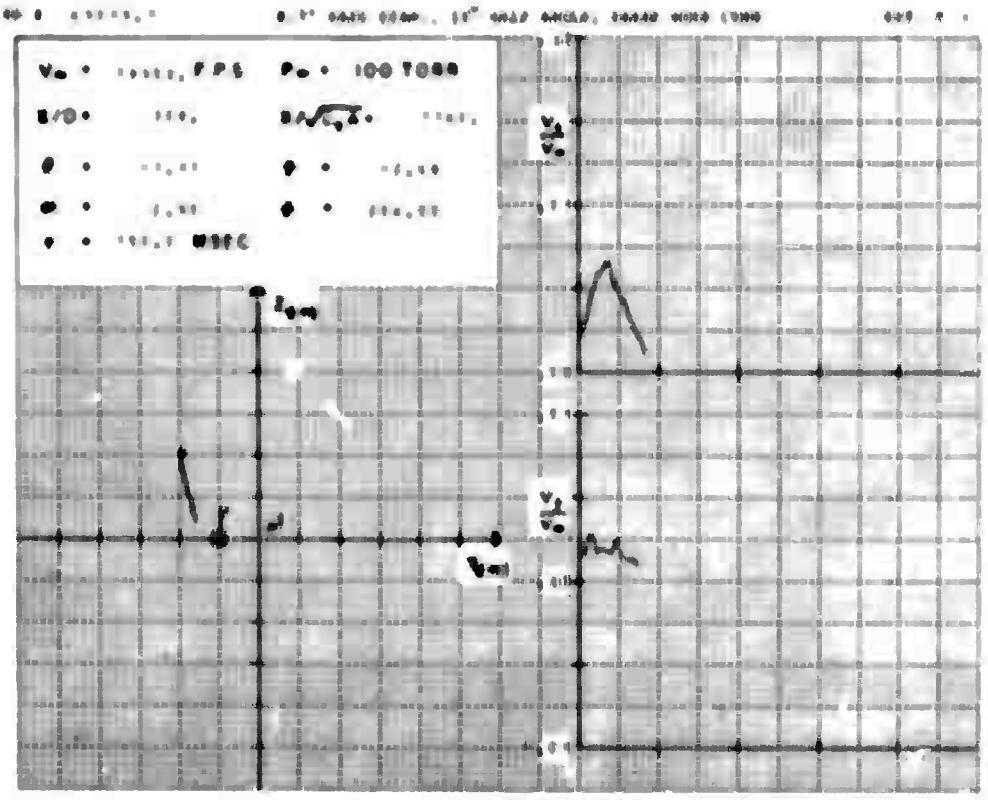

Figure 38

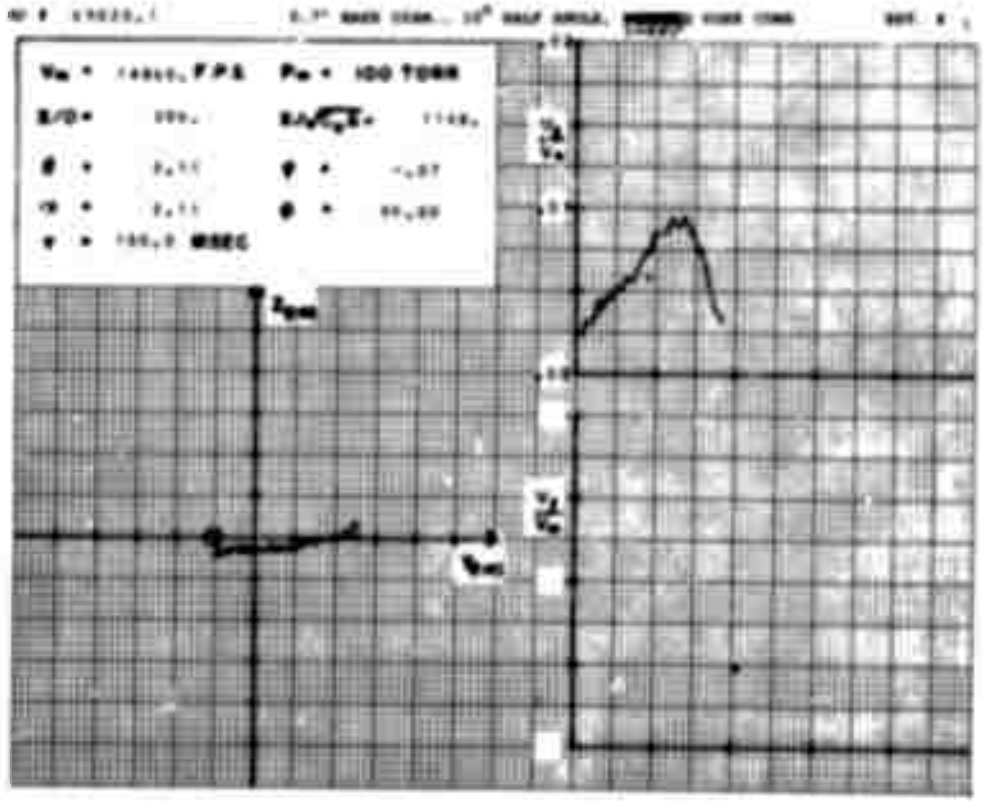

Figure 39

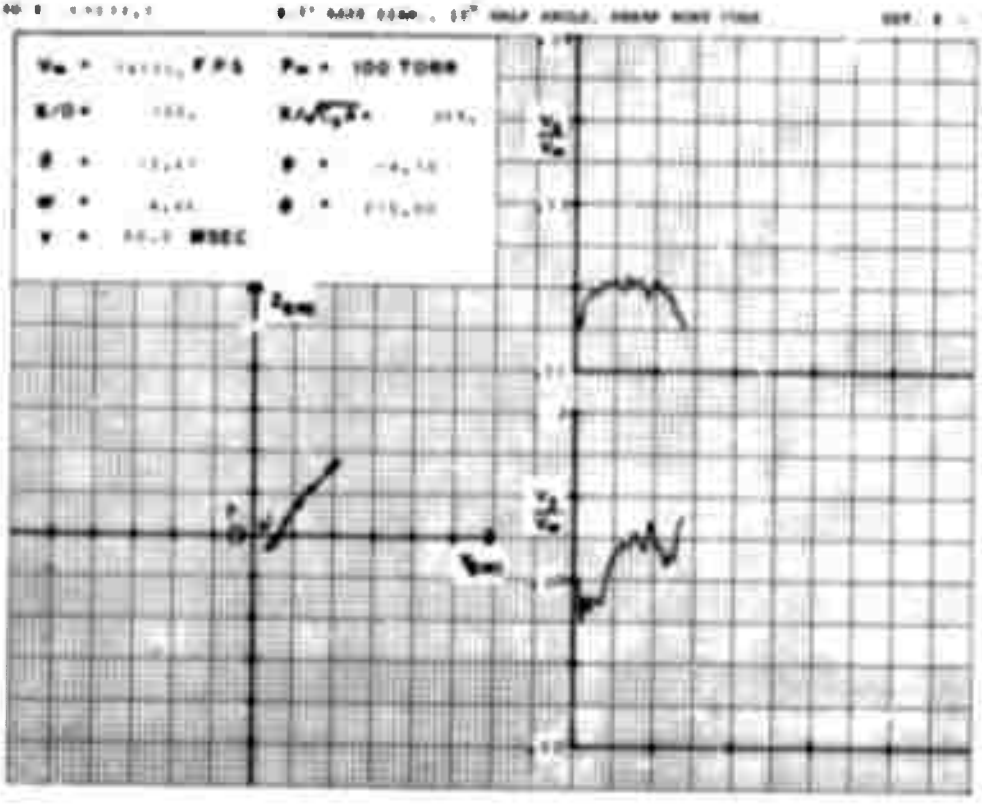

Figure 40

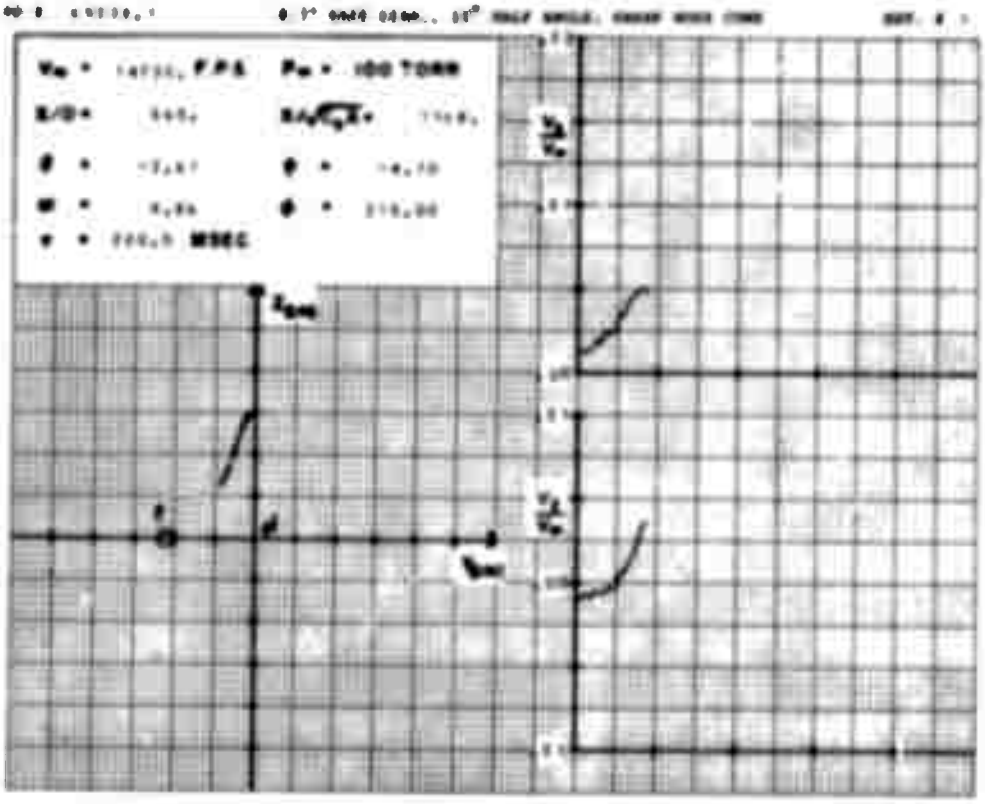

Figure 41

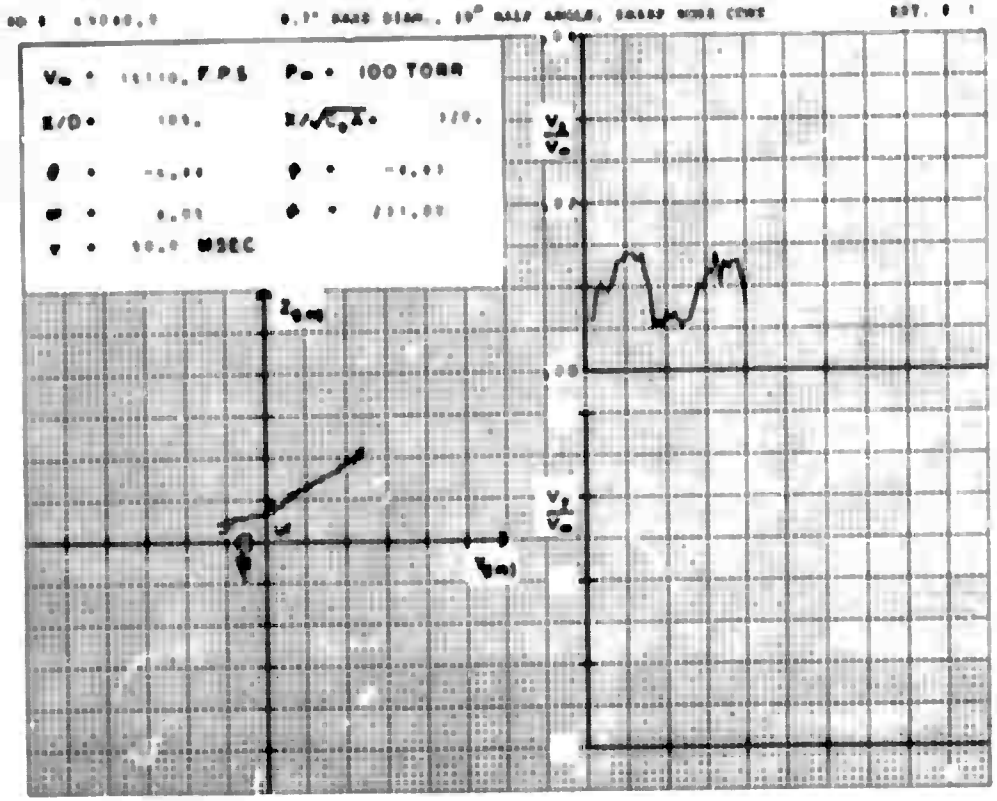

Figure 42

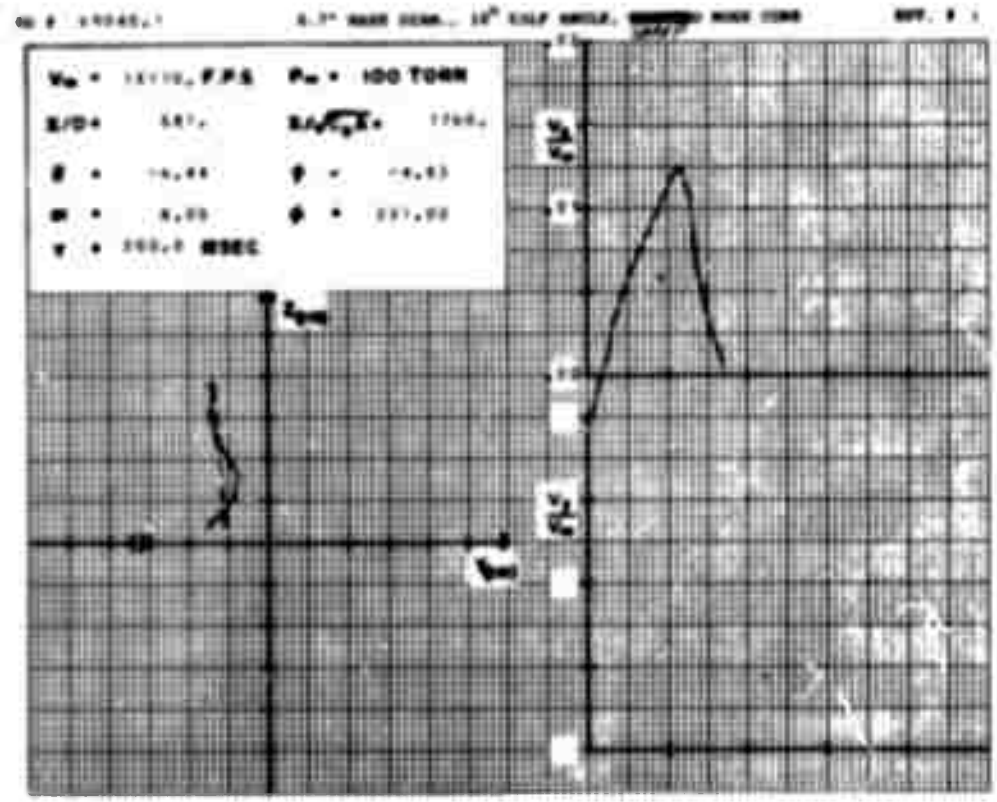

Figure 43

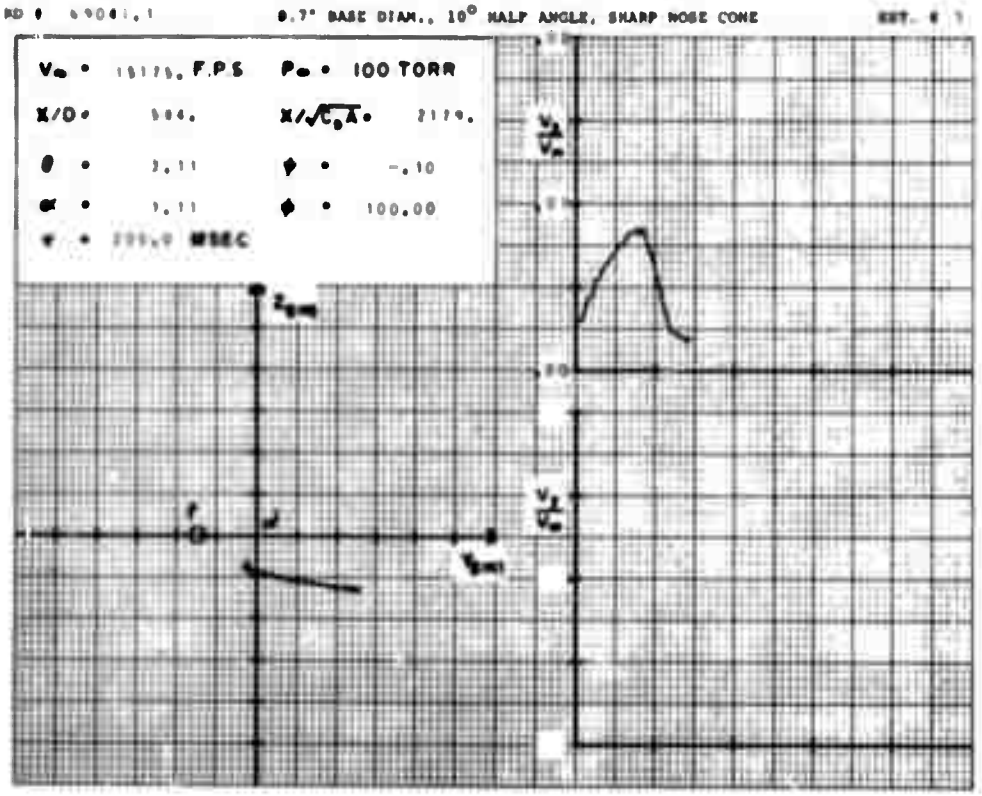

Figure 44

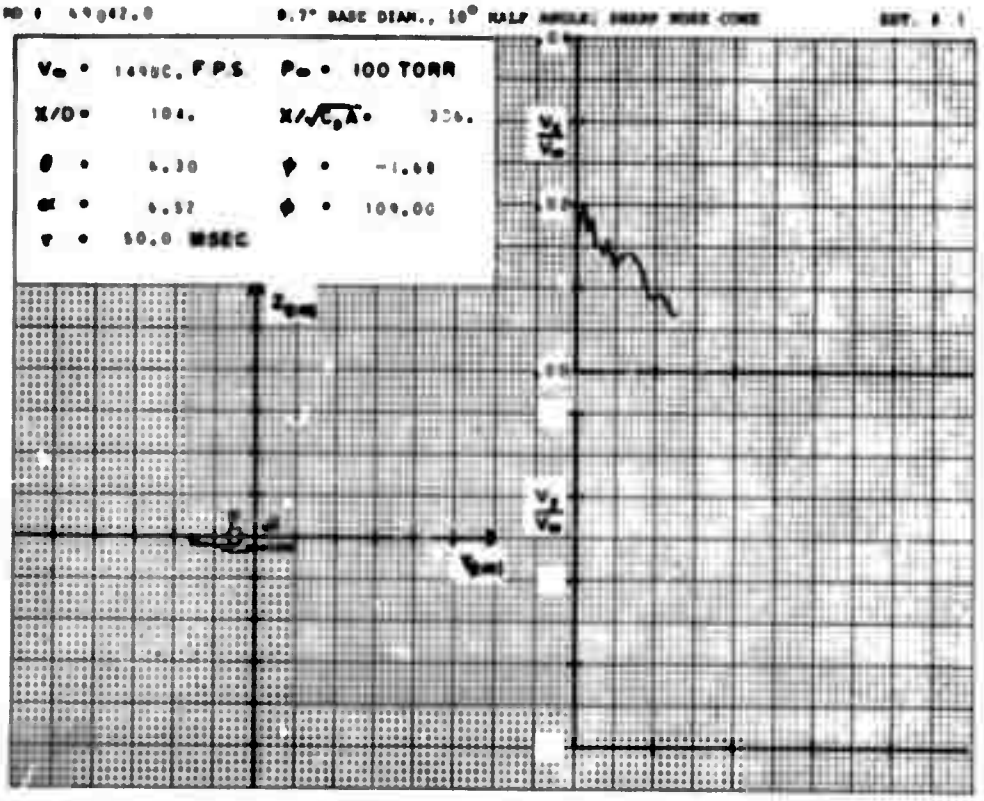

Figure 45

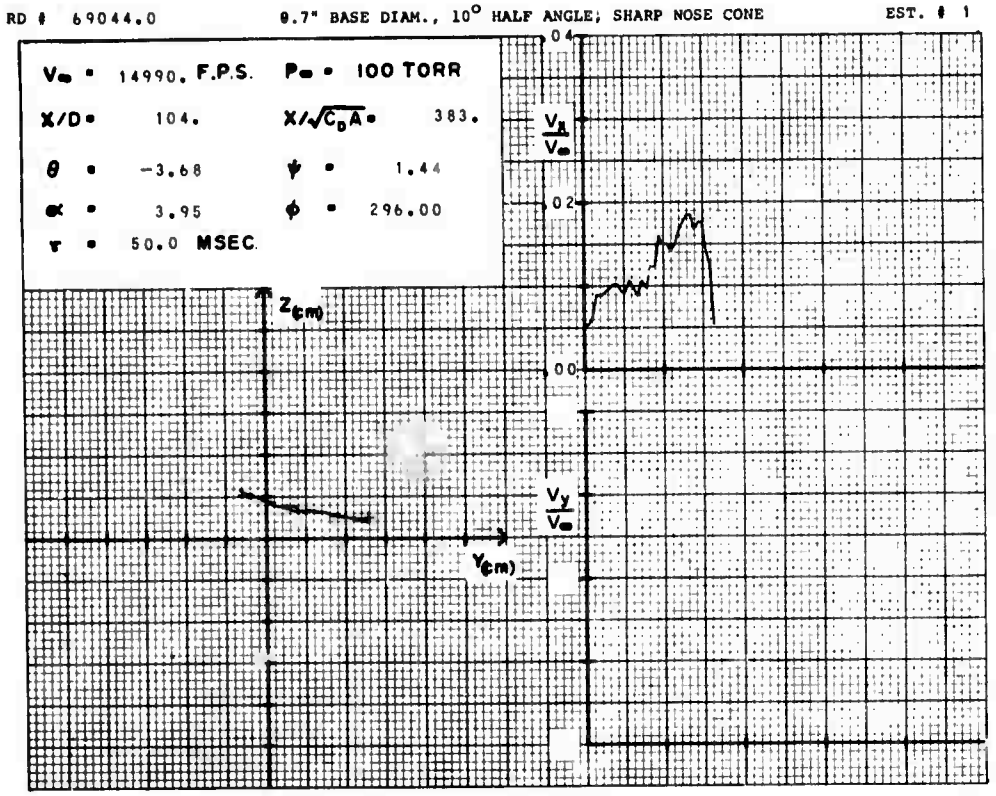

Figure 46

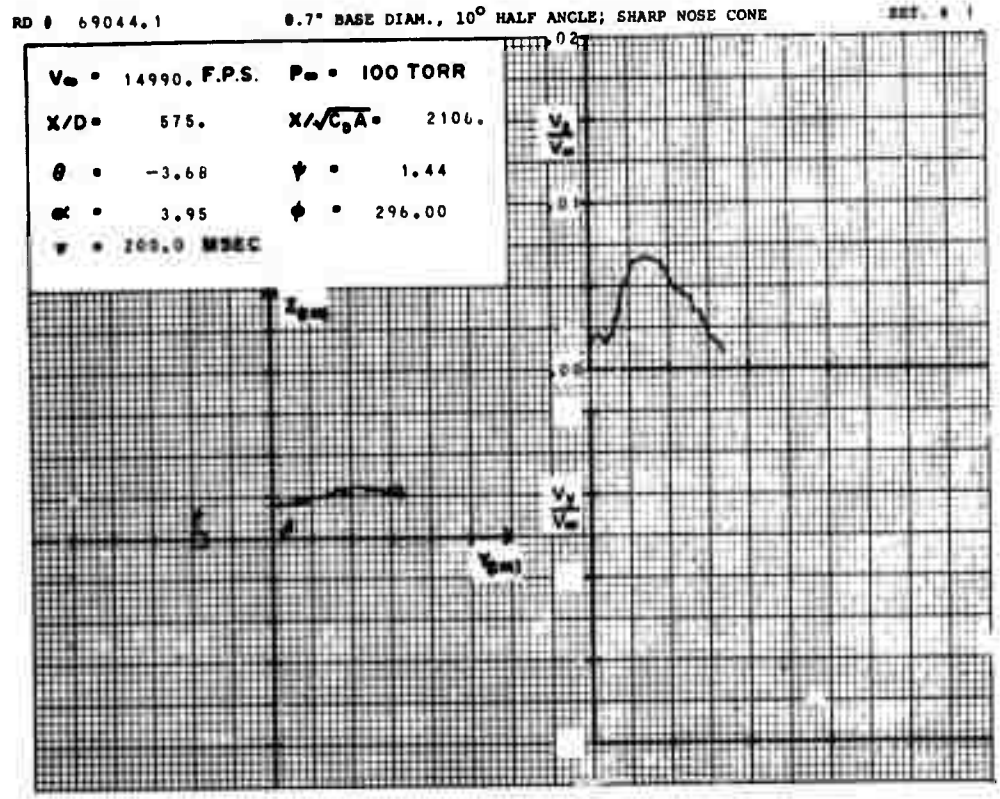

Figure 47

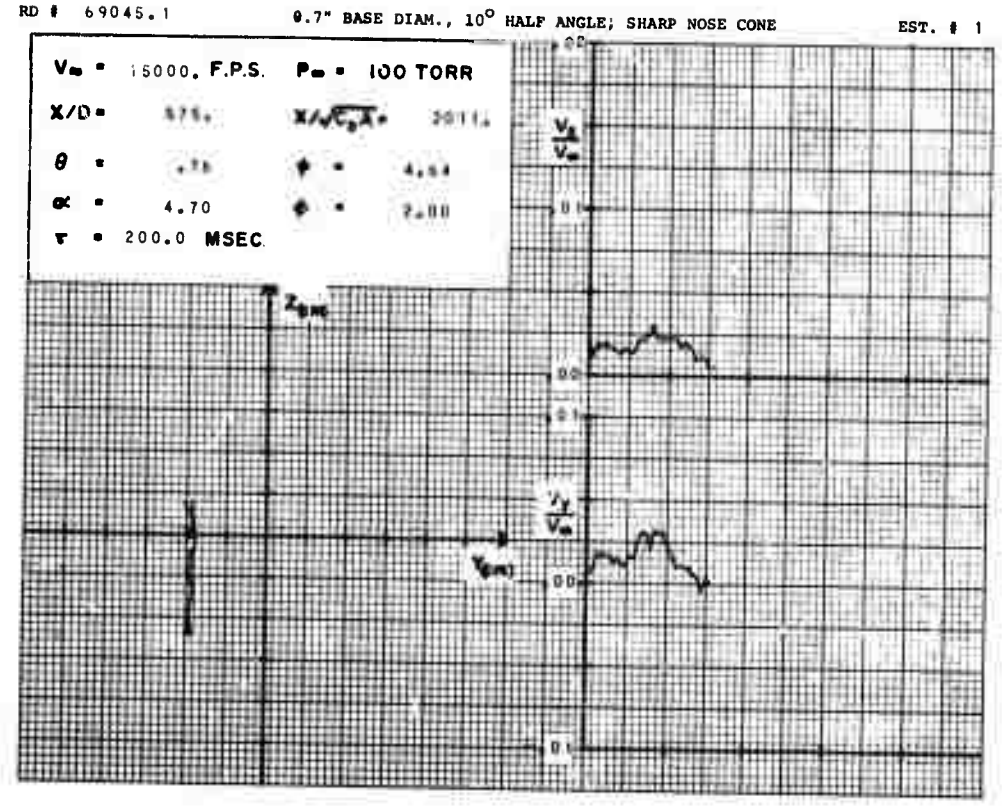

Figure 48

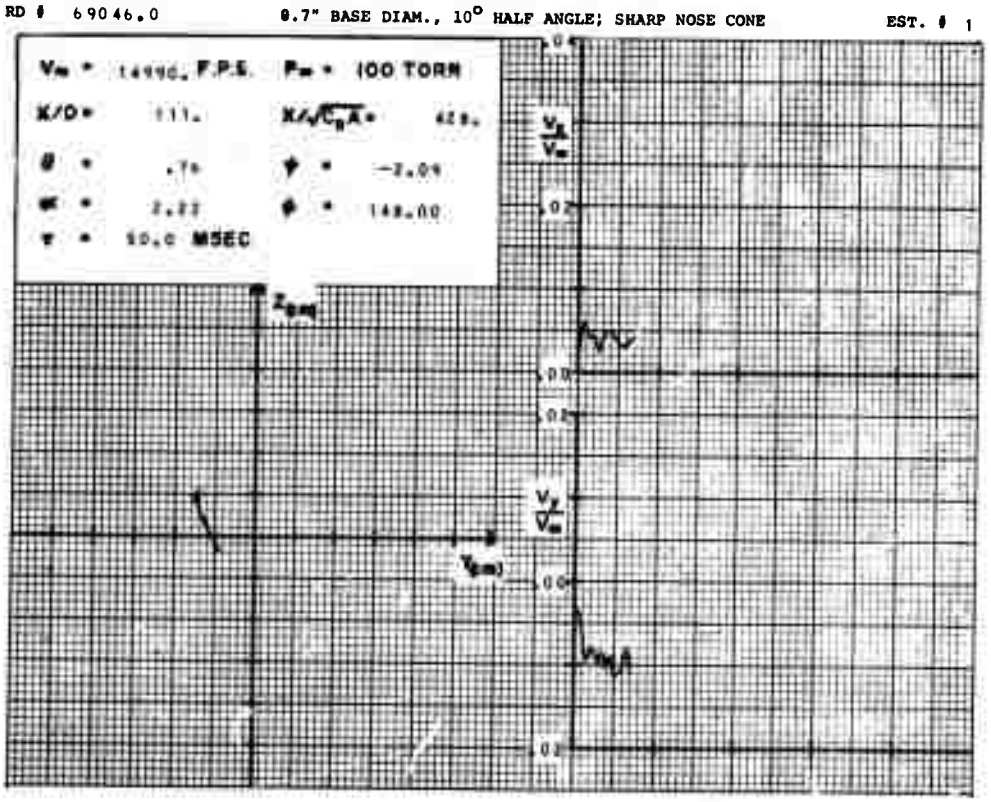

Figure 49

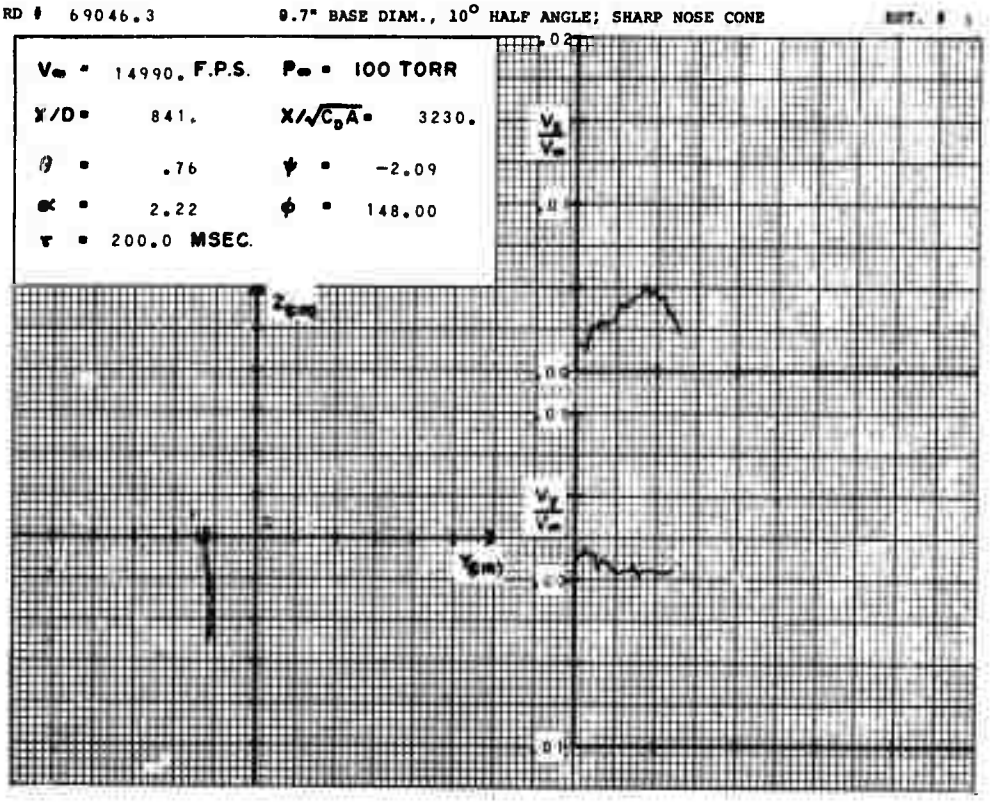

Figure 50

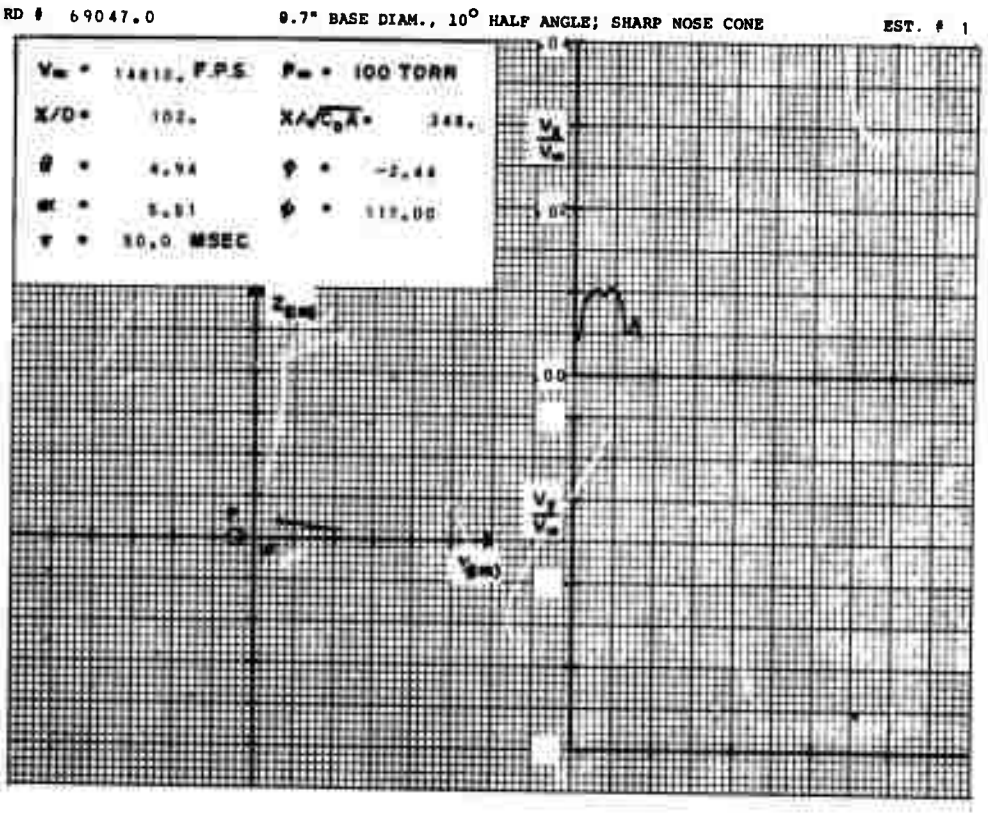

Figure 51

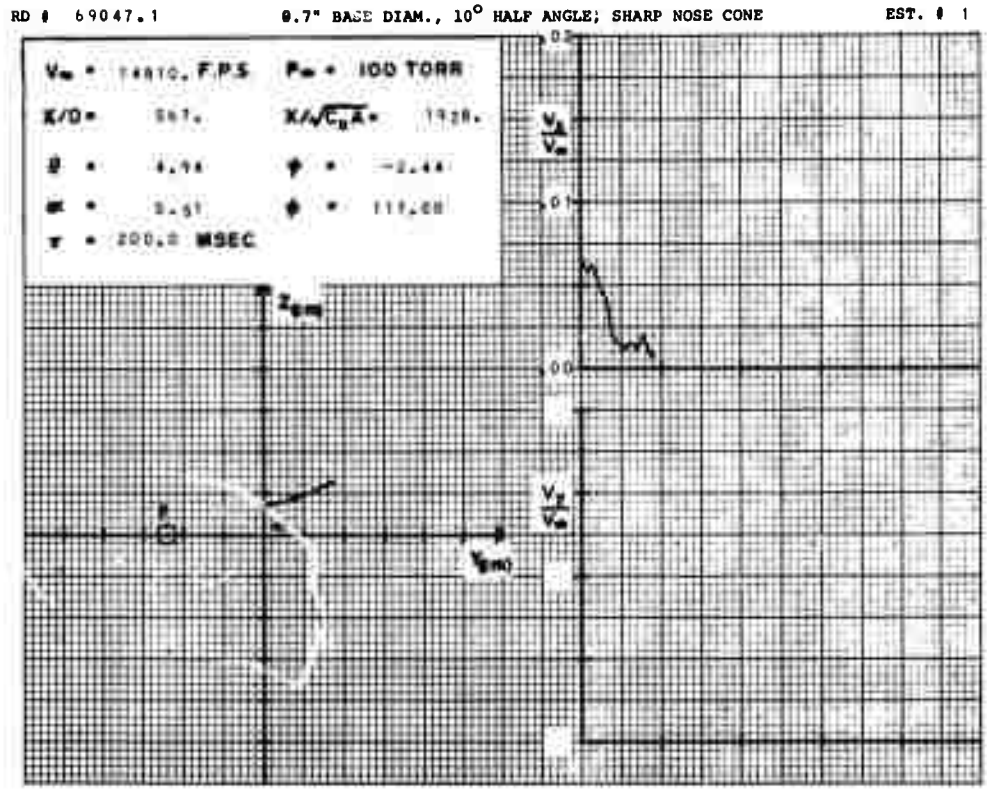

Figure 52

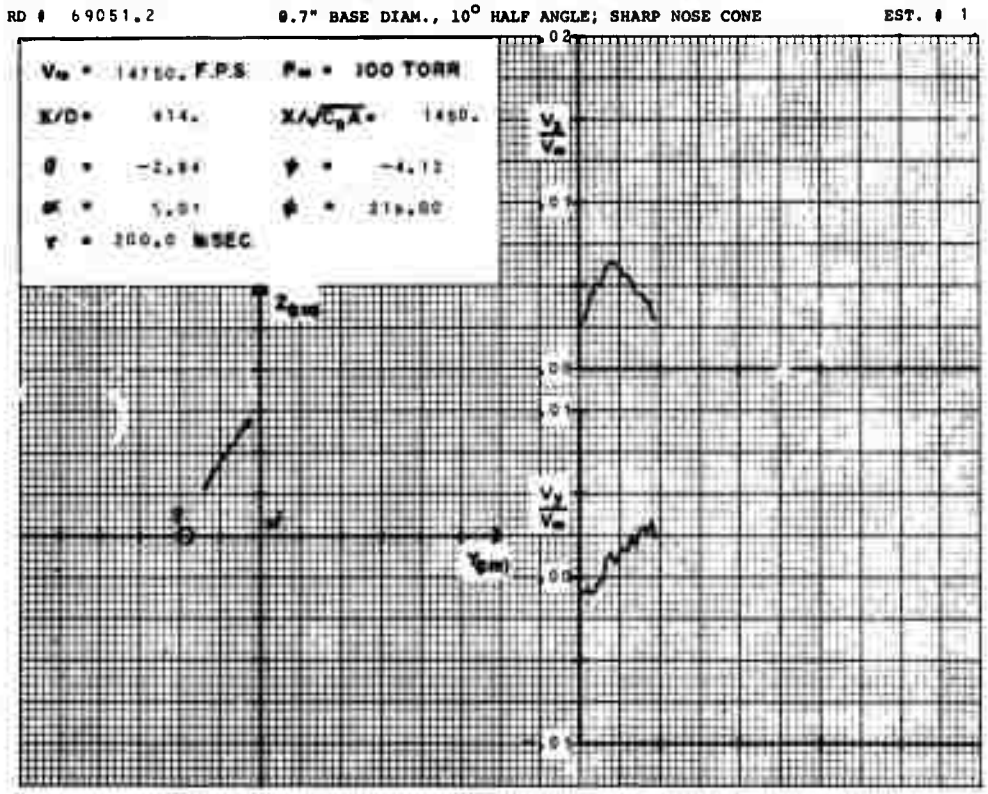

Figure 53

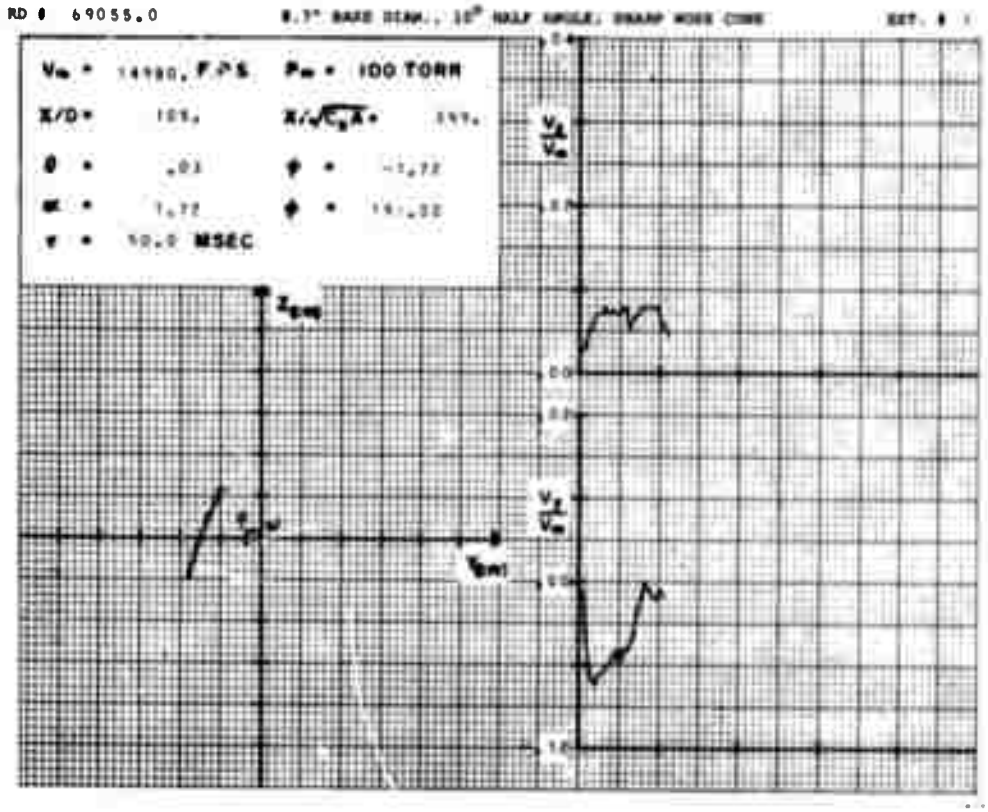

Figure 54

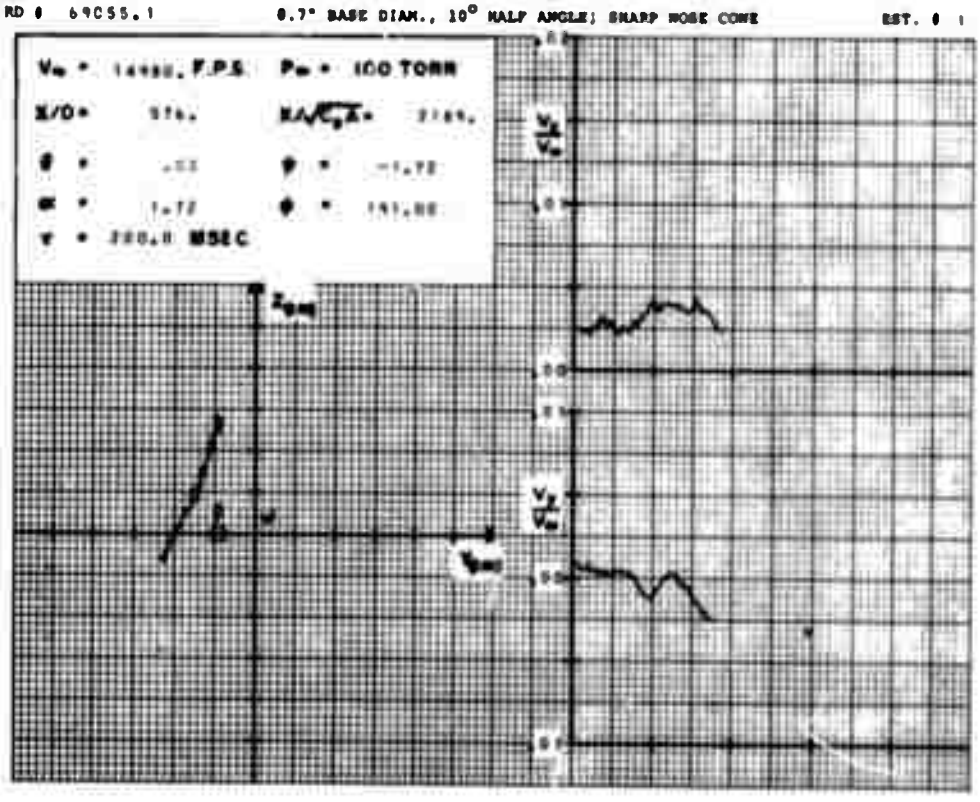

Figure 55

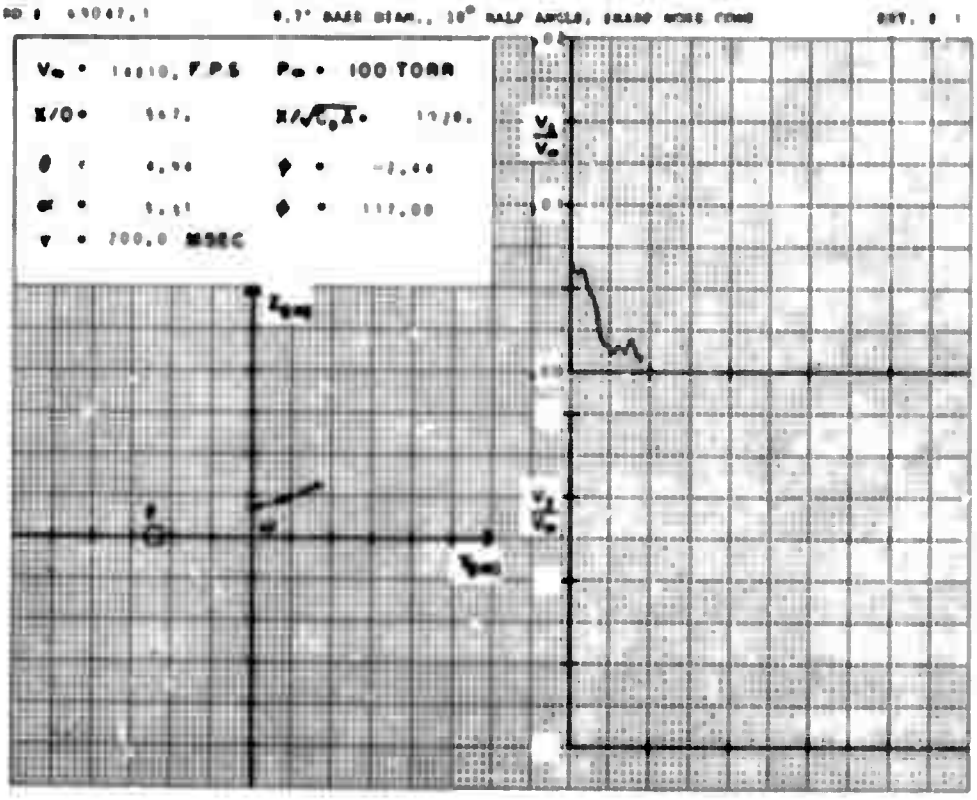

Figure 52

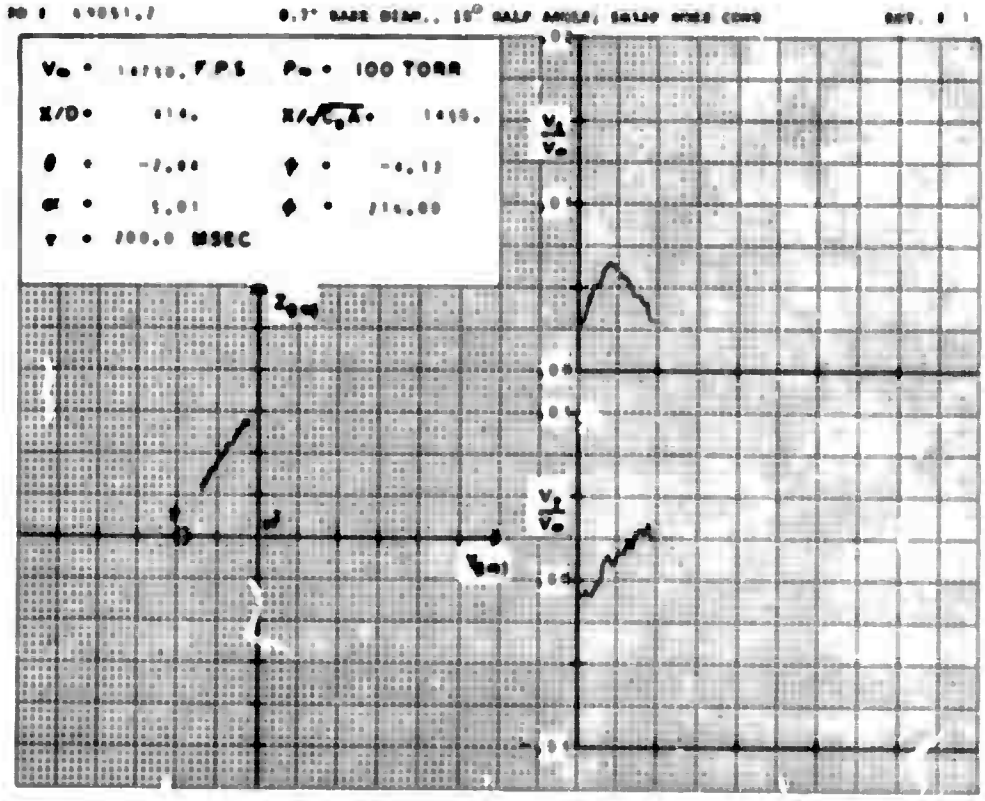

Figure 53

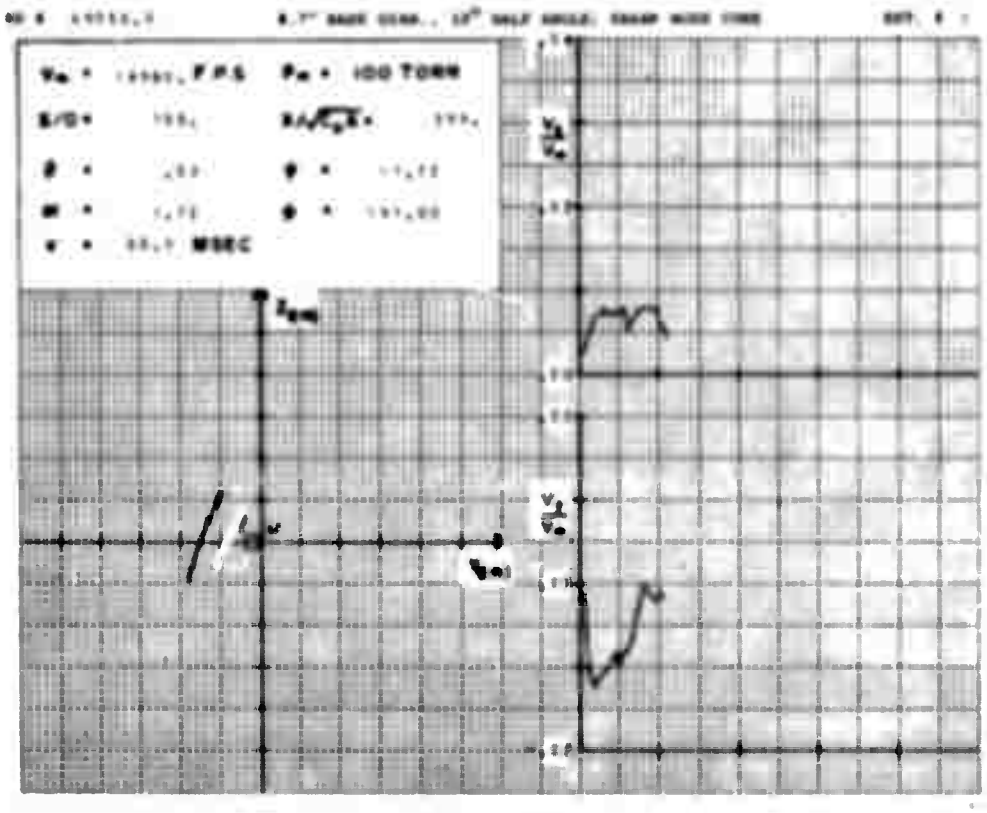

Figure 54

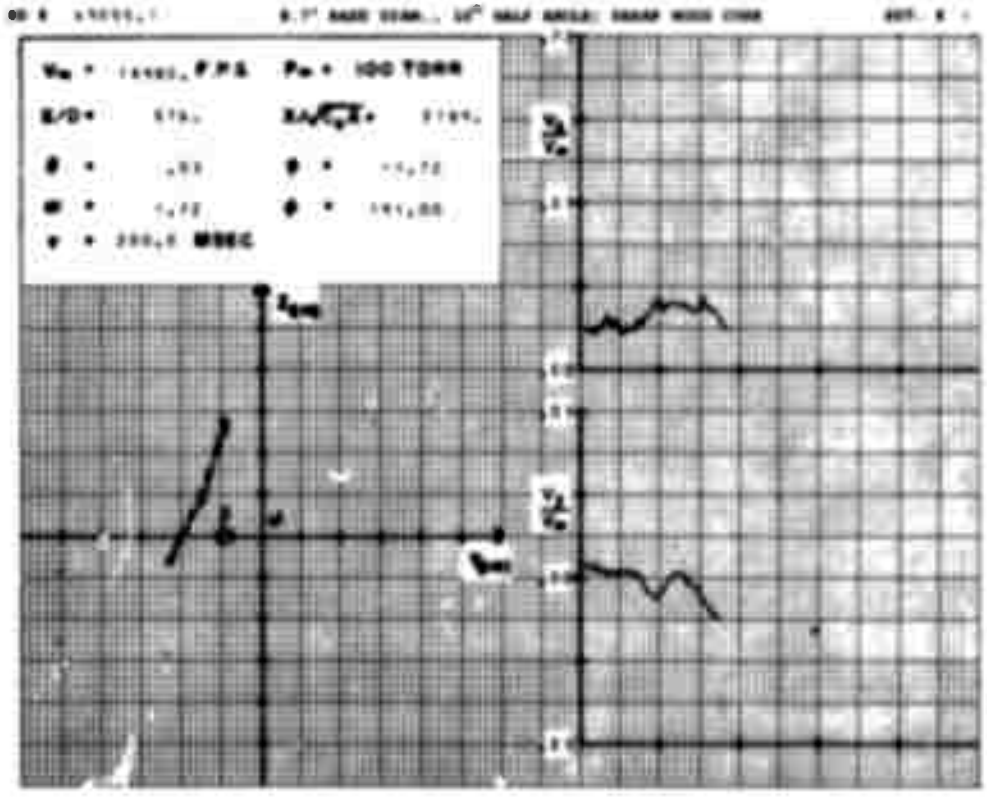

Figure 55

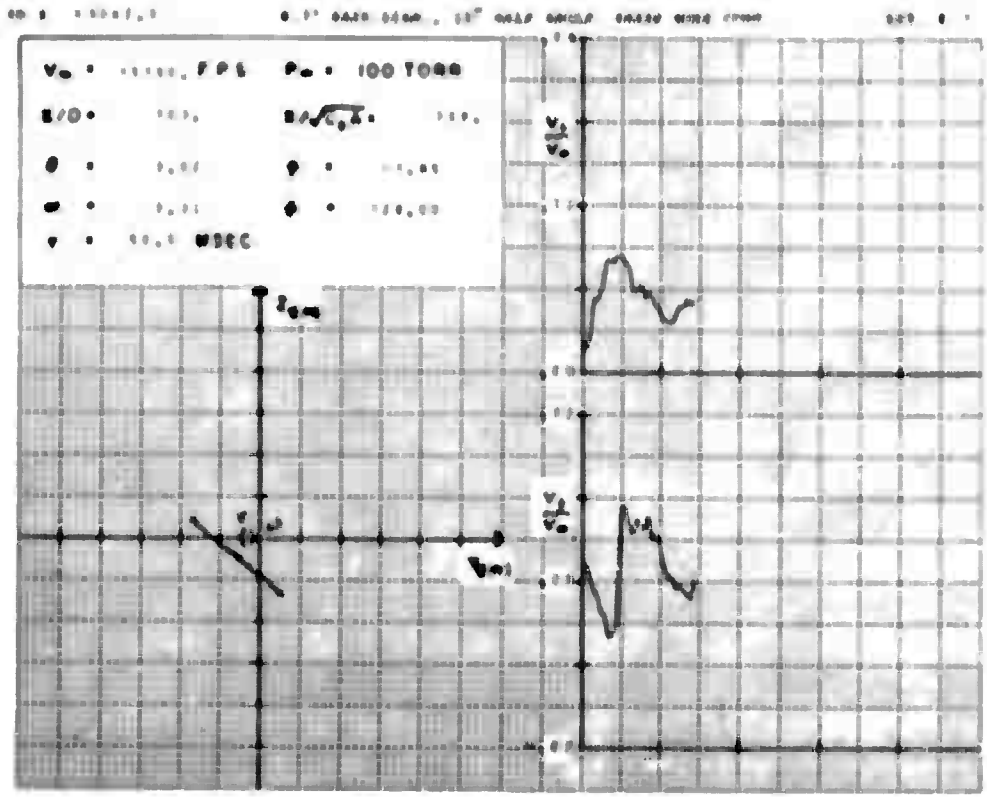

Figure 56

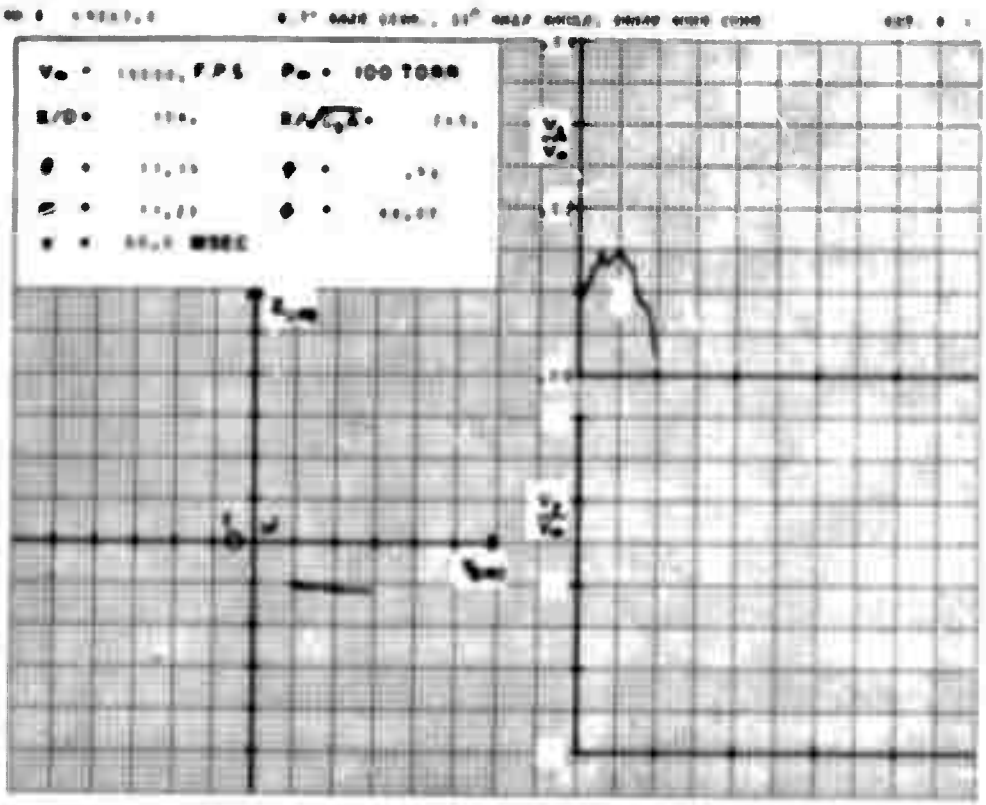

Figure 57

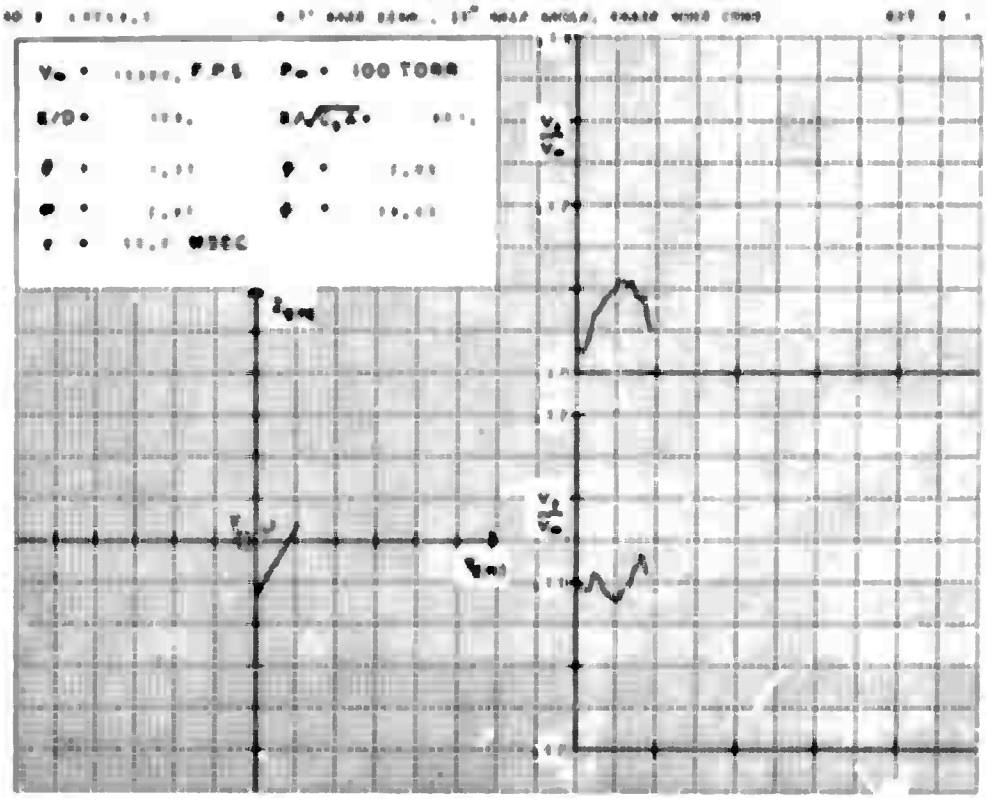

Figure 58

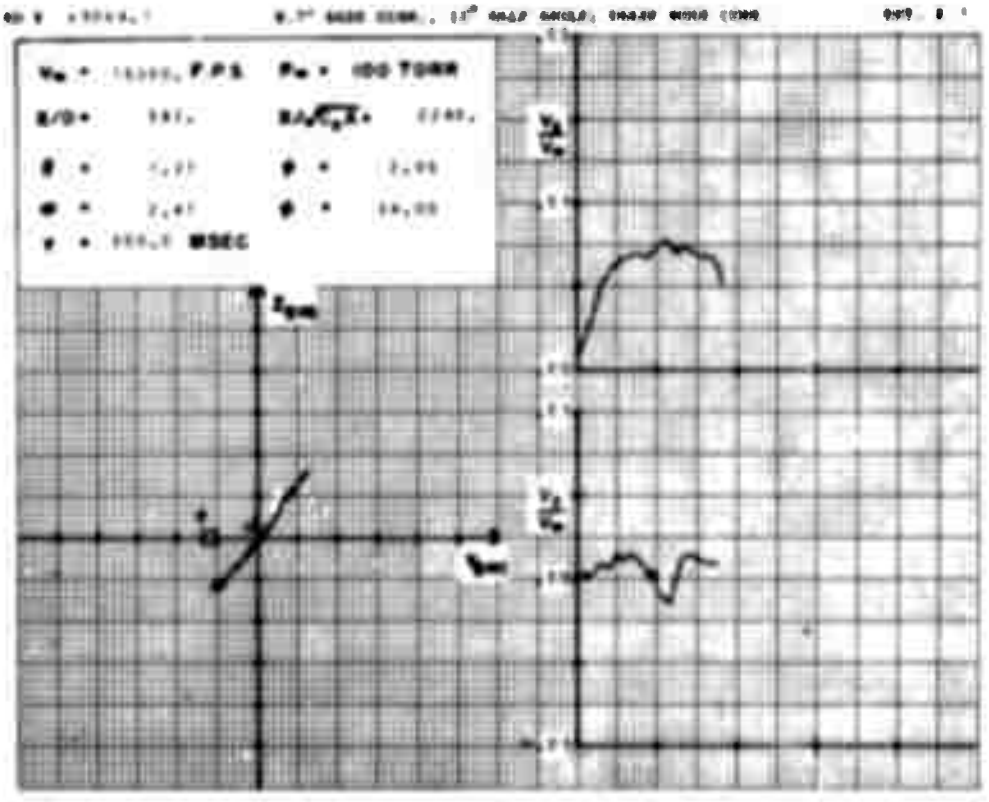

Figure 59

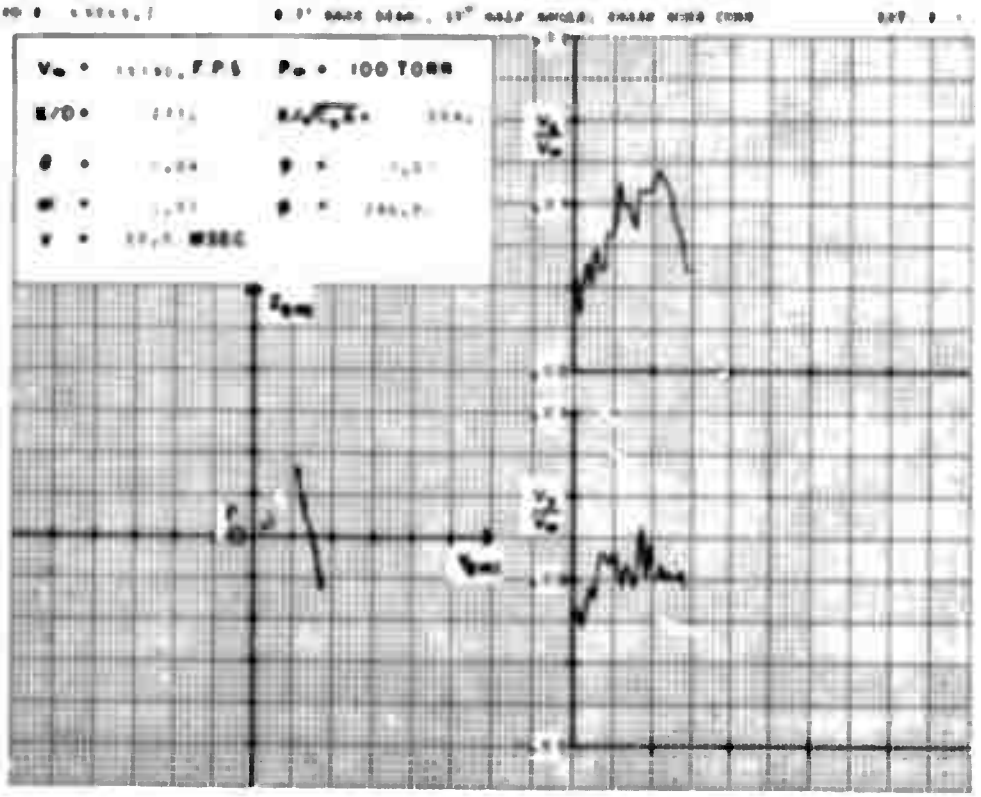

Figure 60

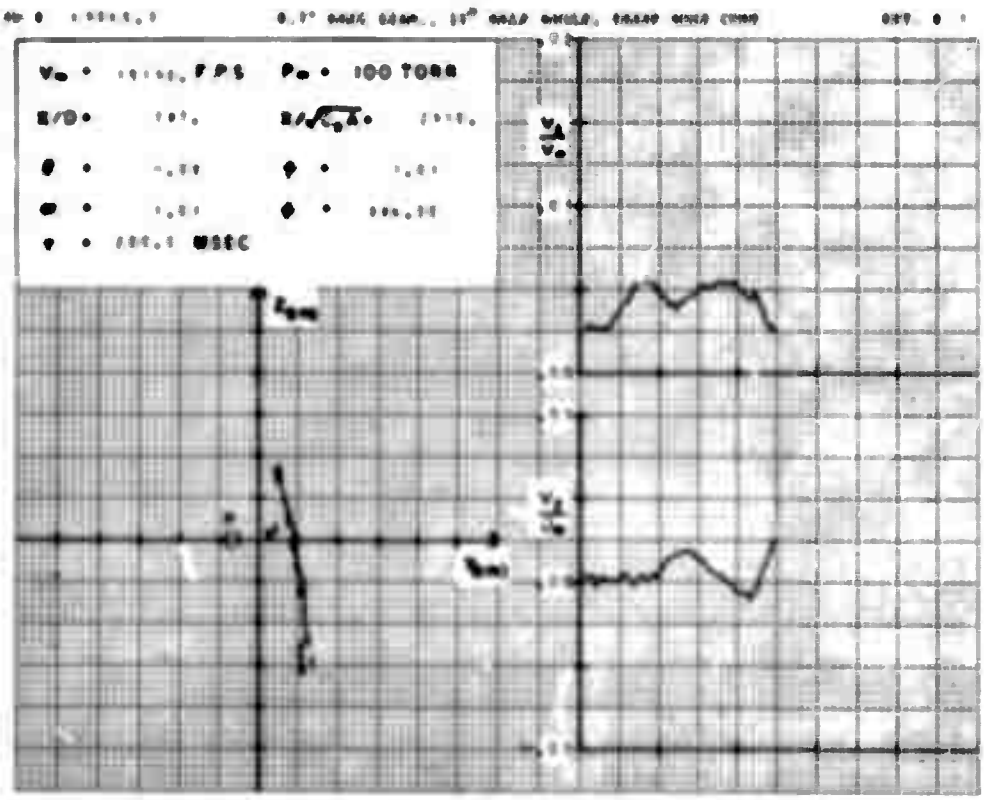

Figure 61

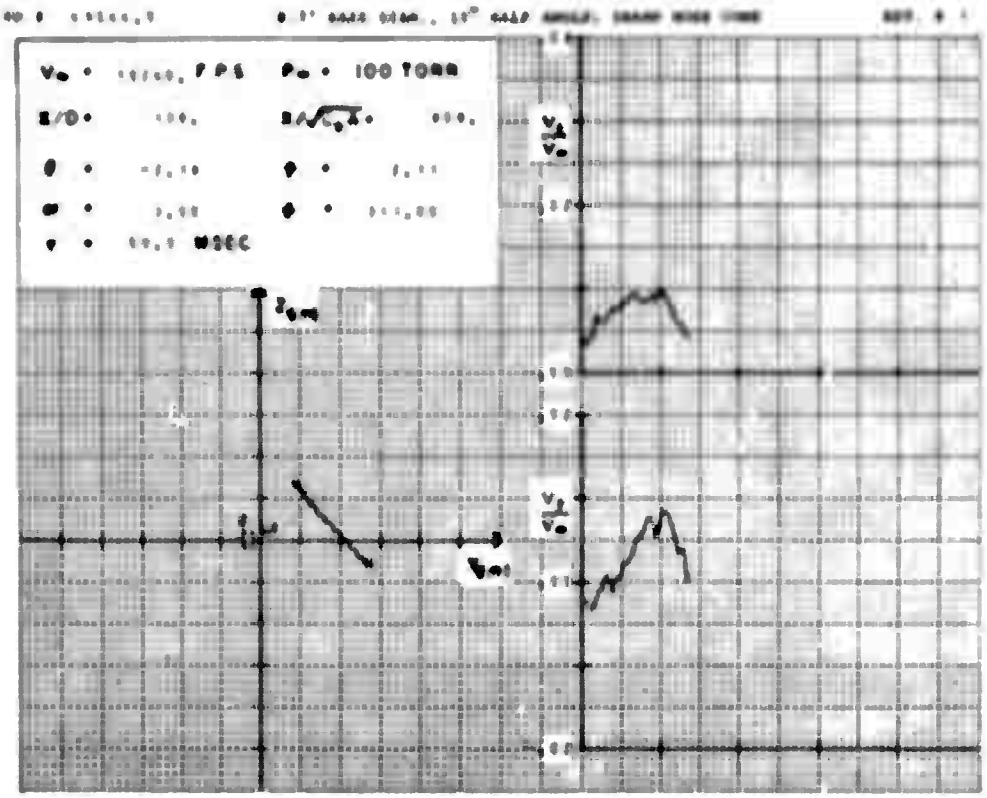

Figure 62

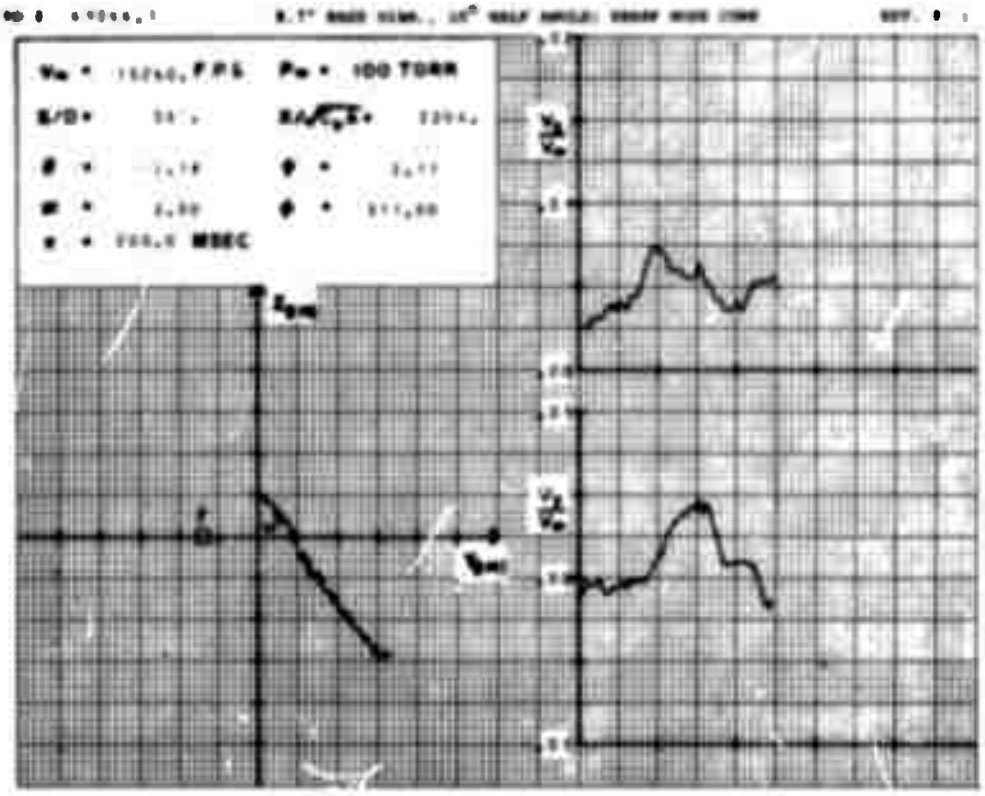

Figure 63

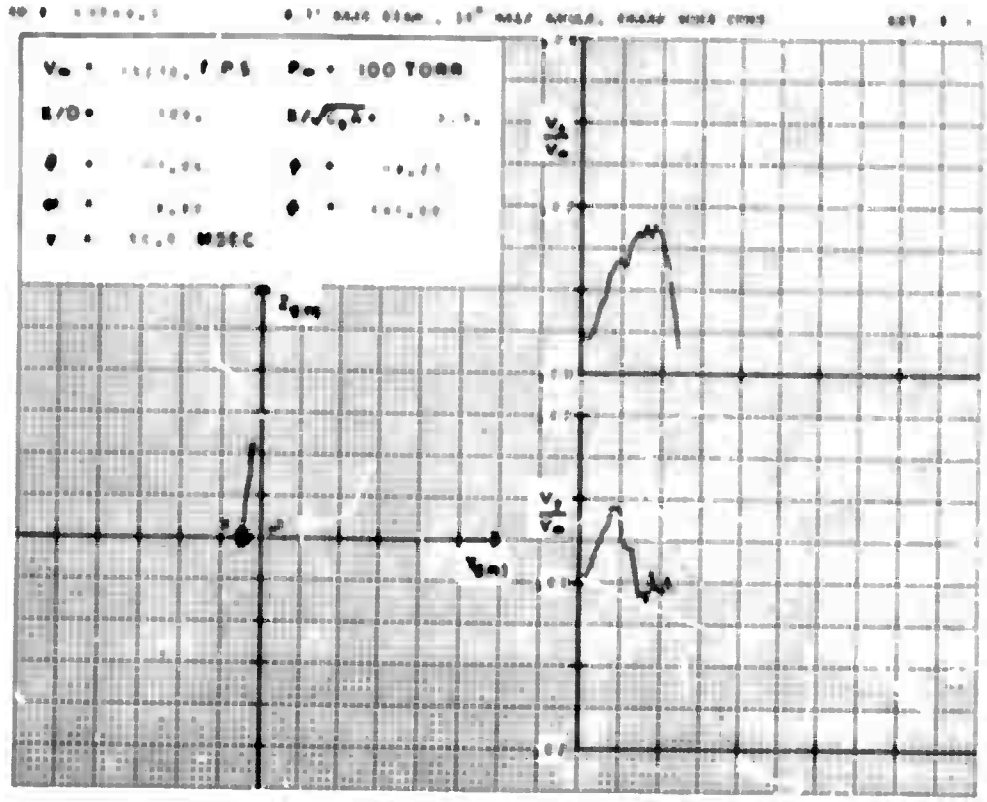

Figure 64

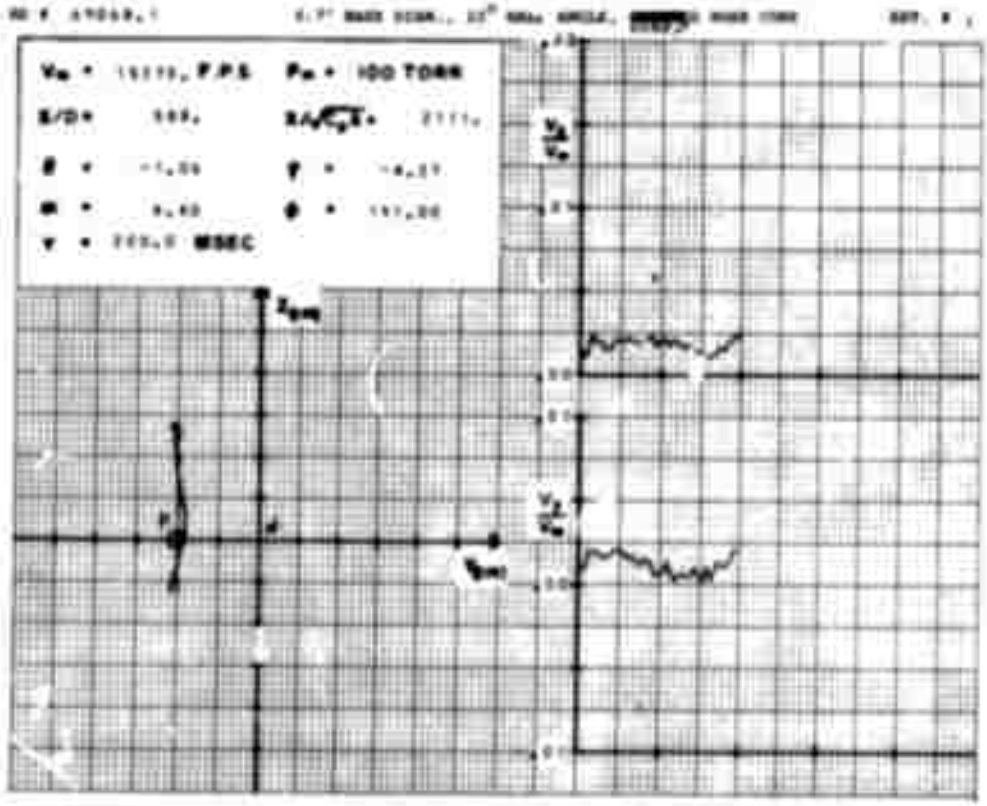

Figure 65

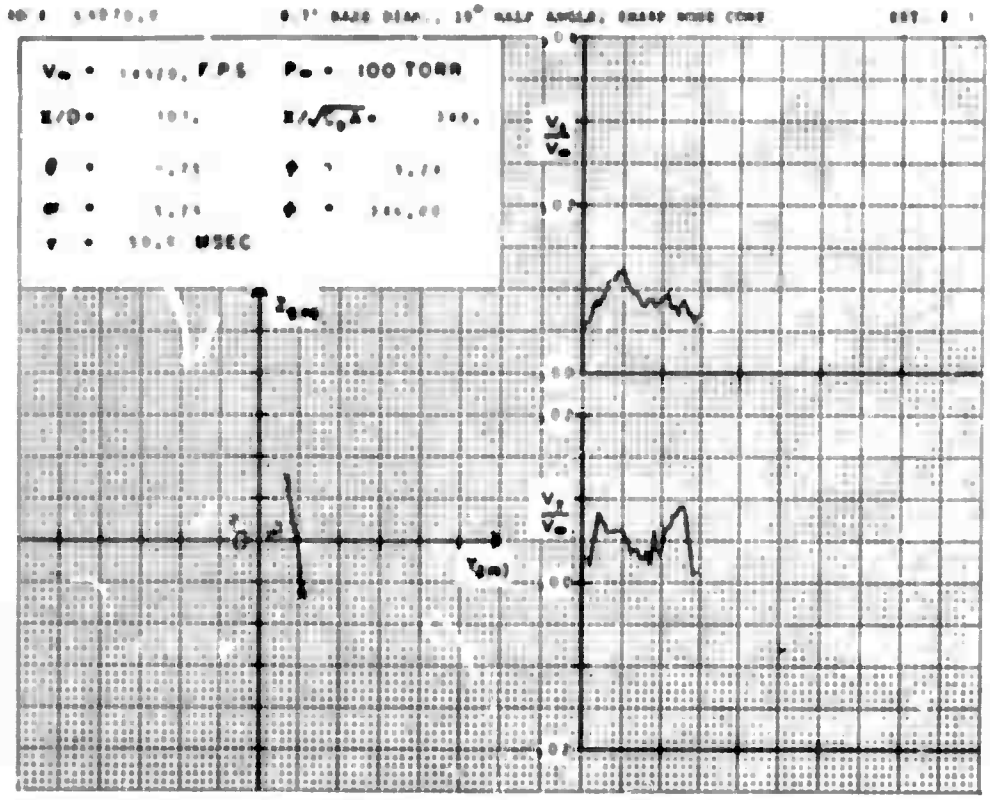

Figure 66

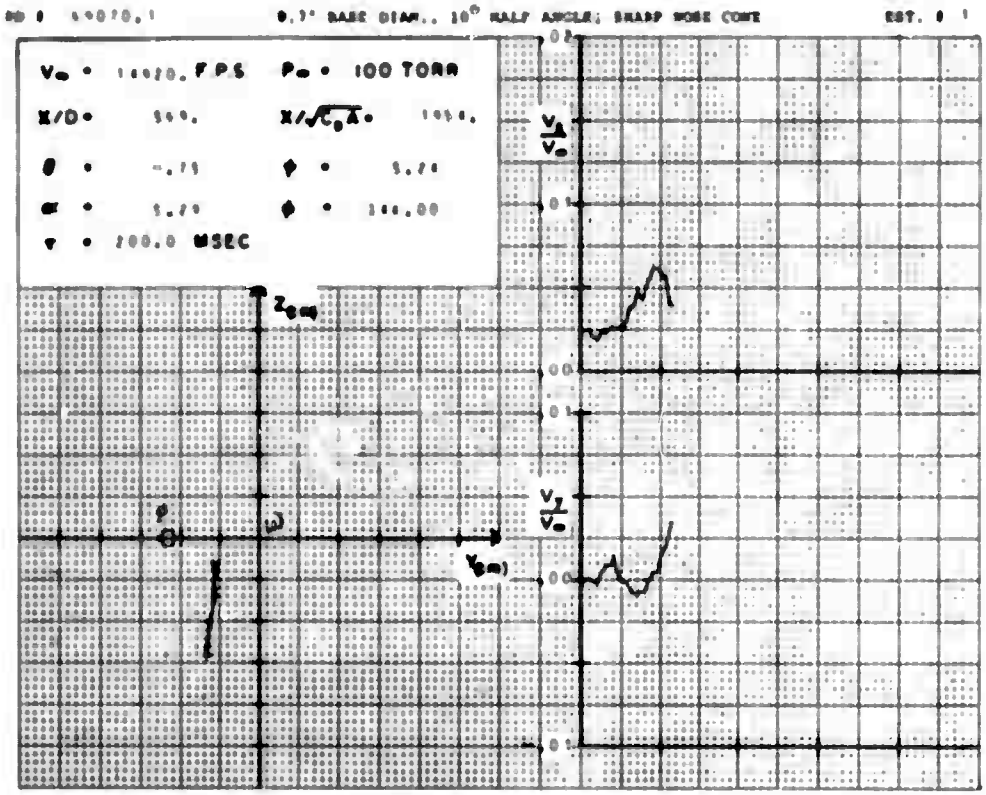

Figure 67

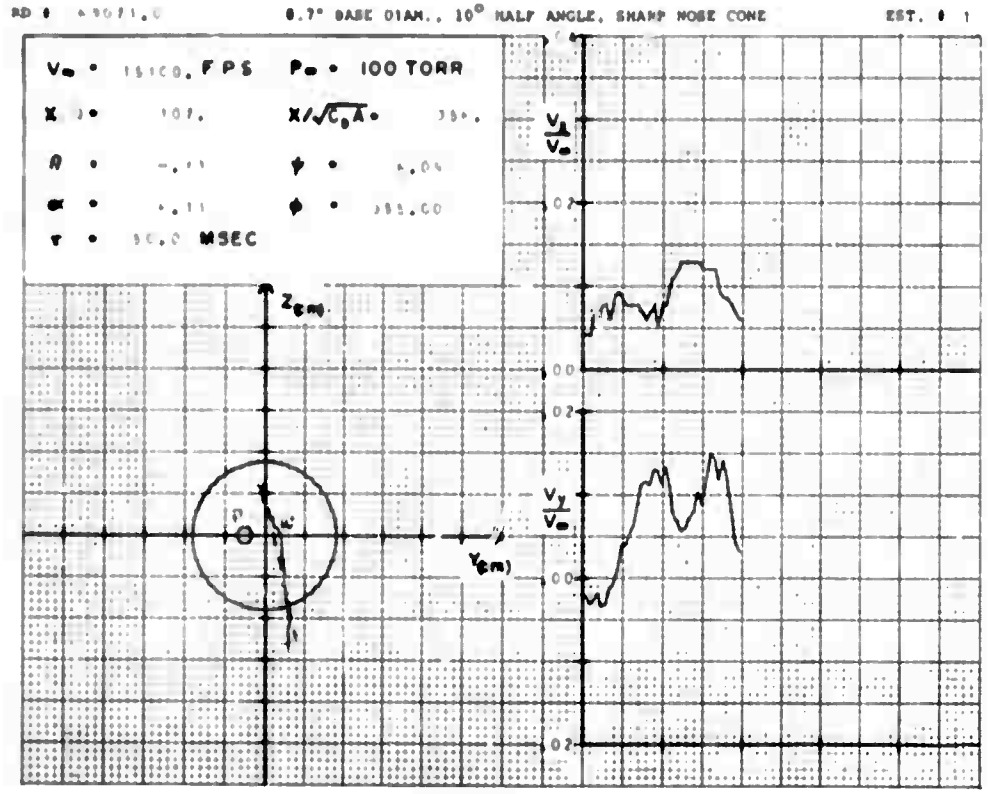

Figure 68

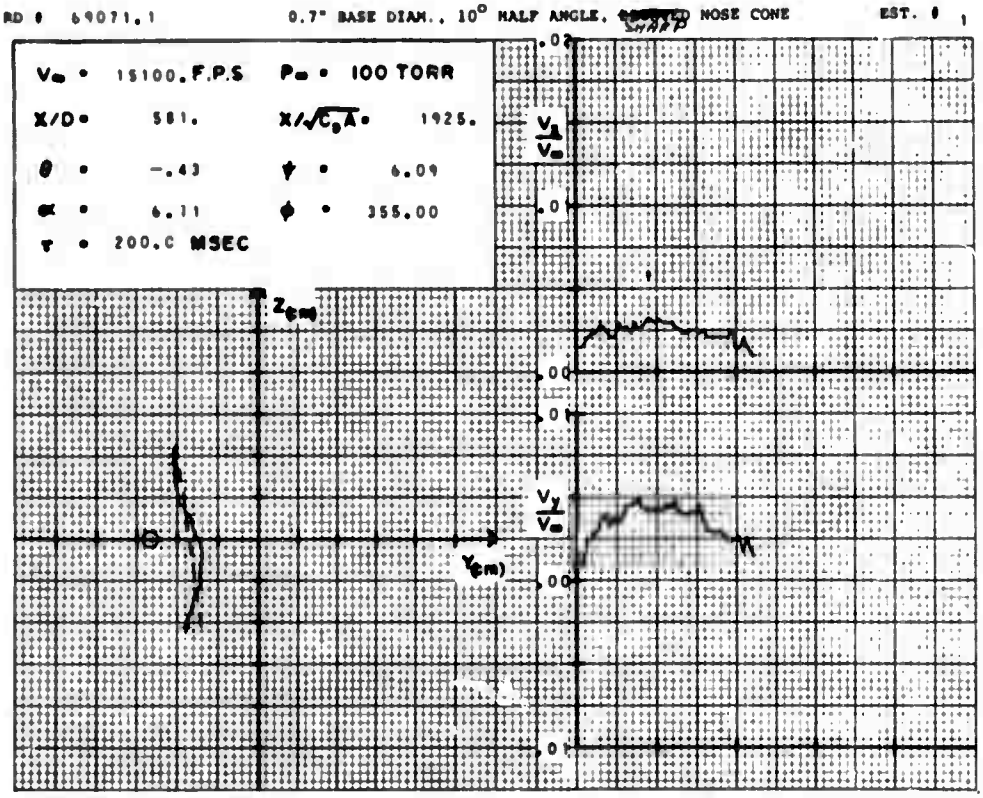

Figure 69

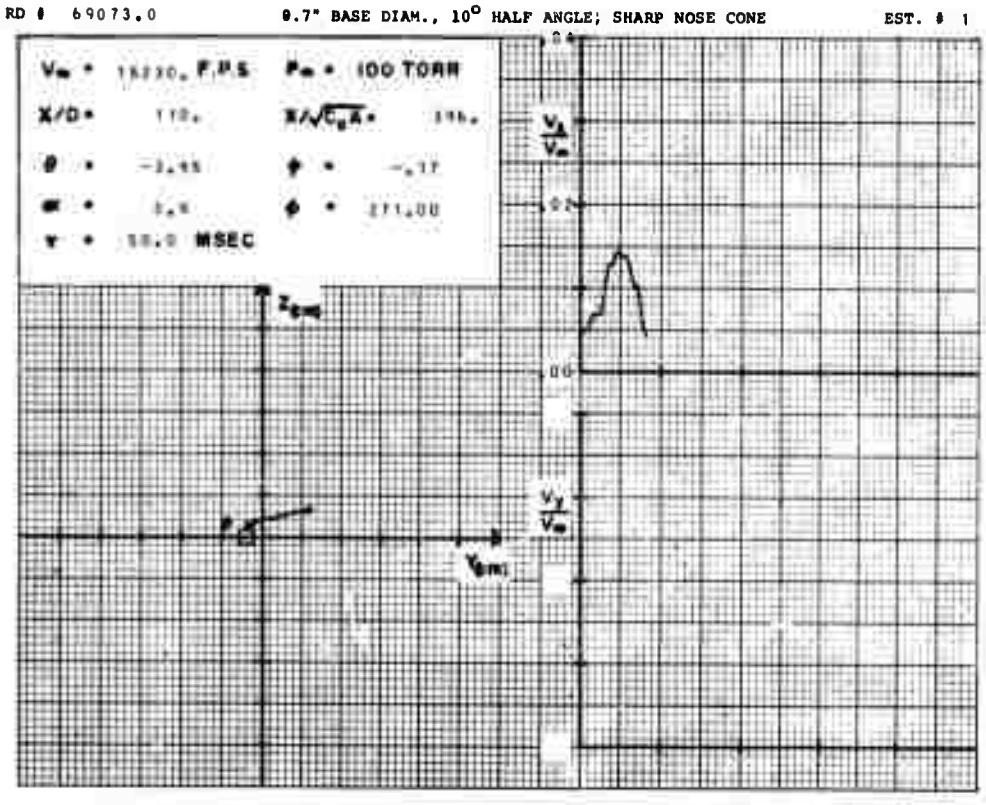

Figure 70

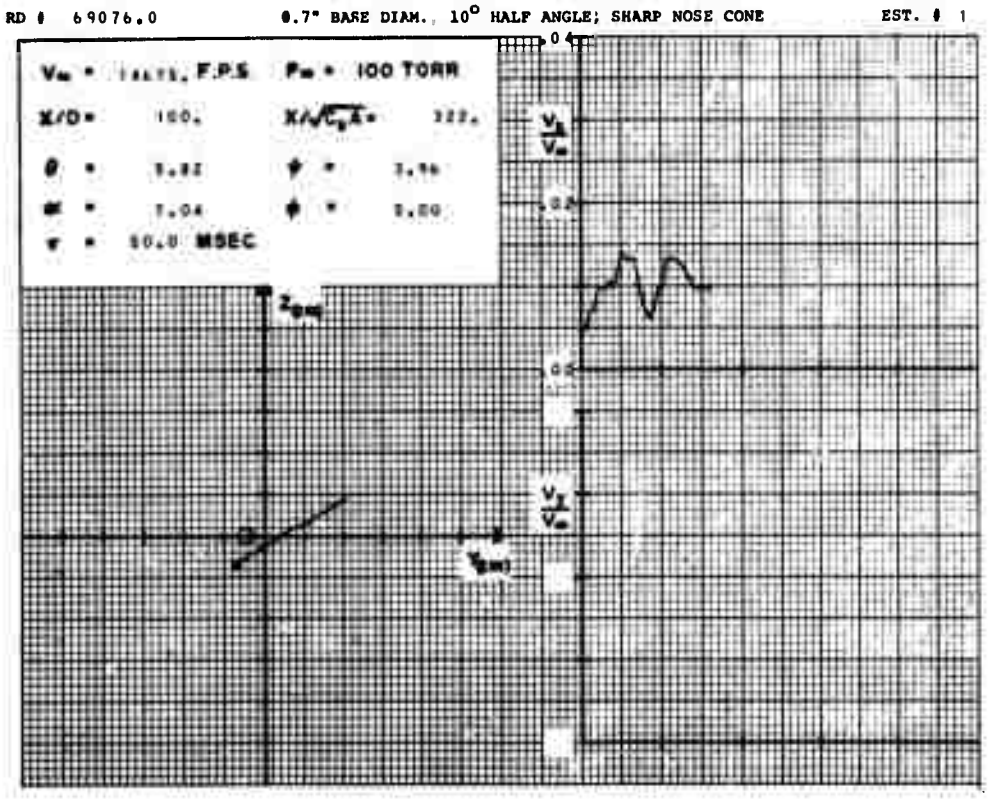

Figure 71

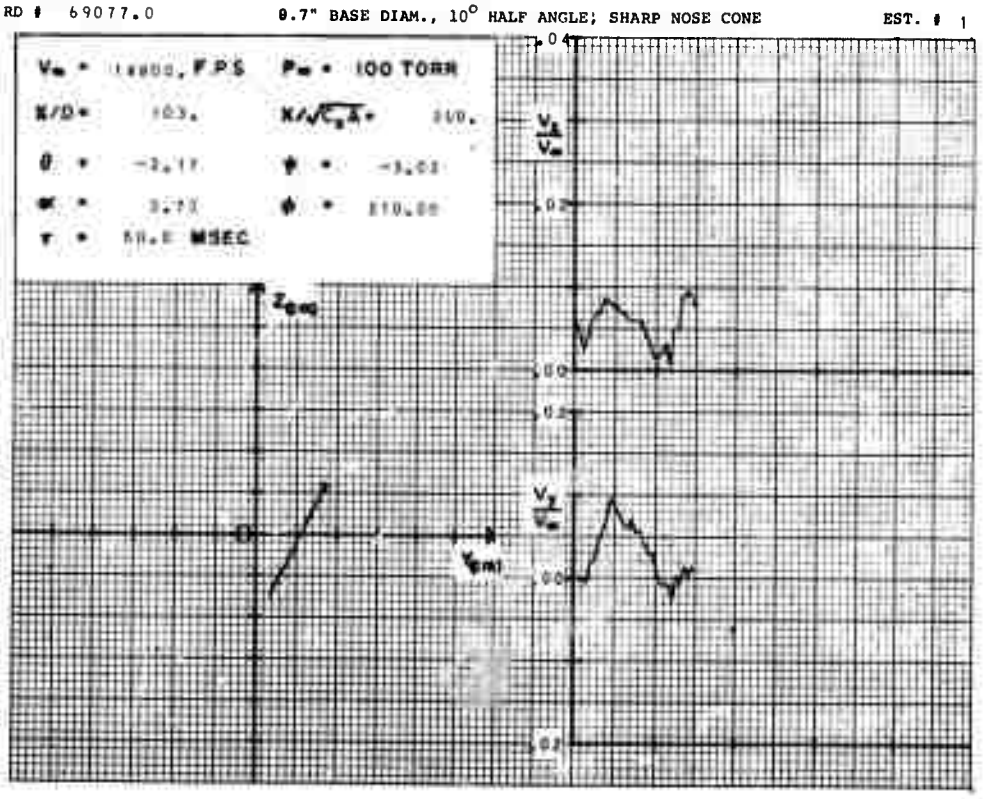

Figure 72

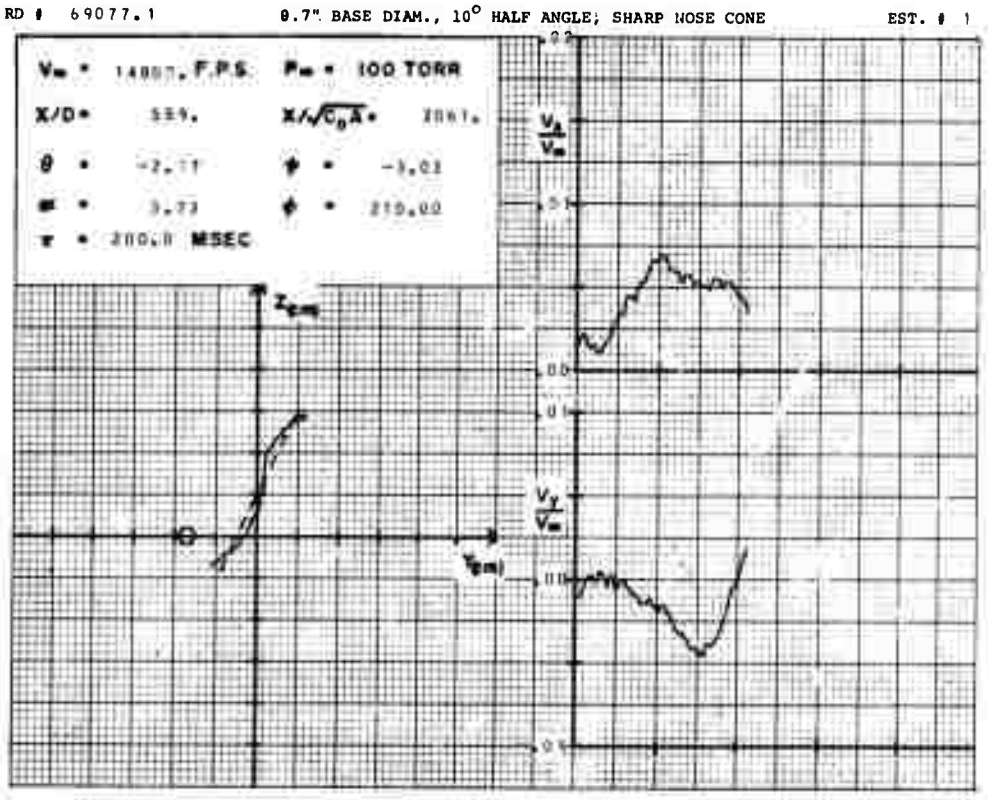

Figure 73

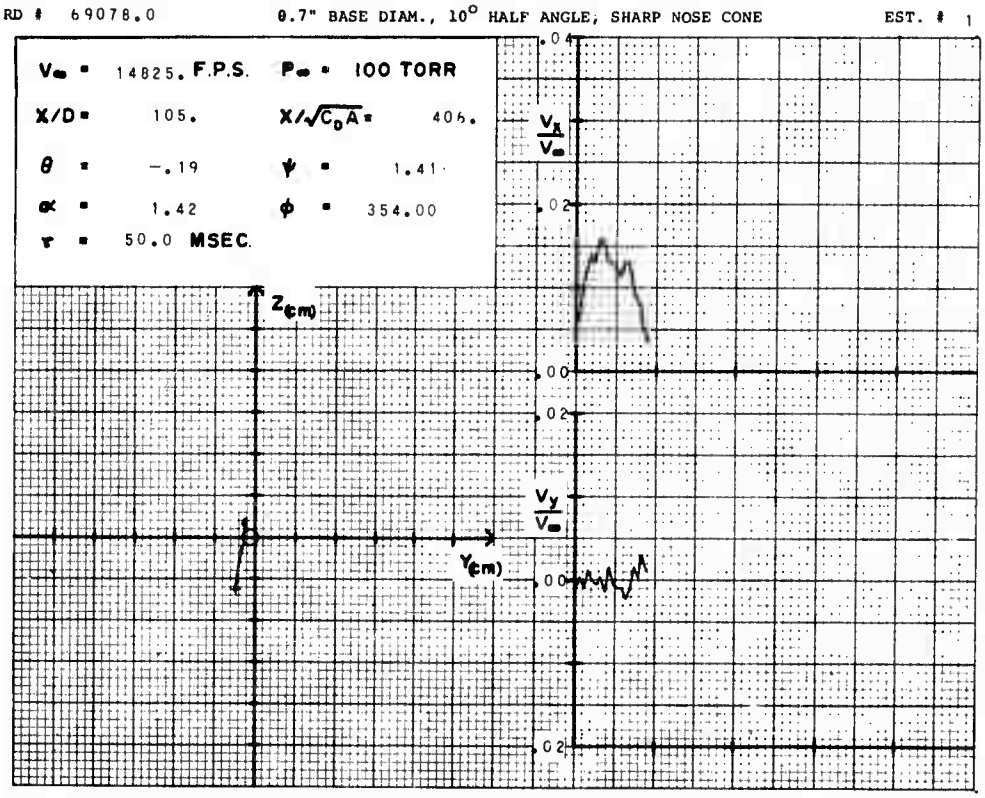

Figure 74

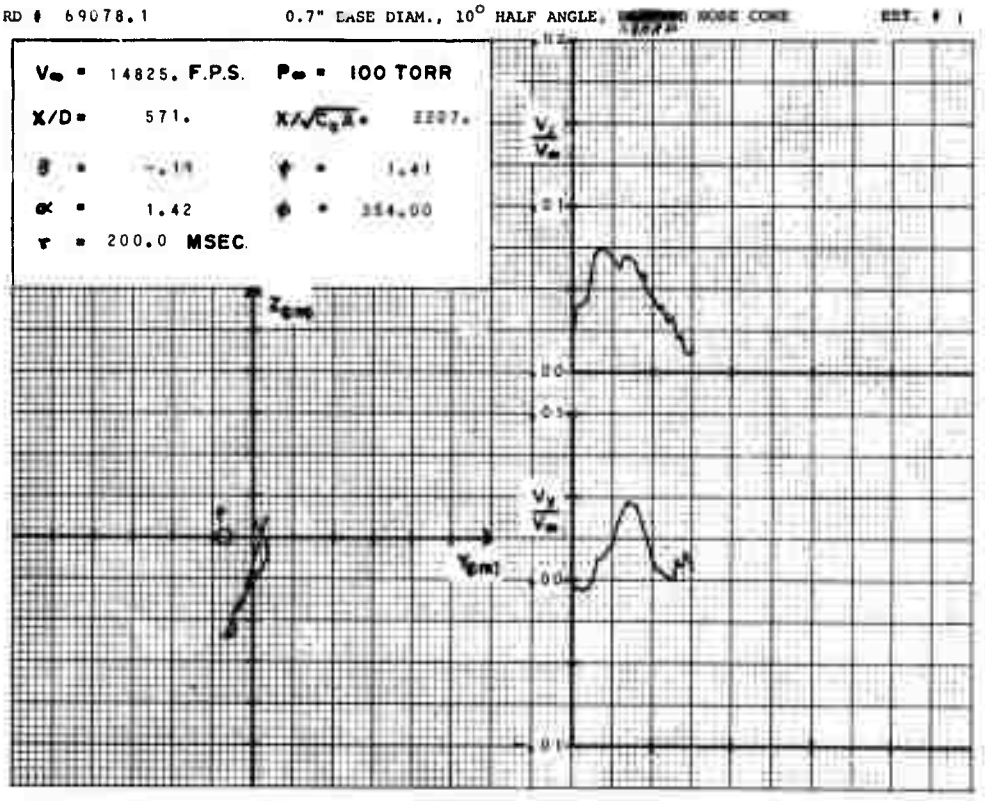

Figure 75

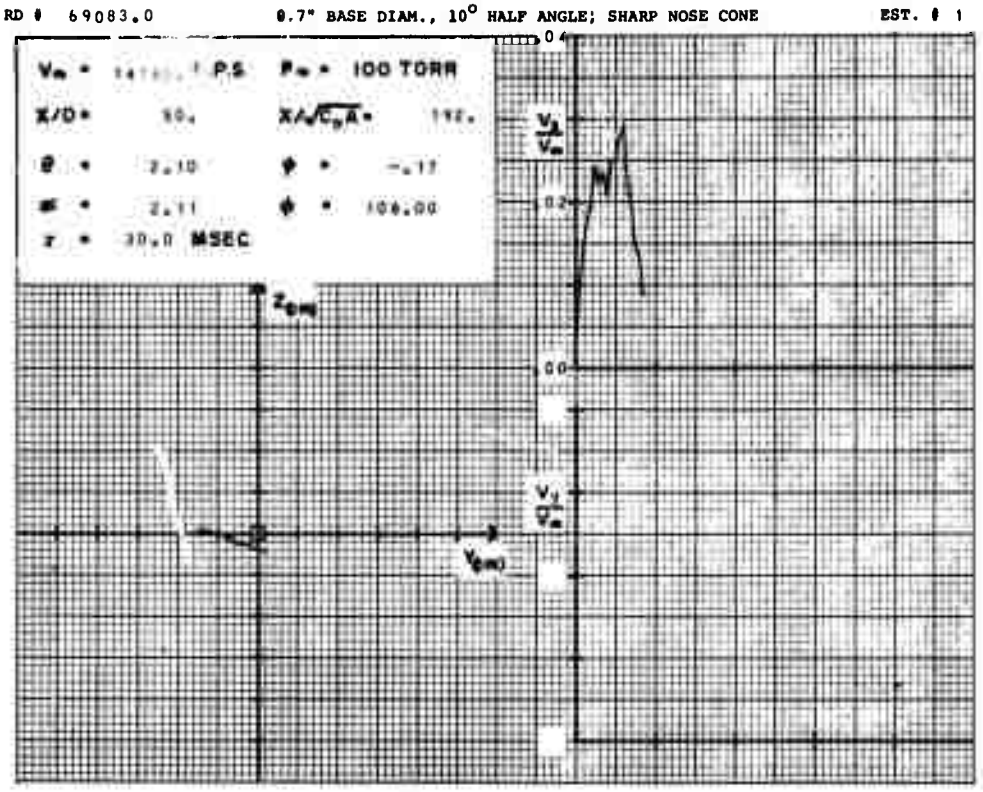

Figure 76

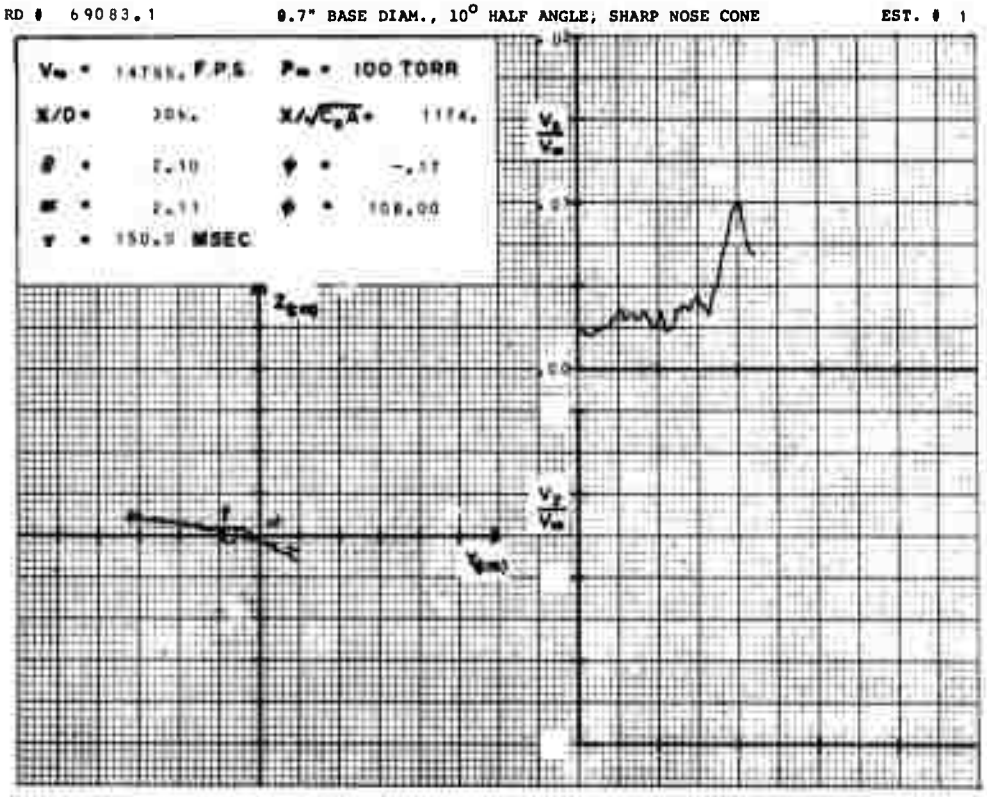

Figure 77

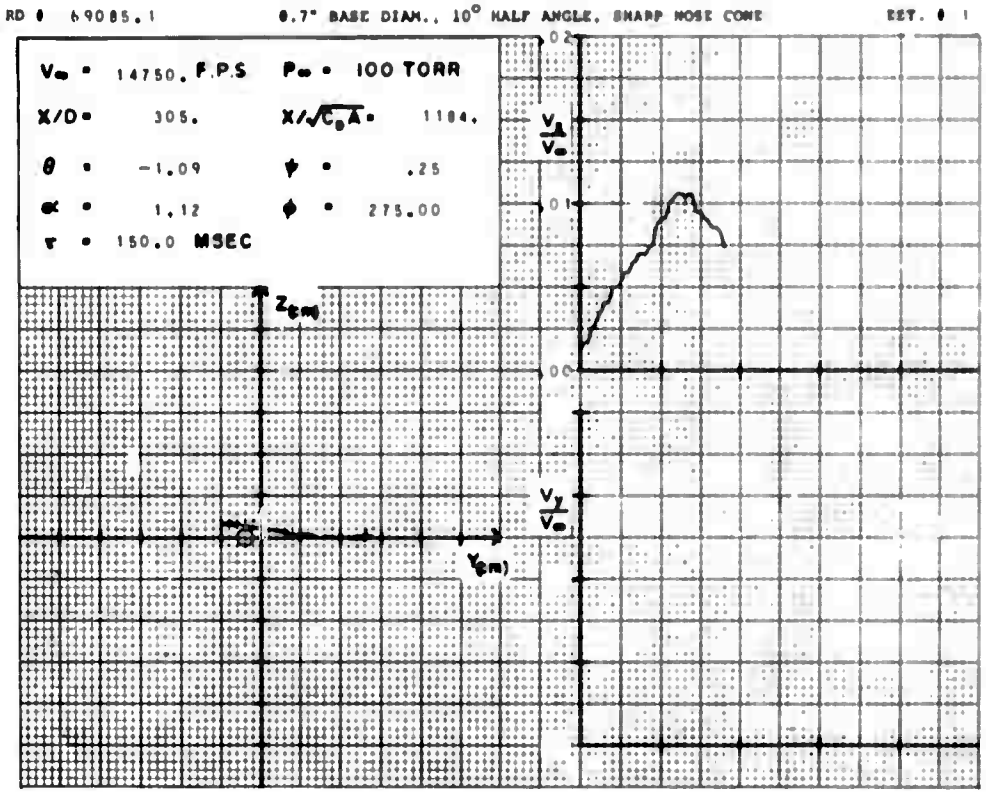

Figure 78

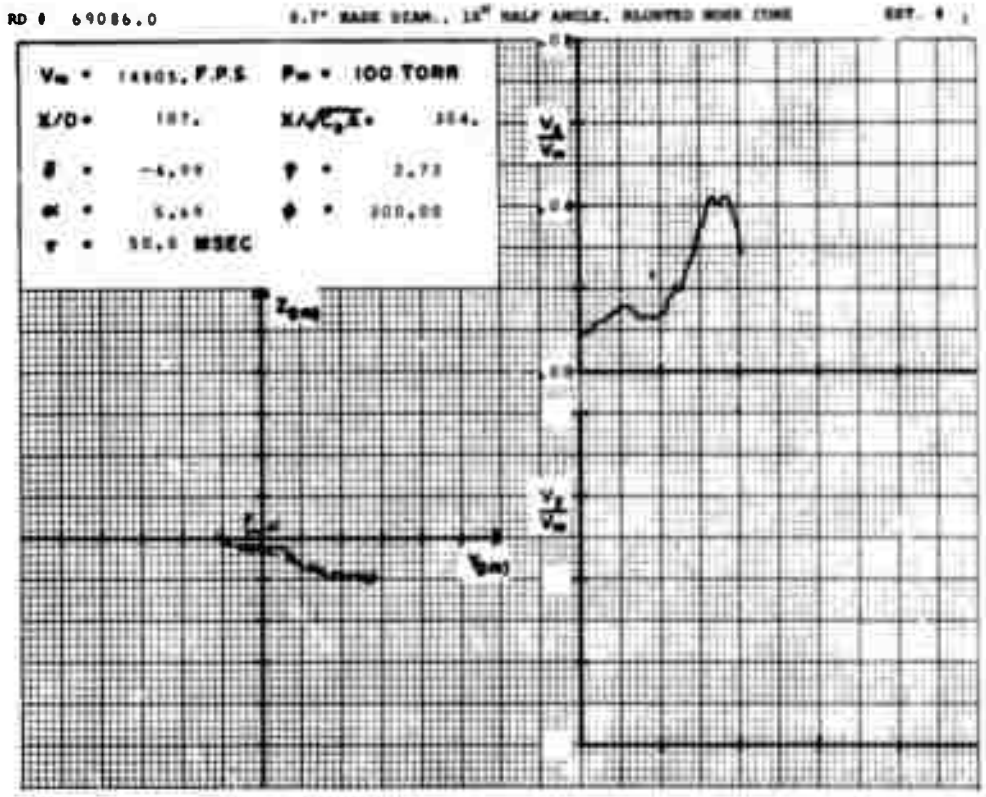

Figure 79

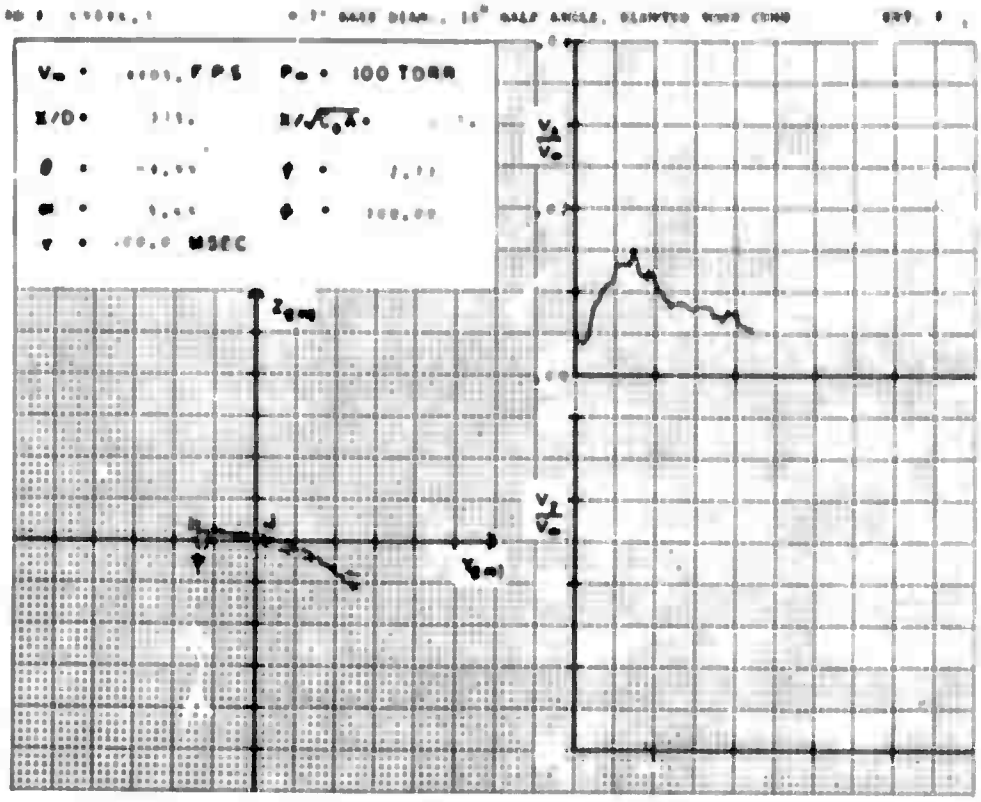

Figure 80

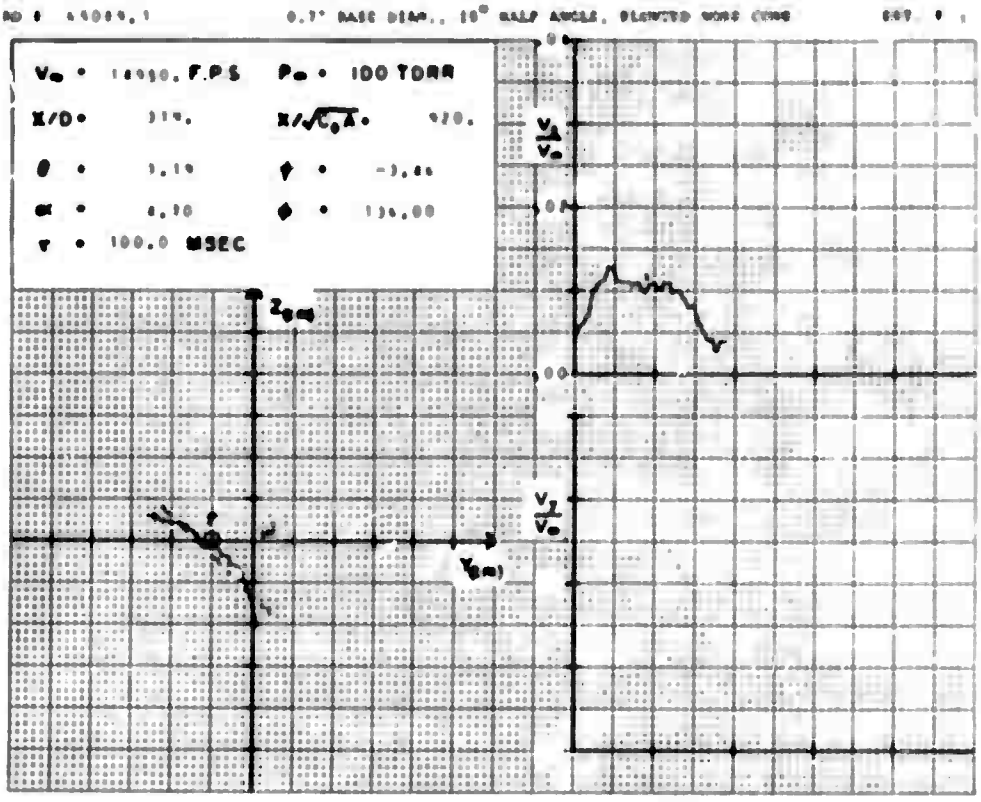

Figure 81

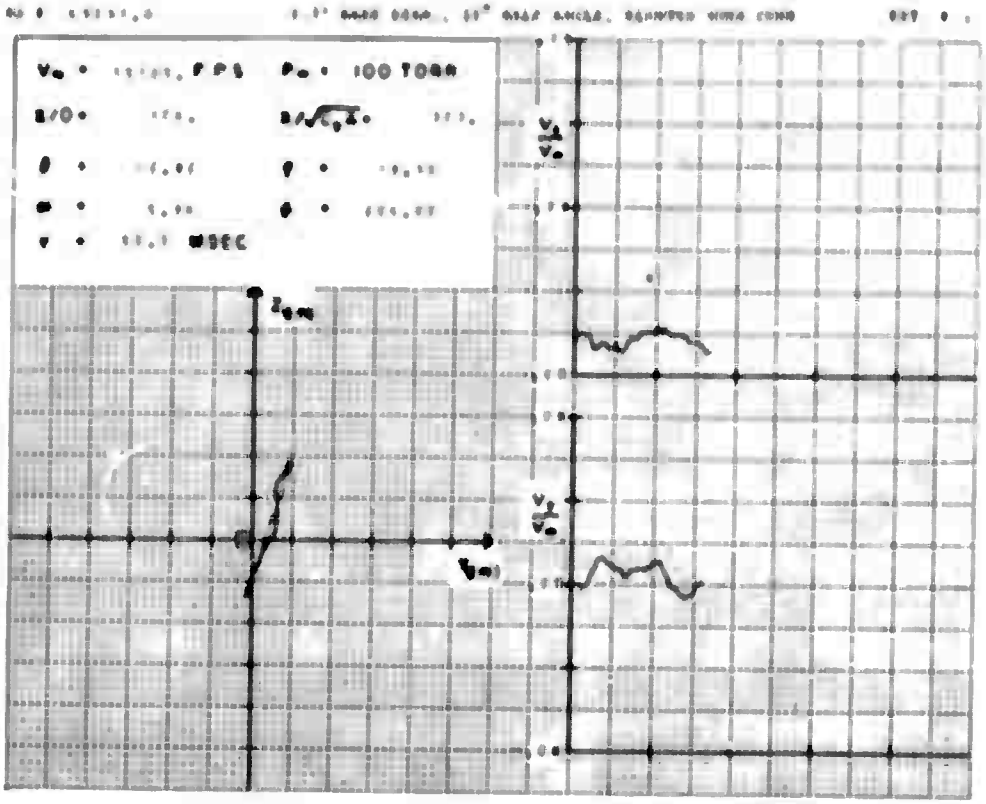

Figure 82

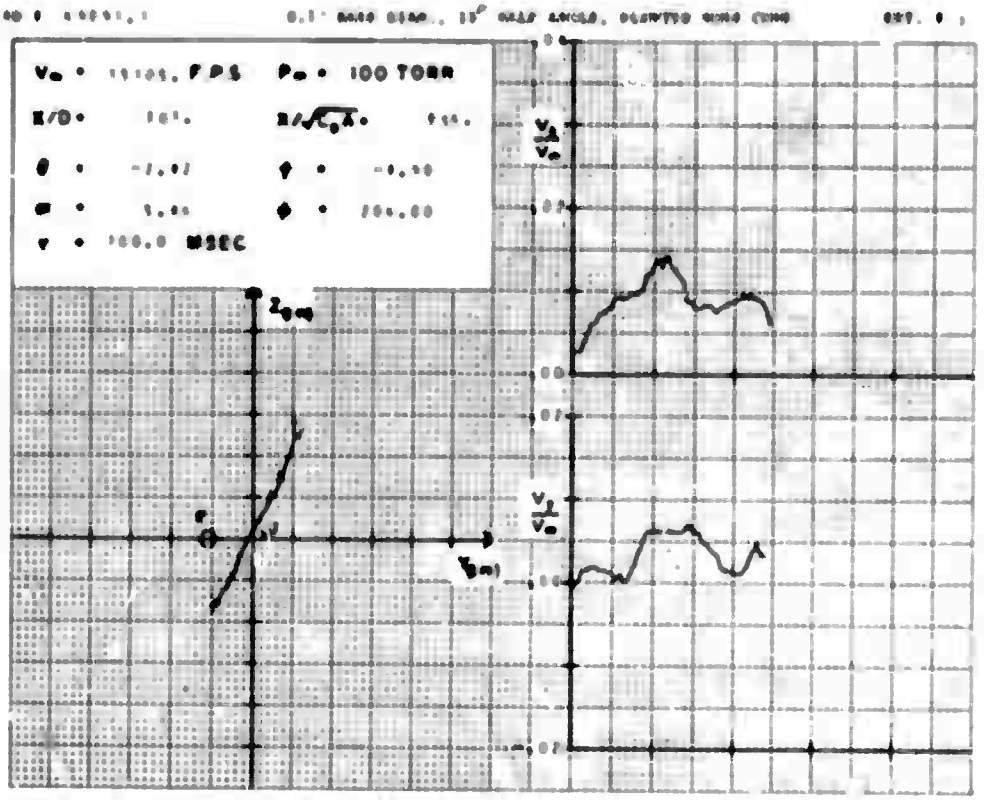

Figure 83

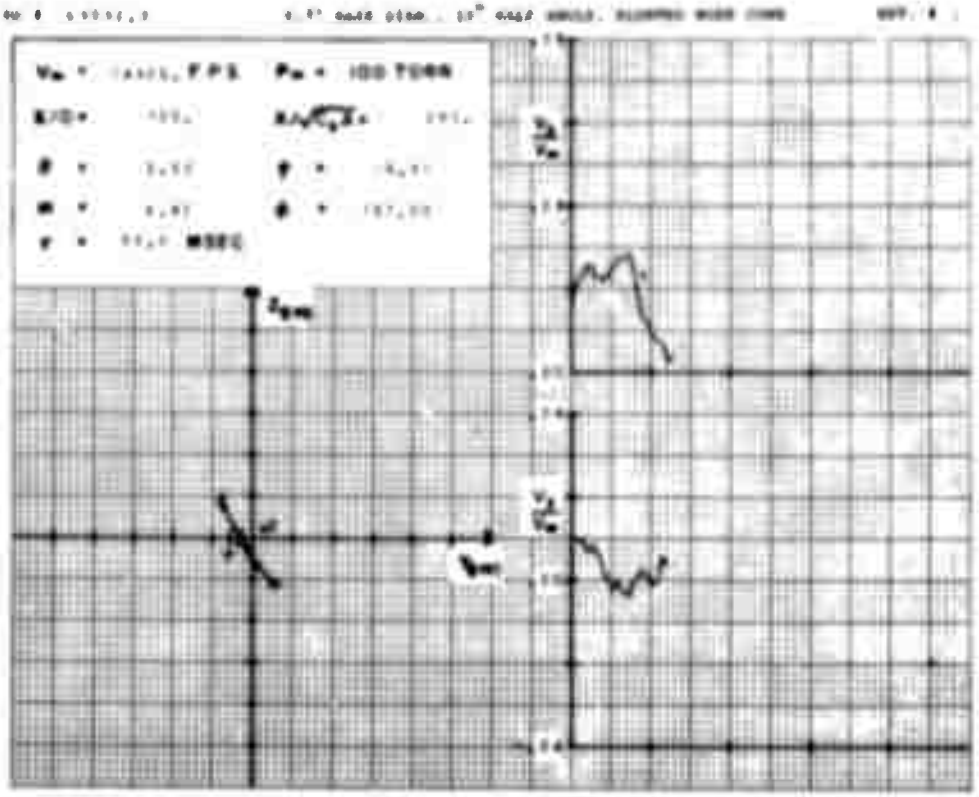

Figure 84

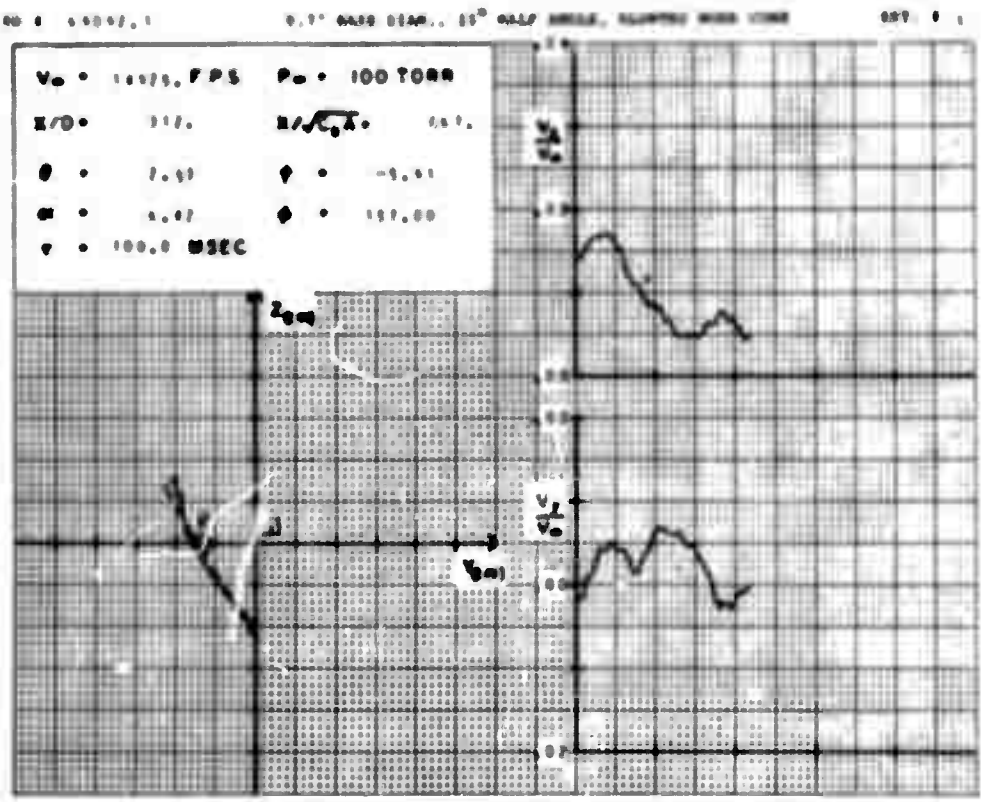

Figure 85

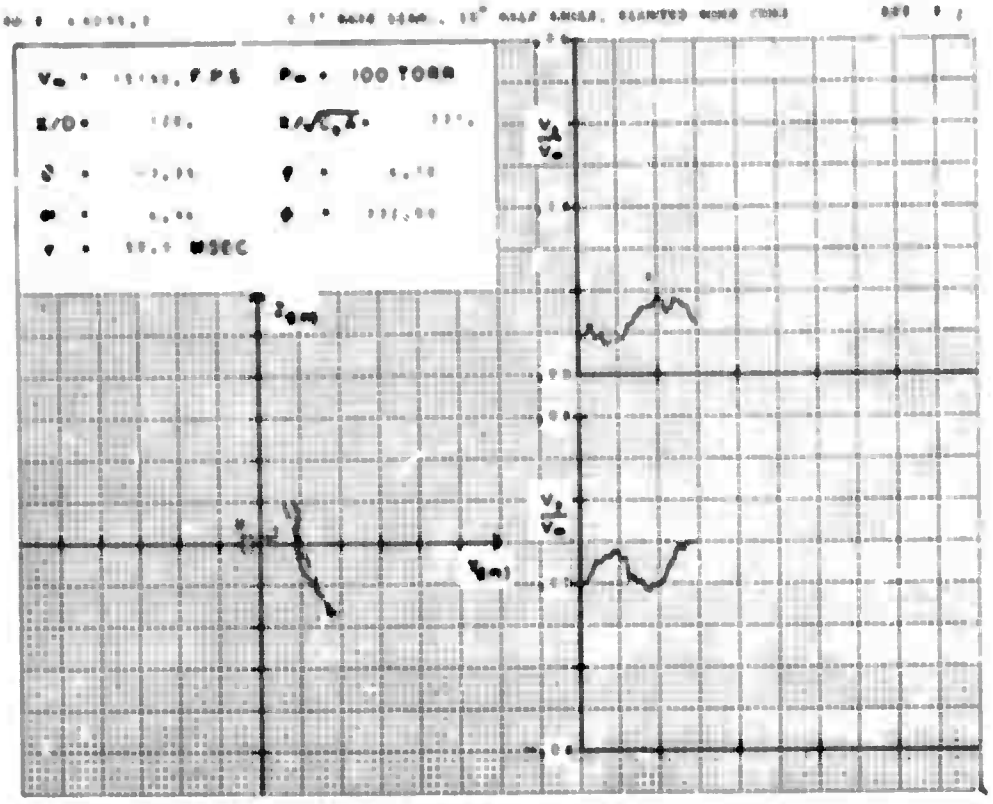

Figure 86

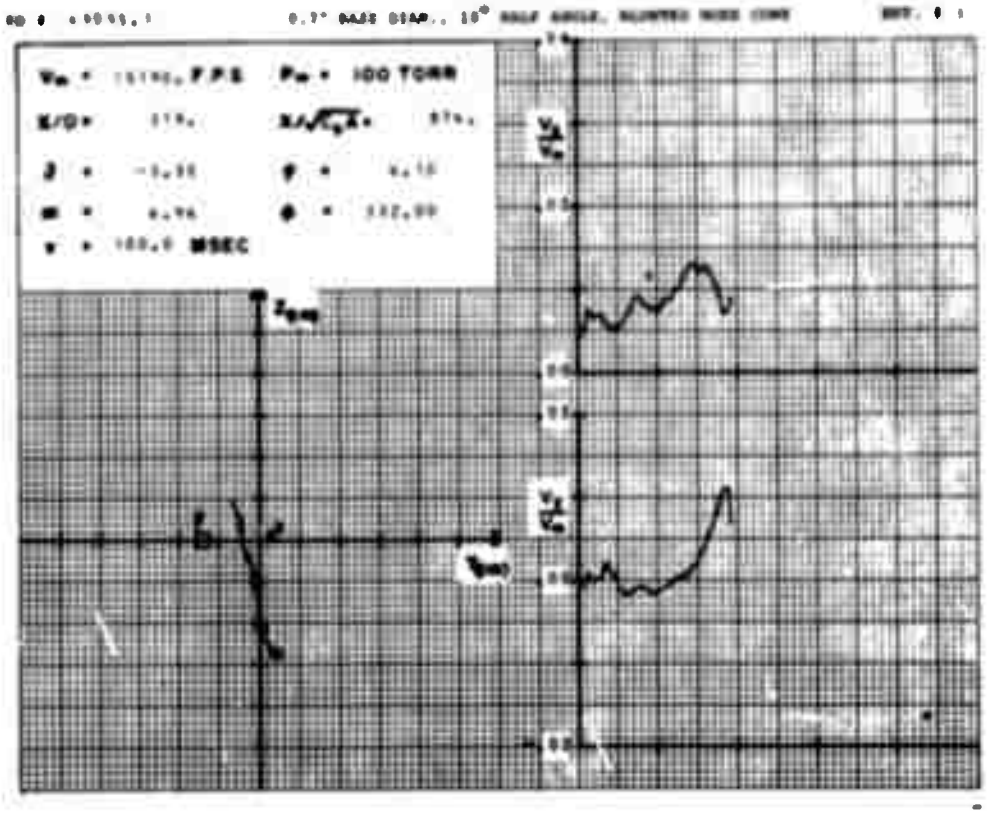

Figure 87

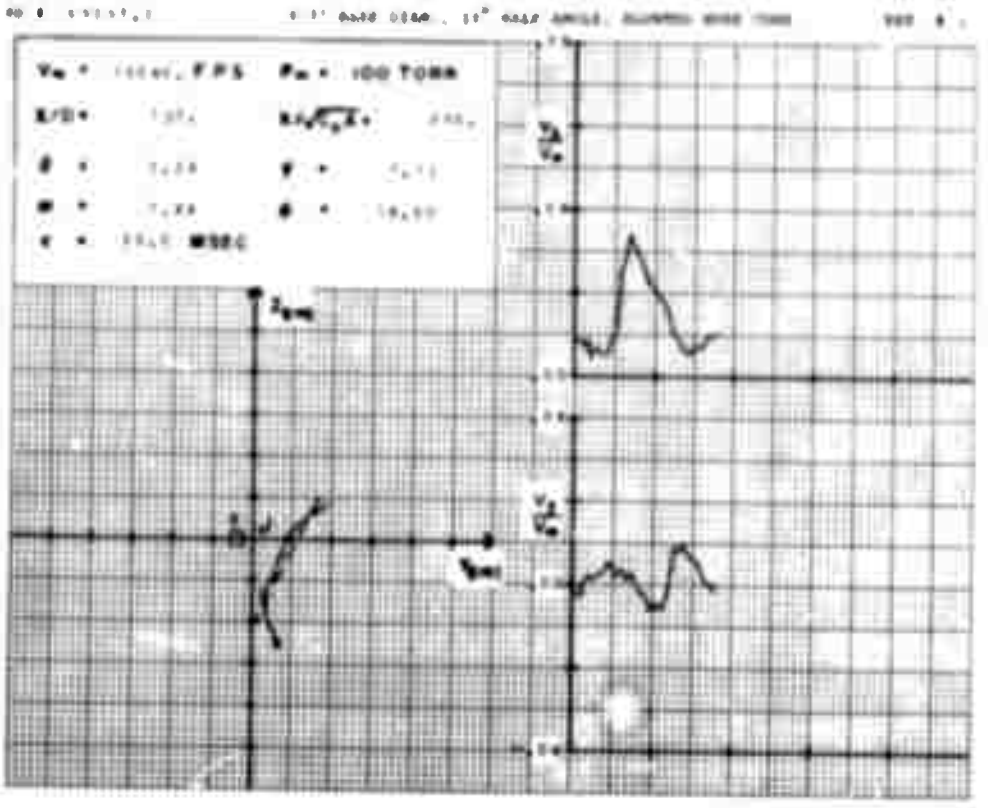

Figure 88

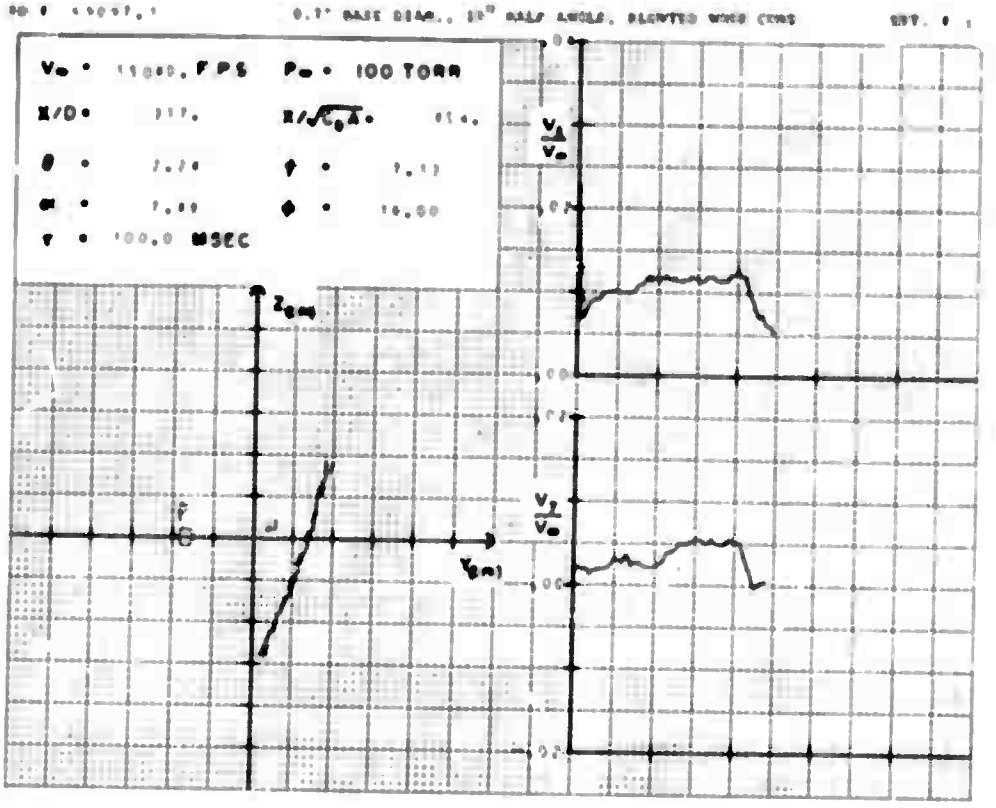

Figure 89

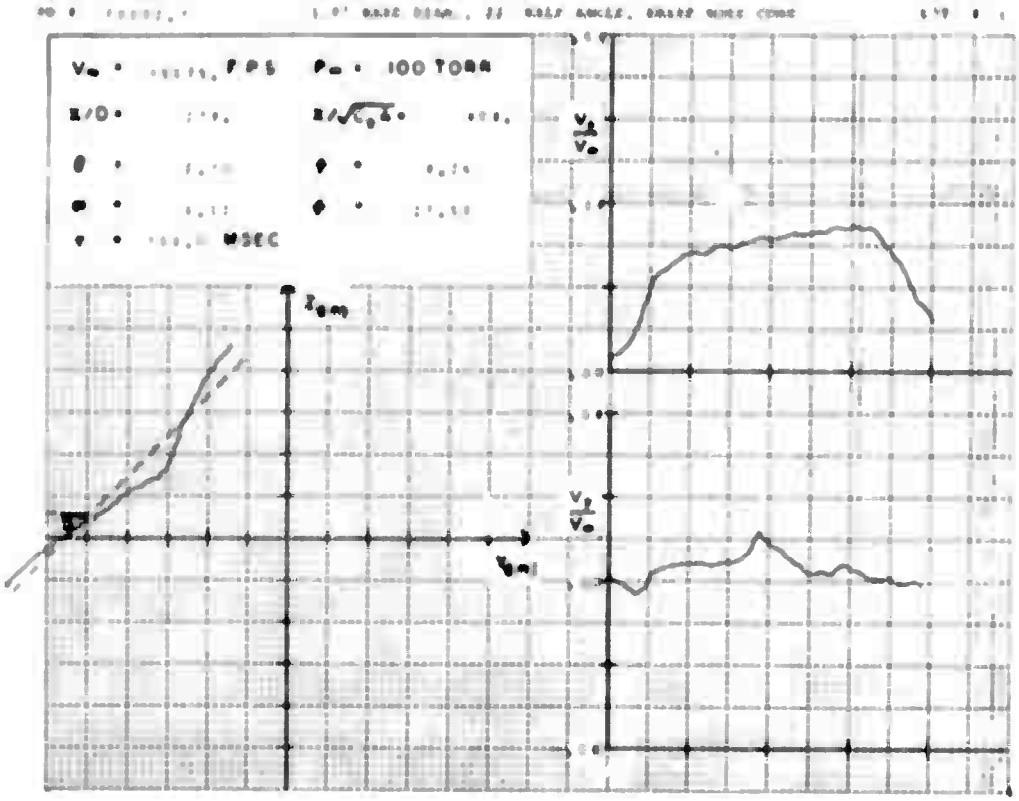

Figure 90

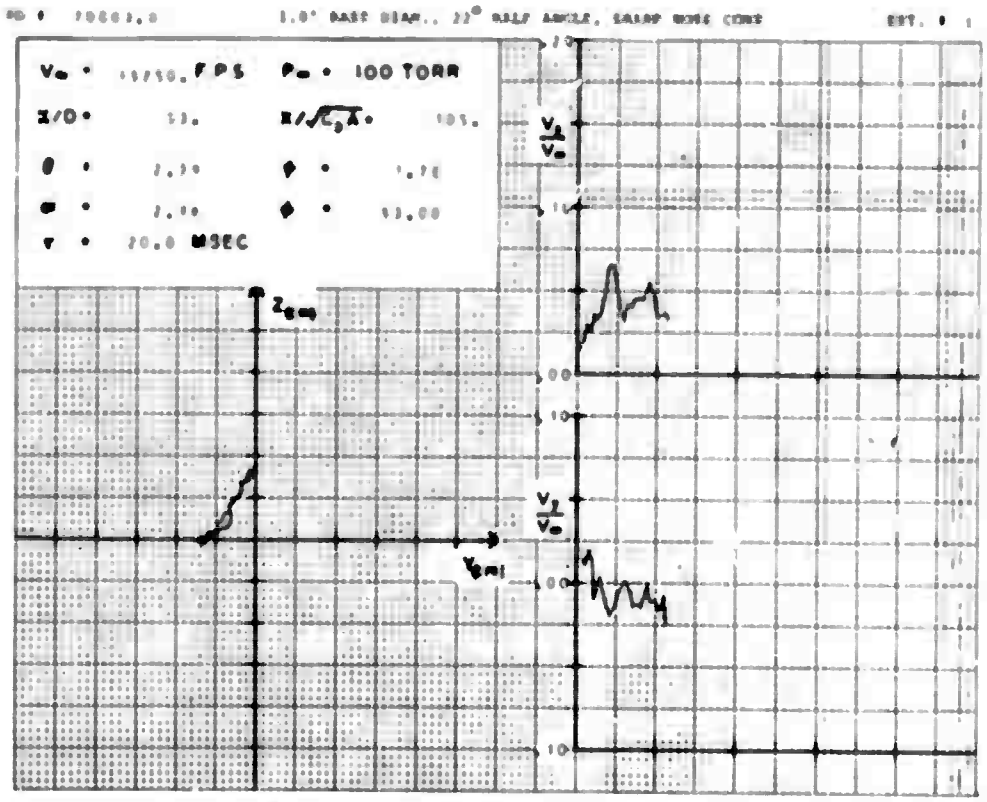

Figure 91

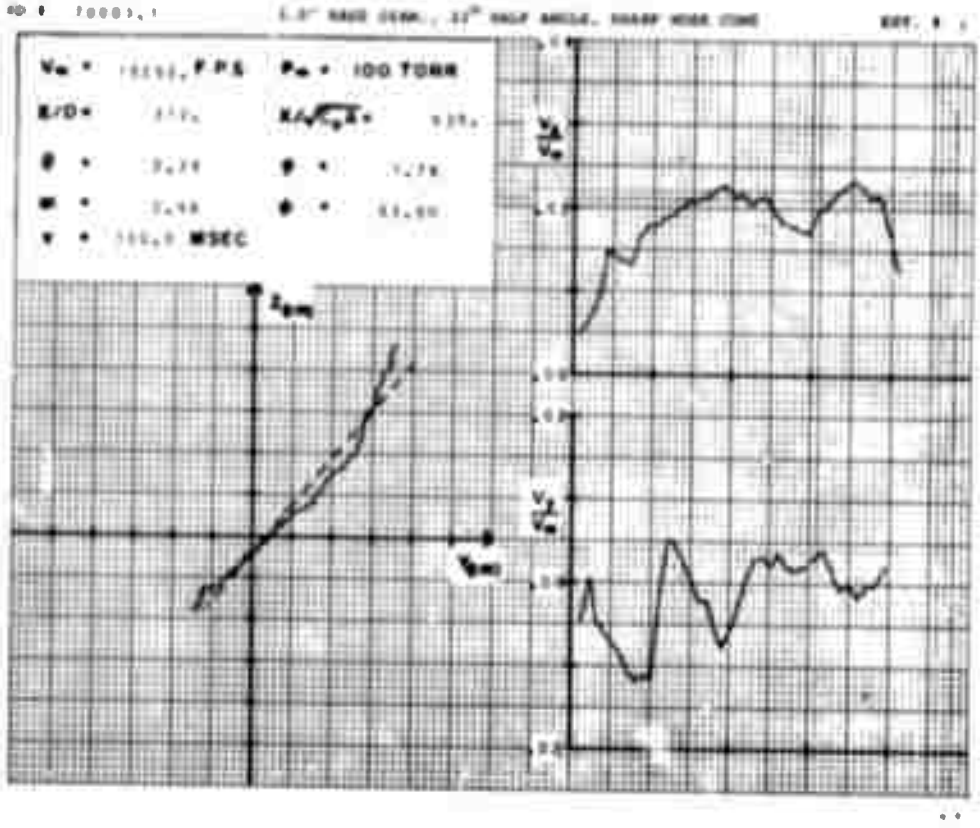

Figure 92

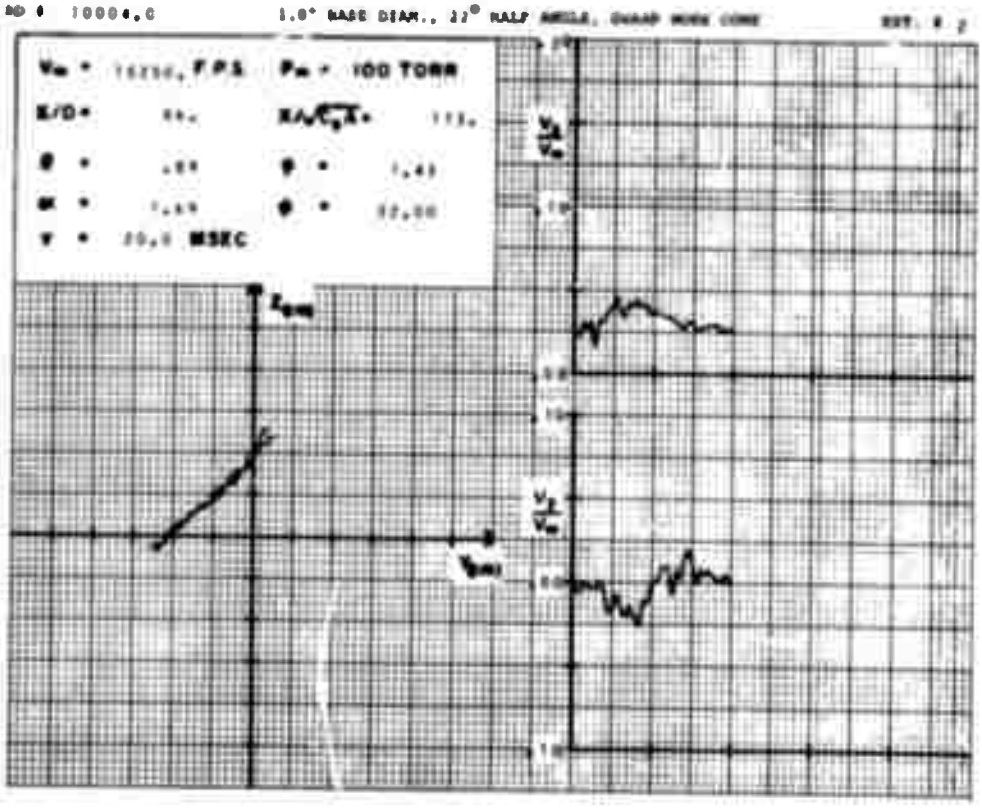

Figure 93

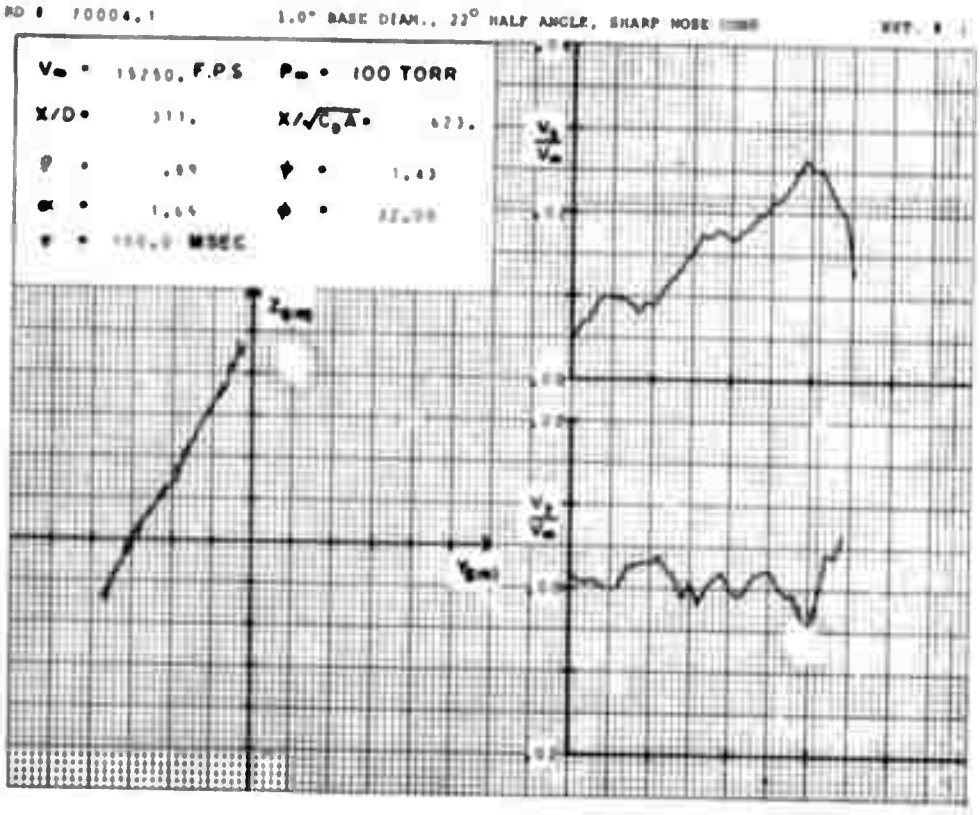

Figure 94

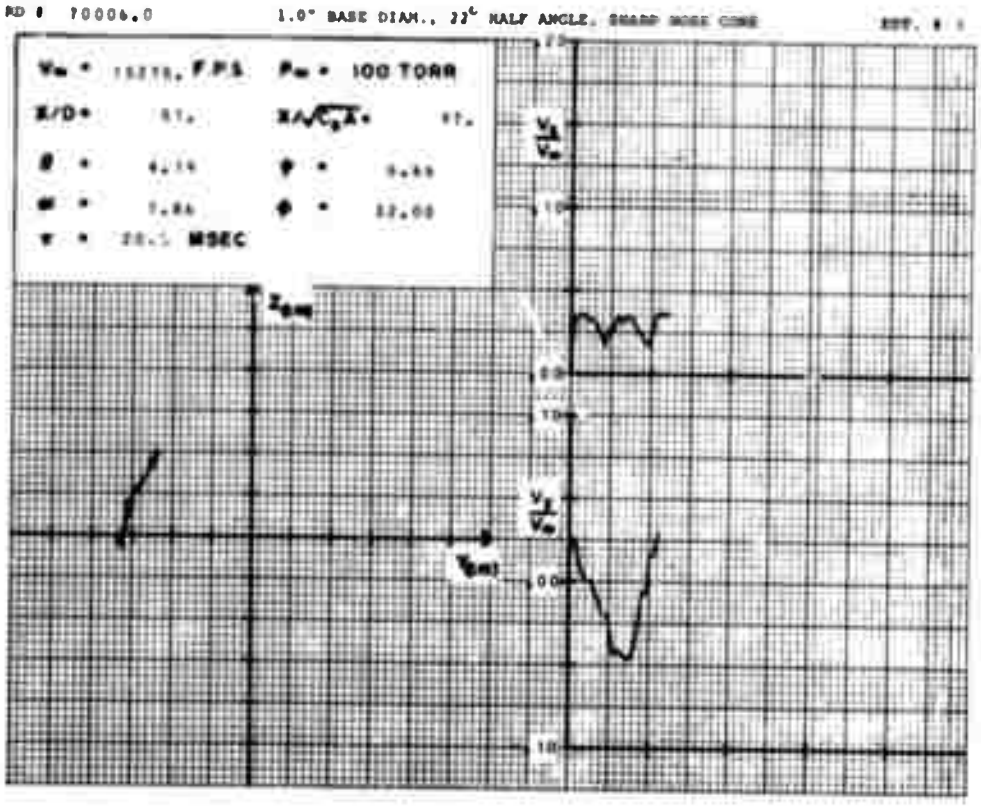

Figure 95

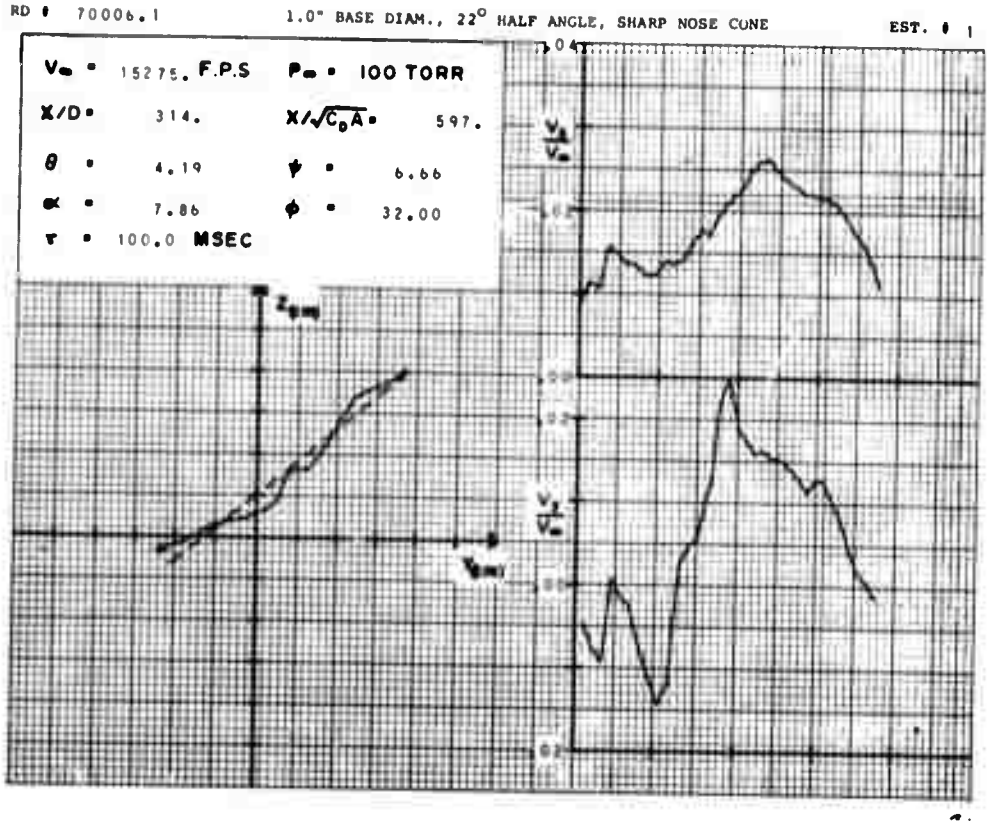

Figure 96

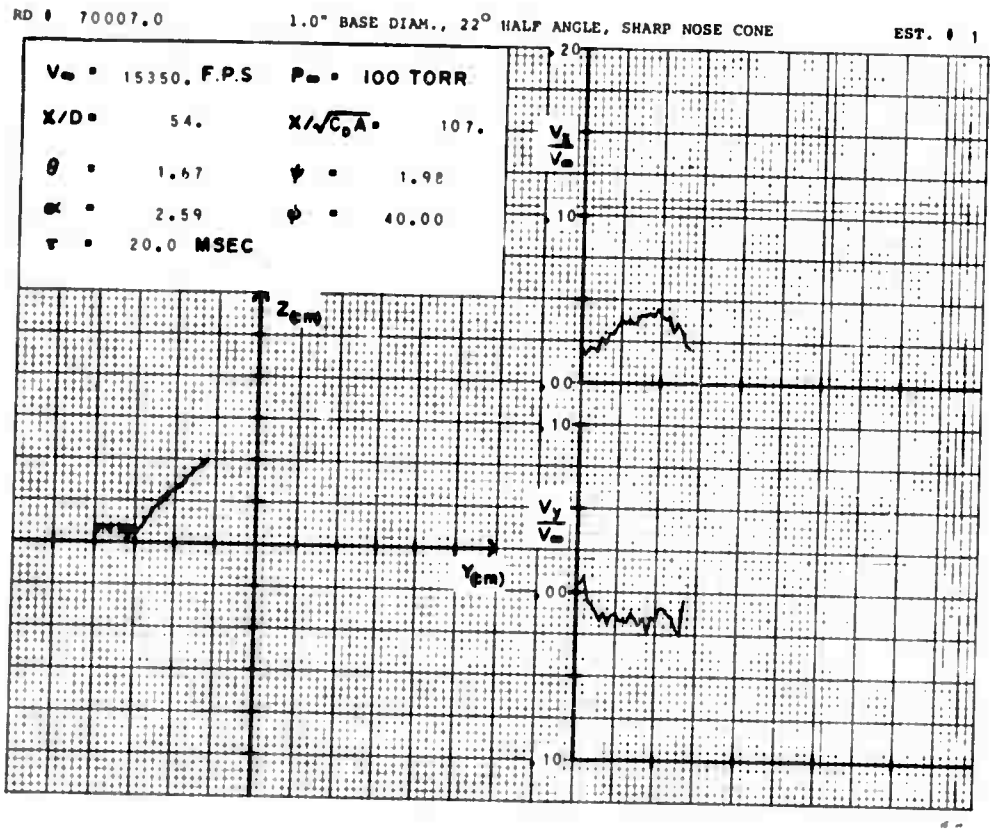

Figure 97

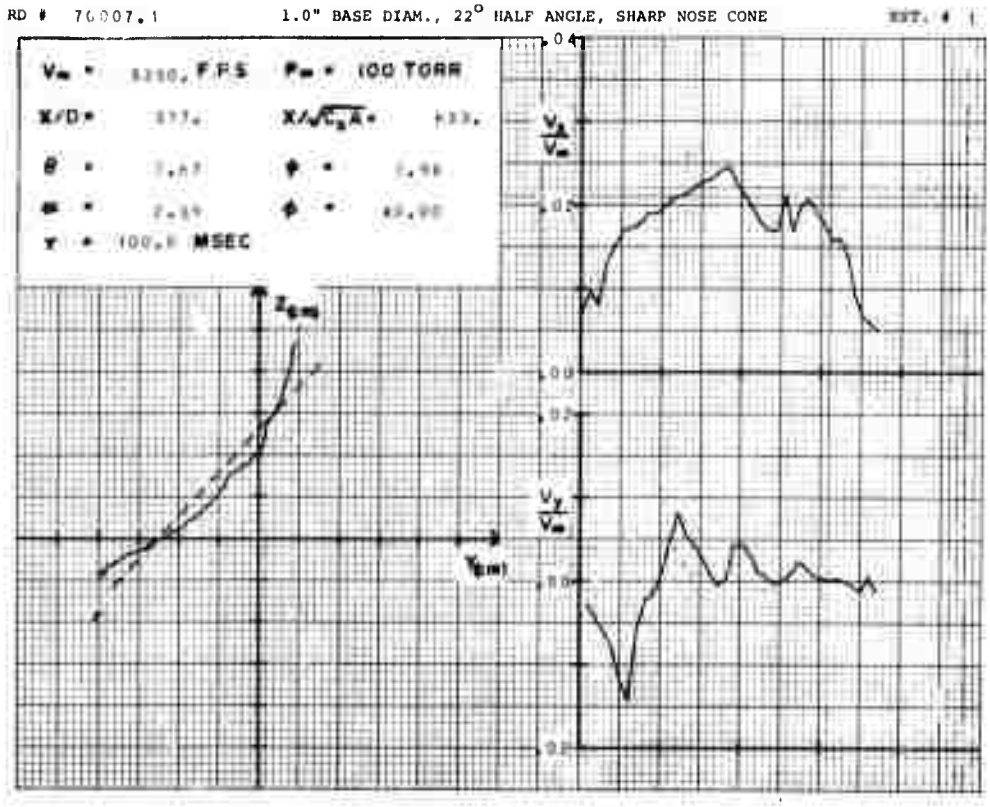

Figure 98

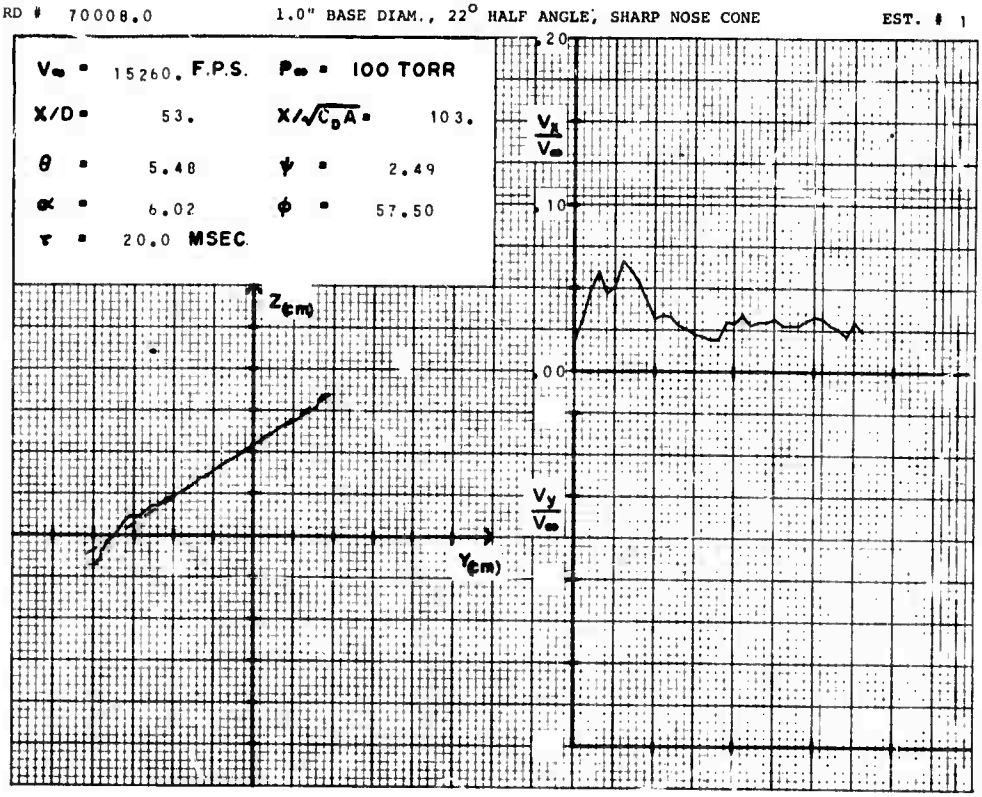

Figure 99

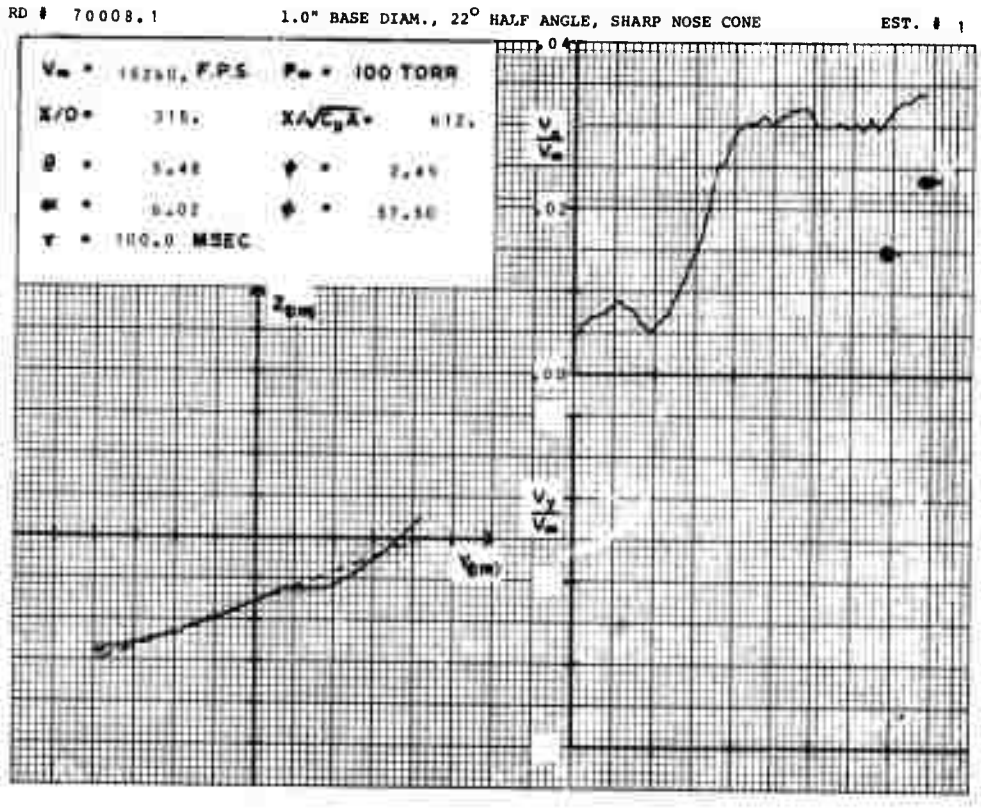

Figure 100

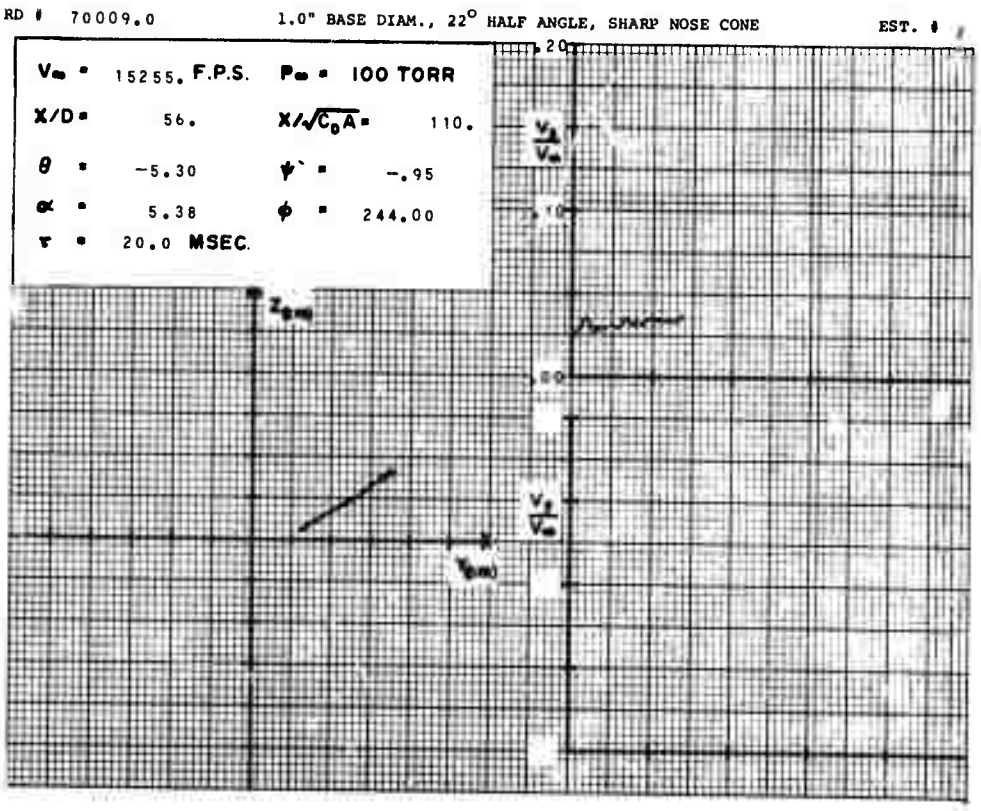

Figure 101

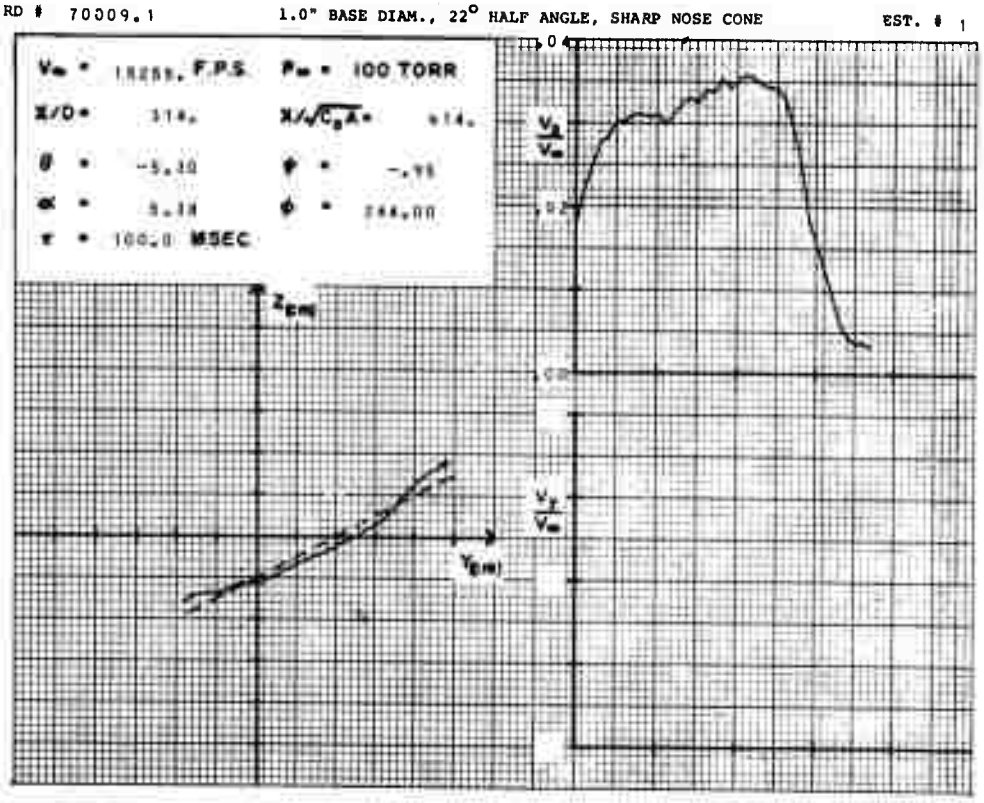

Figure 102

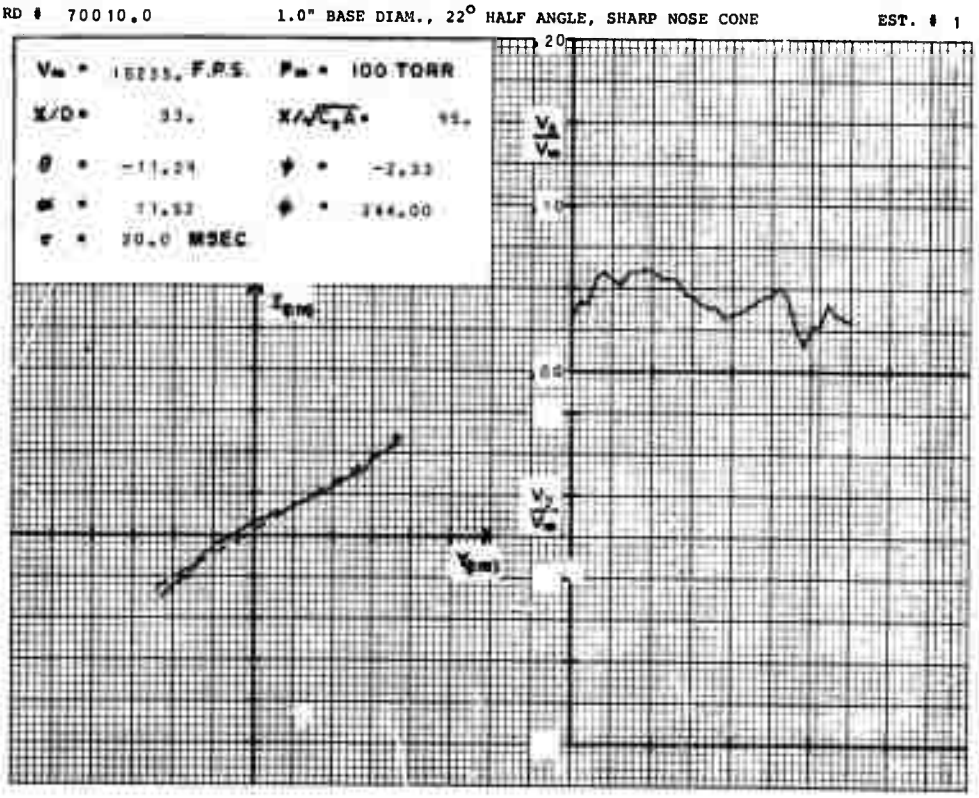

Figure 103

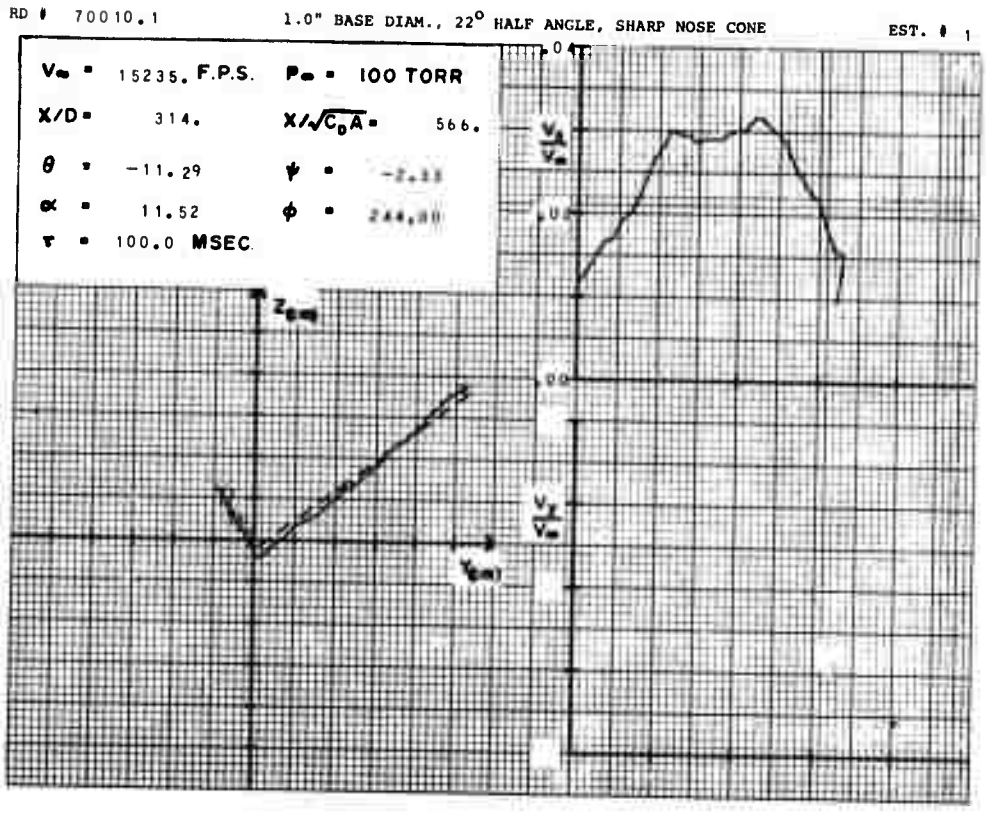

Figure 104

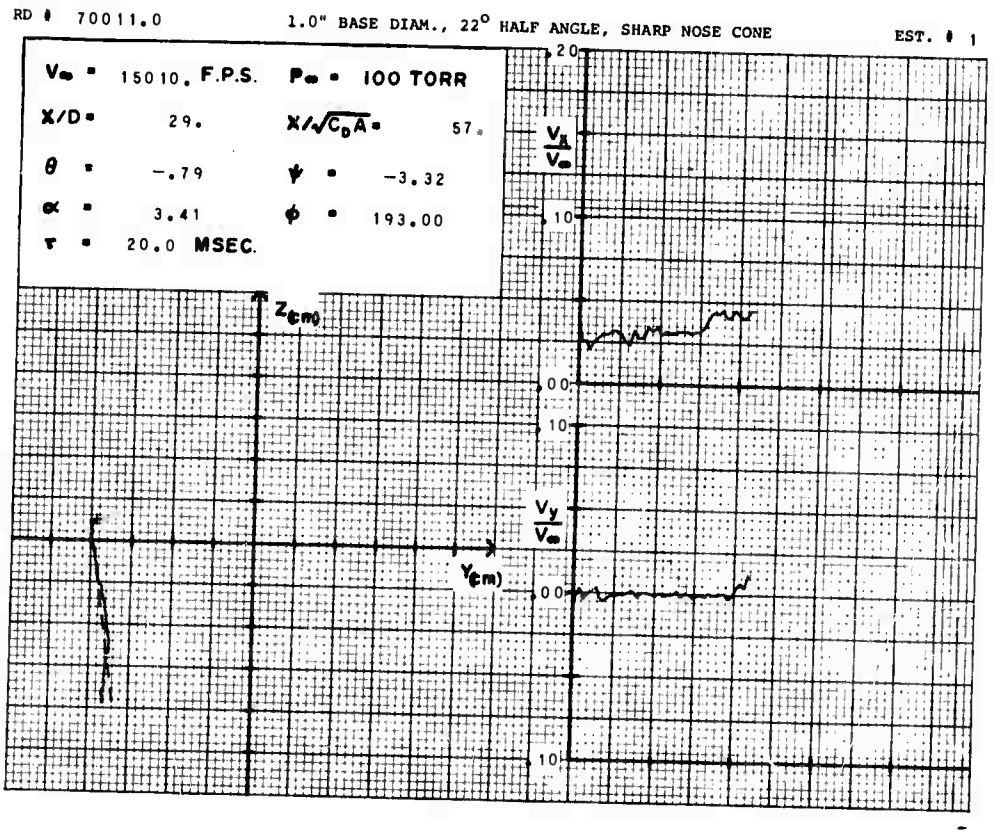

Figure 105

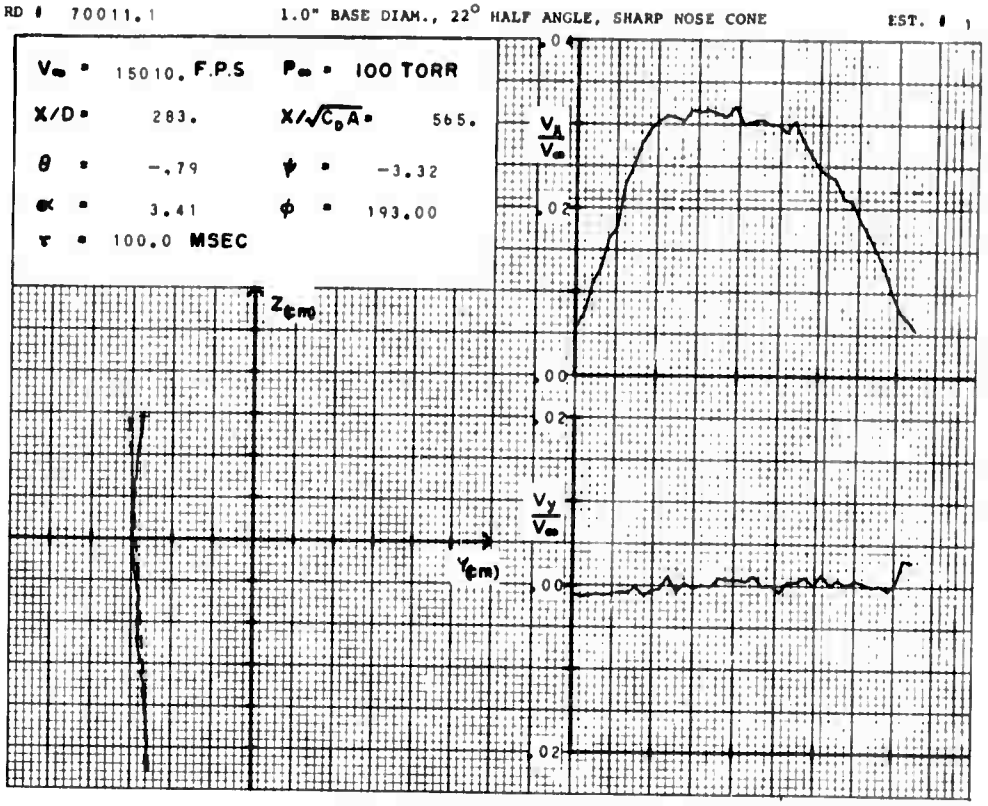

Figure 106

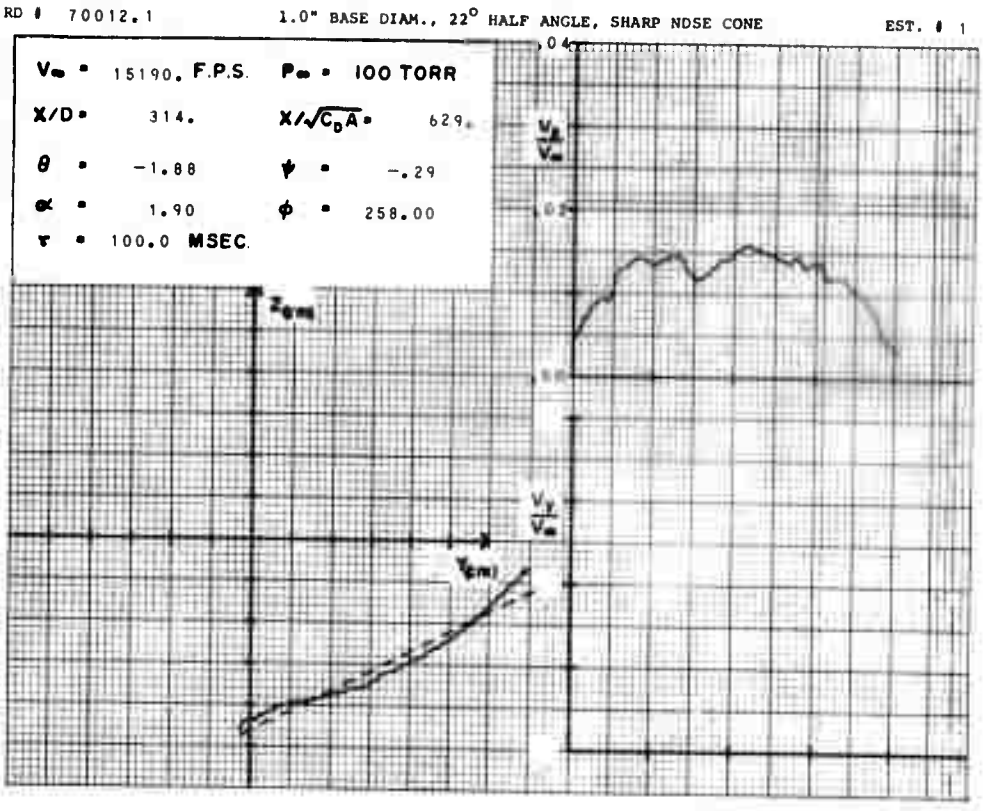

Figure 107

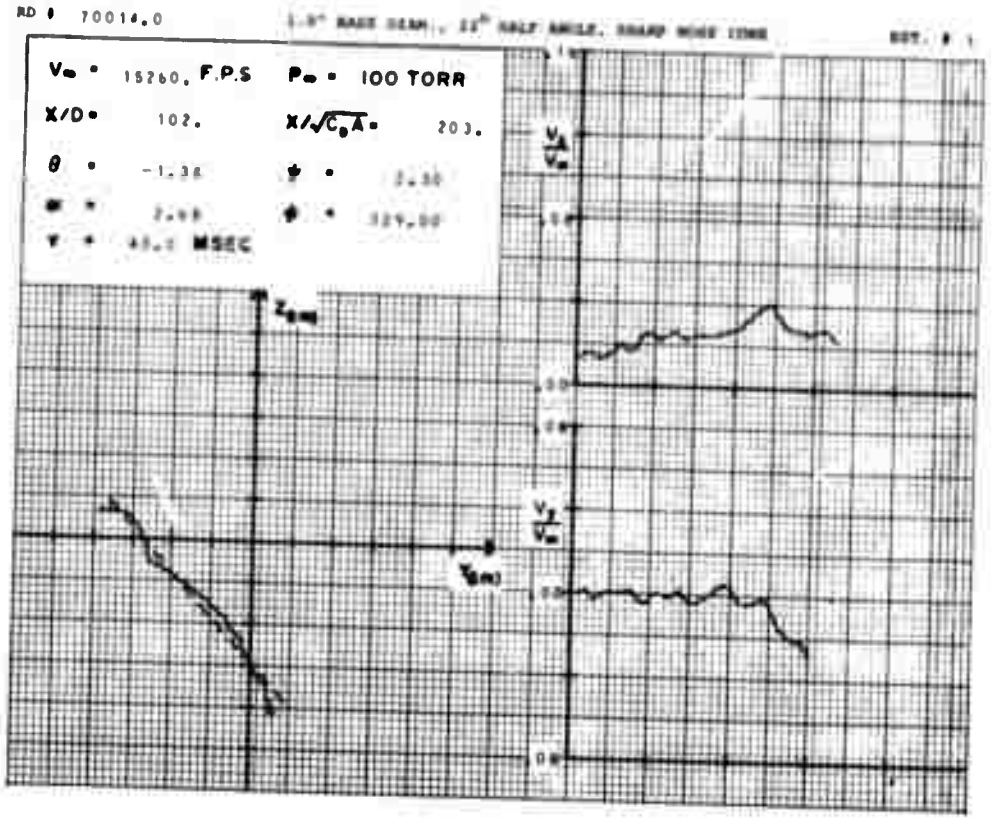

Figure 108

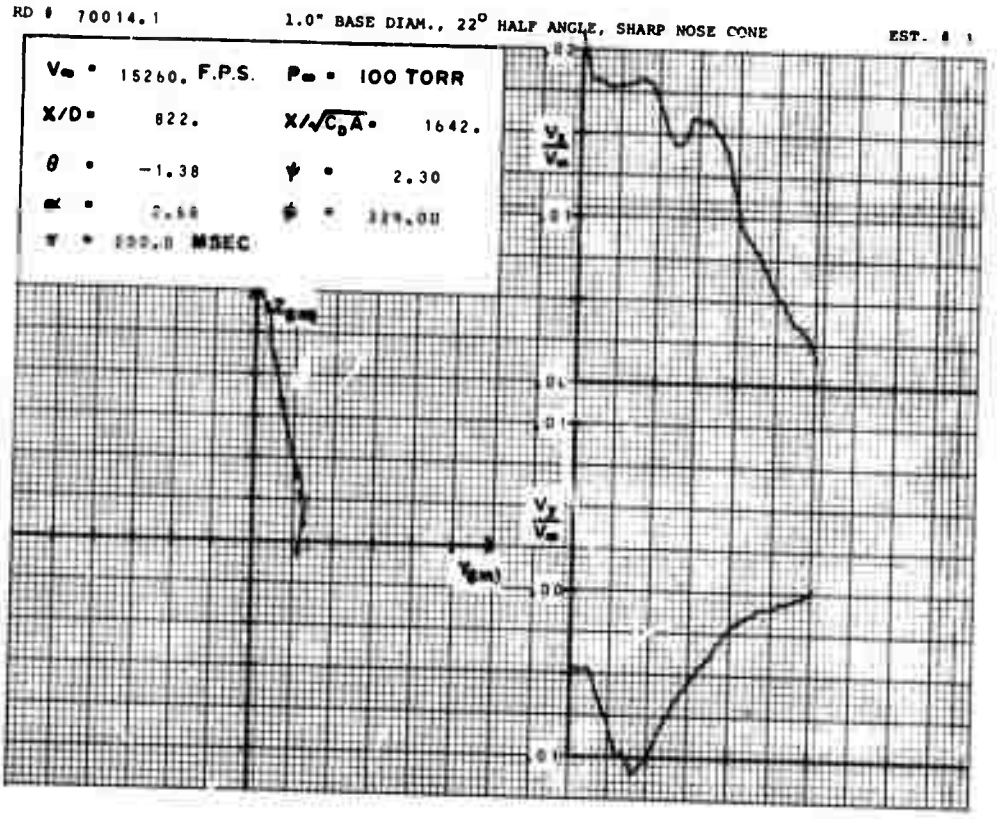

Figure 109

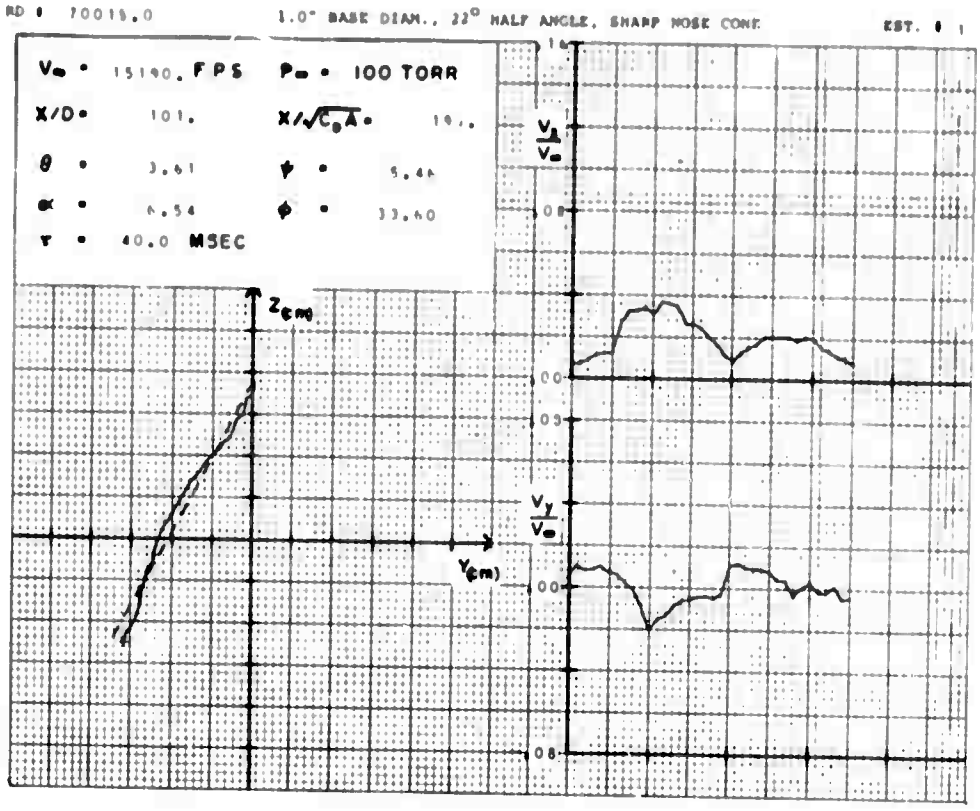

Figure 110

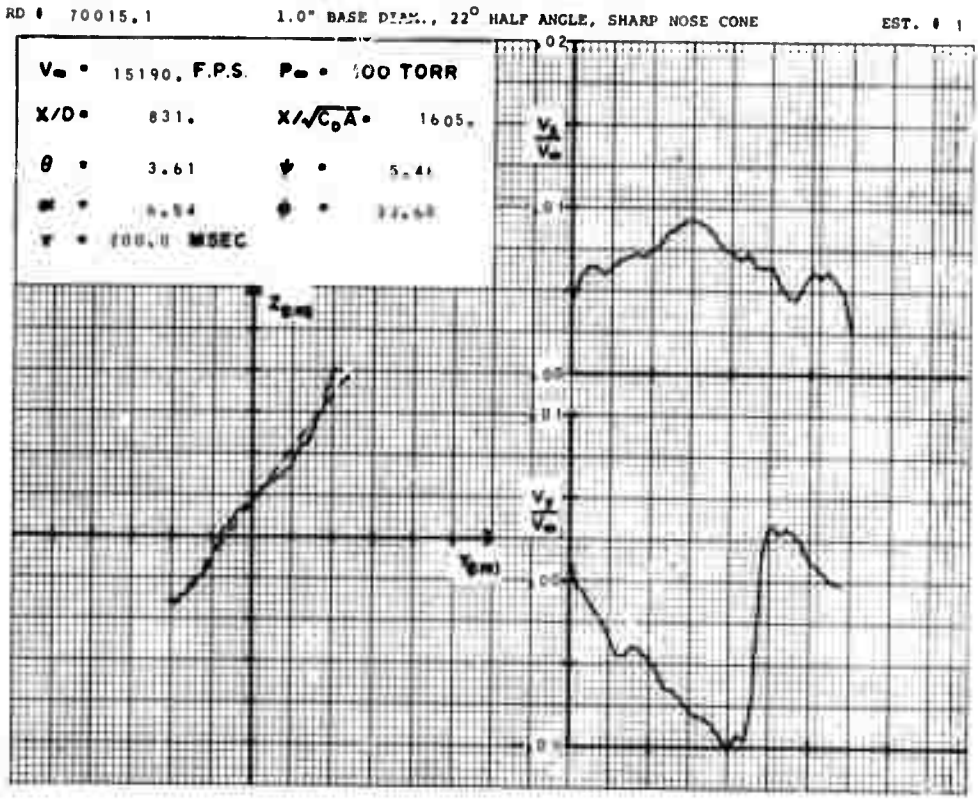

Figure 111

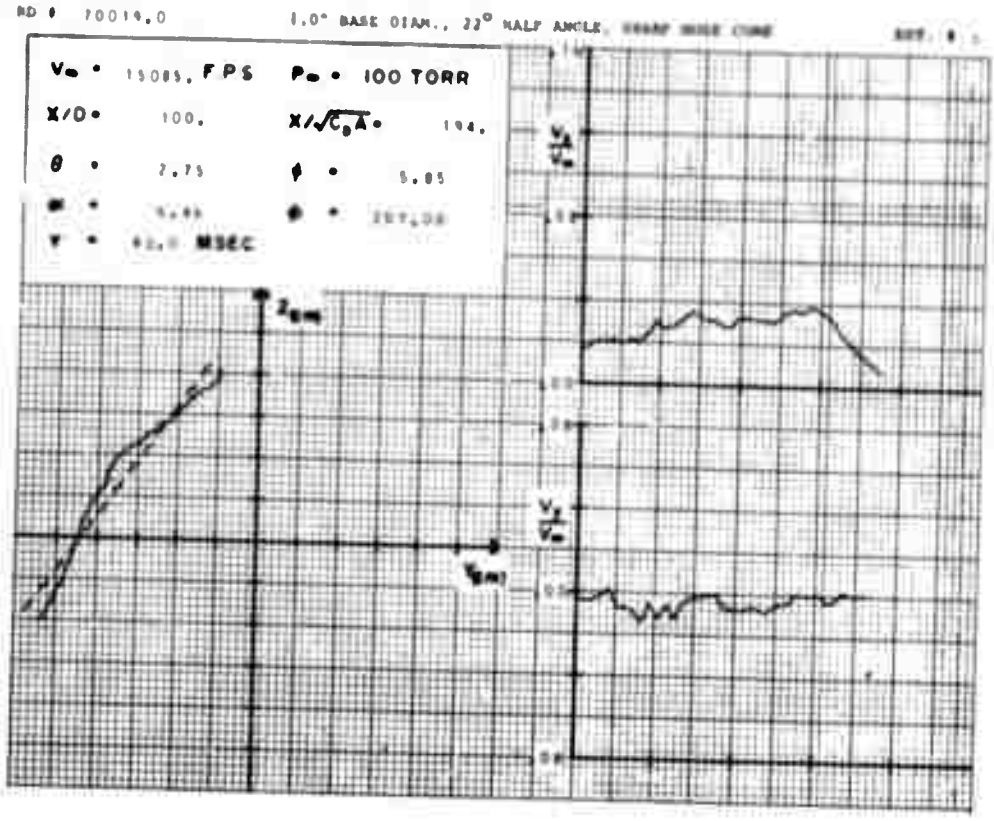

Figure 112

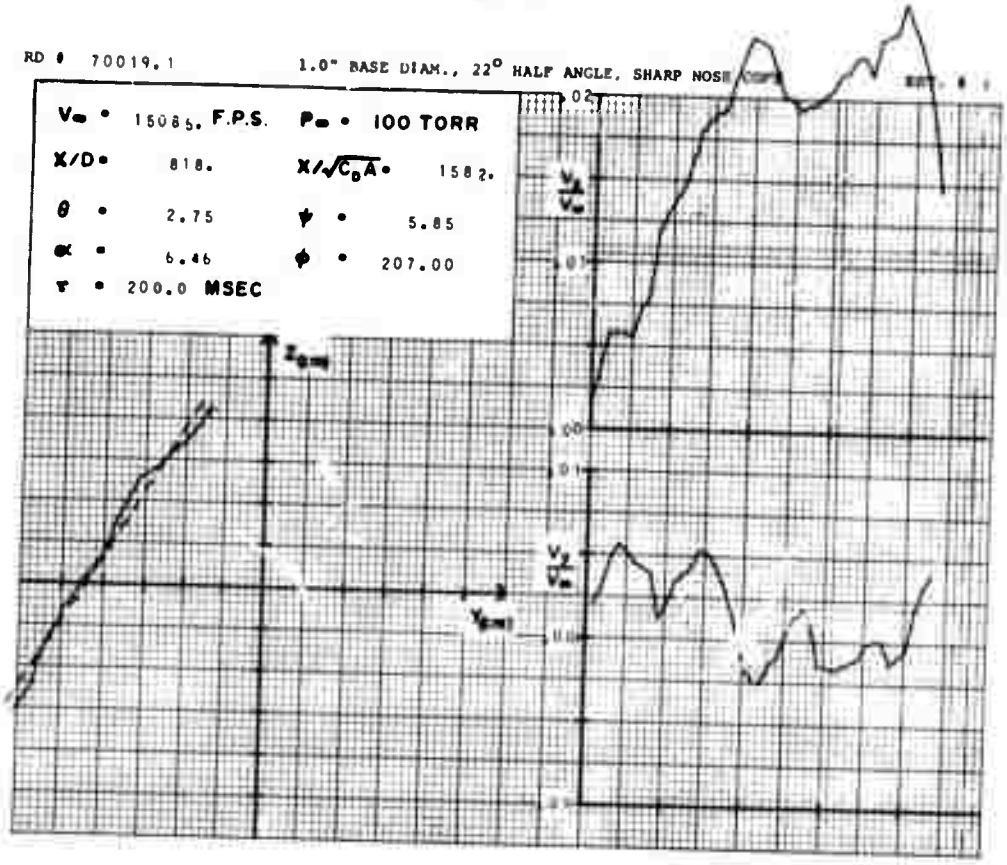

Figure 113

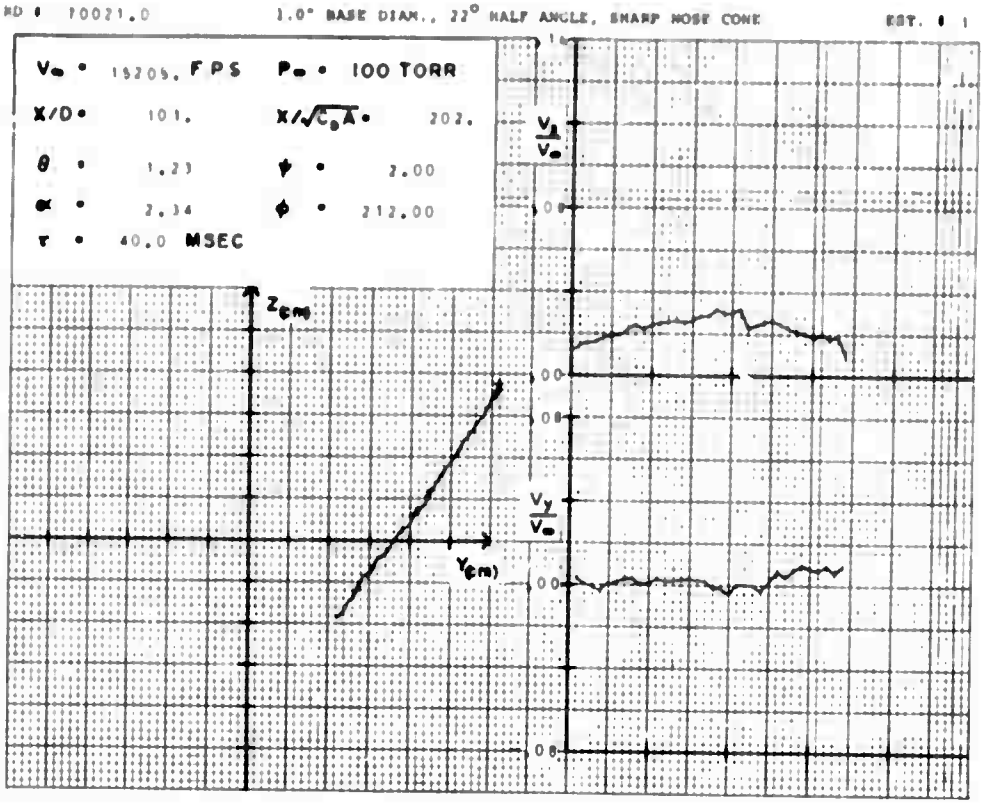

Figure 114

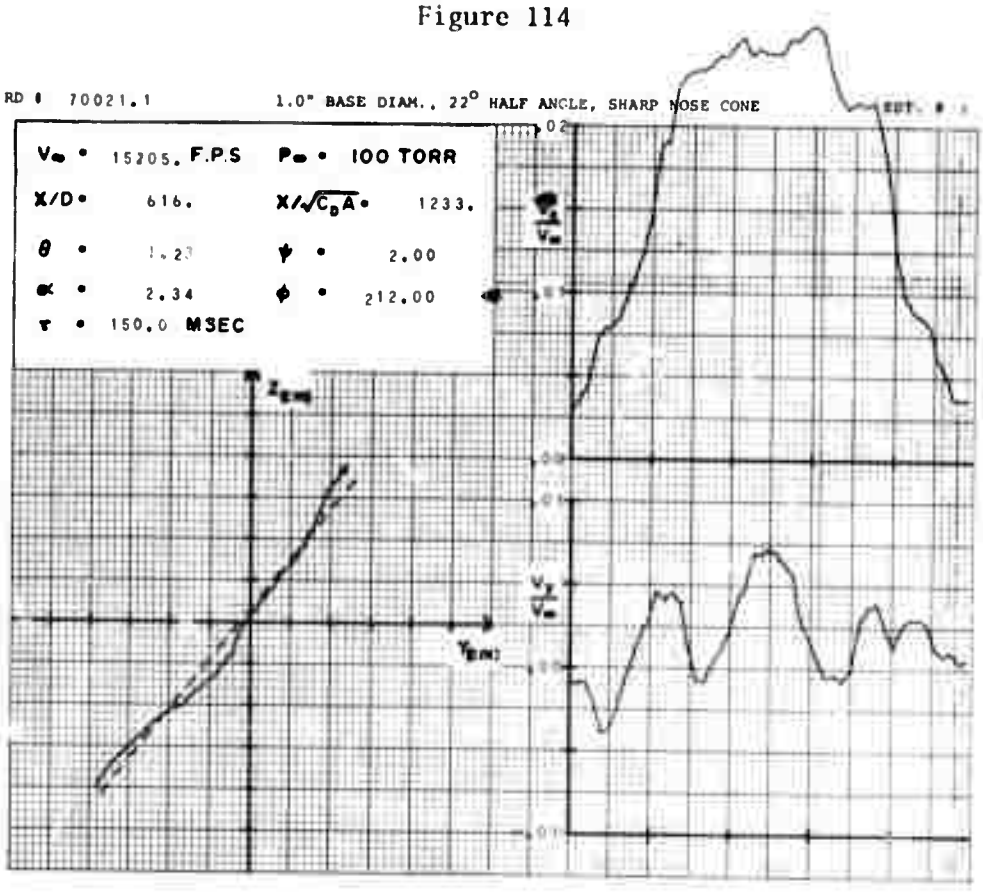

Figure 115

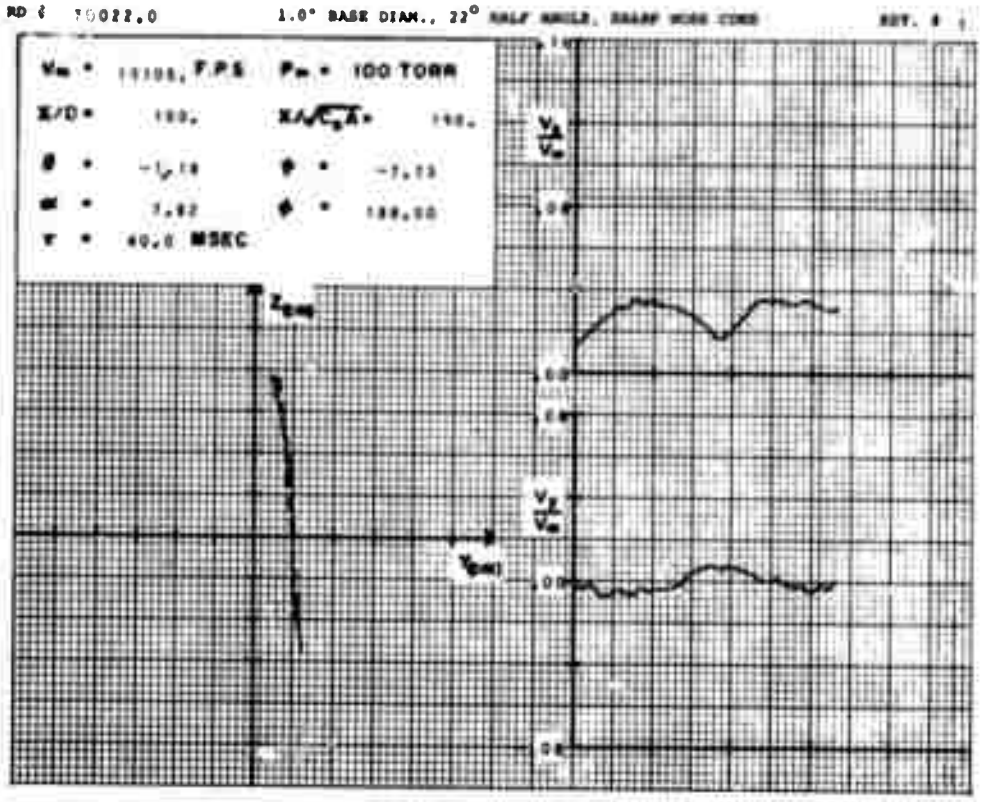

Figure 116

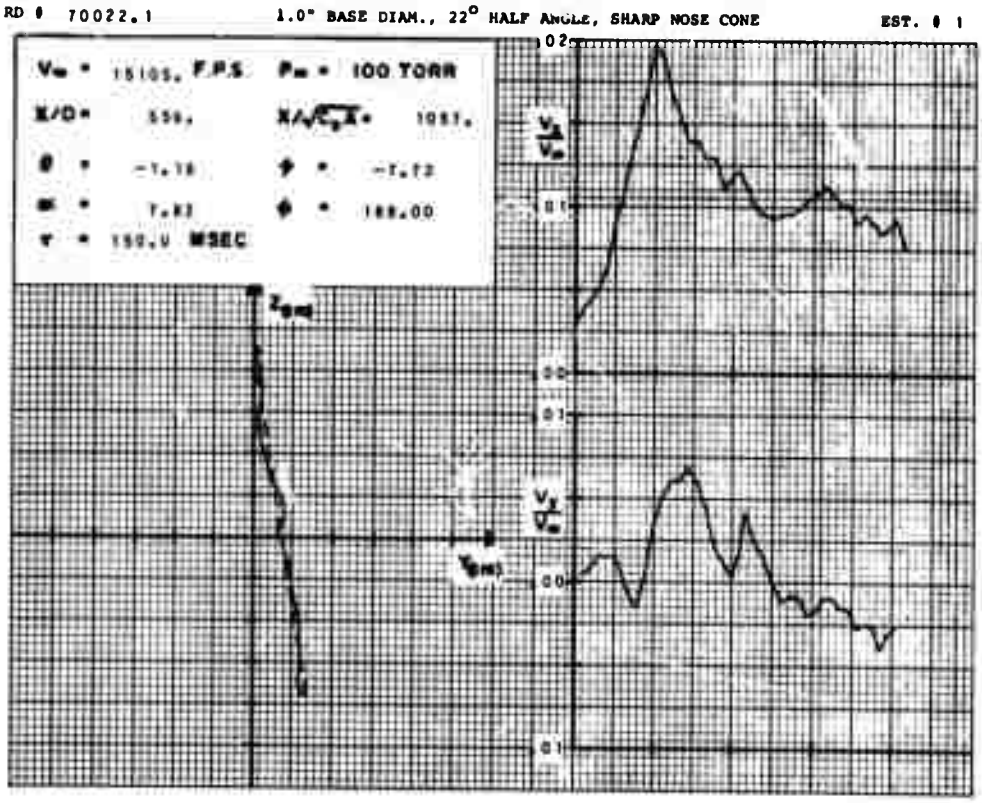

Figure 117

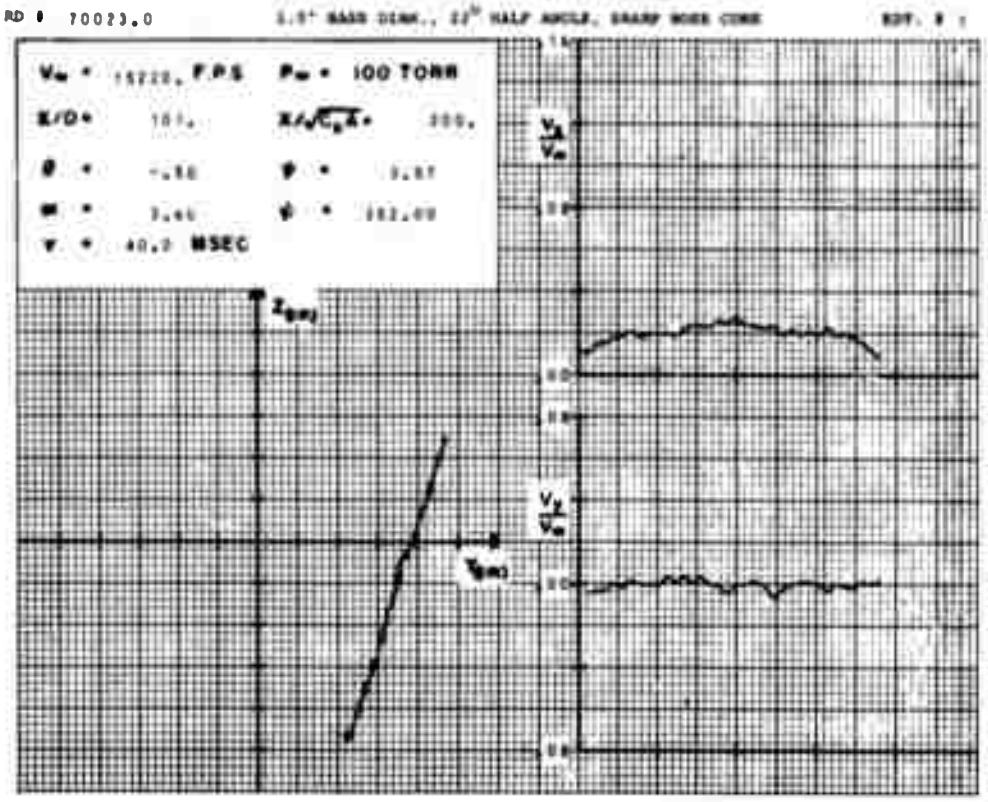

Figure 118

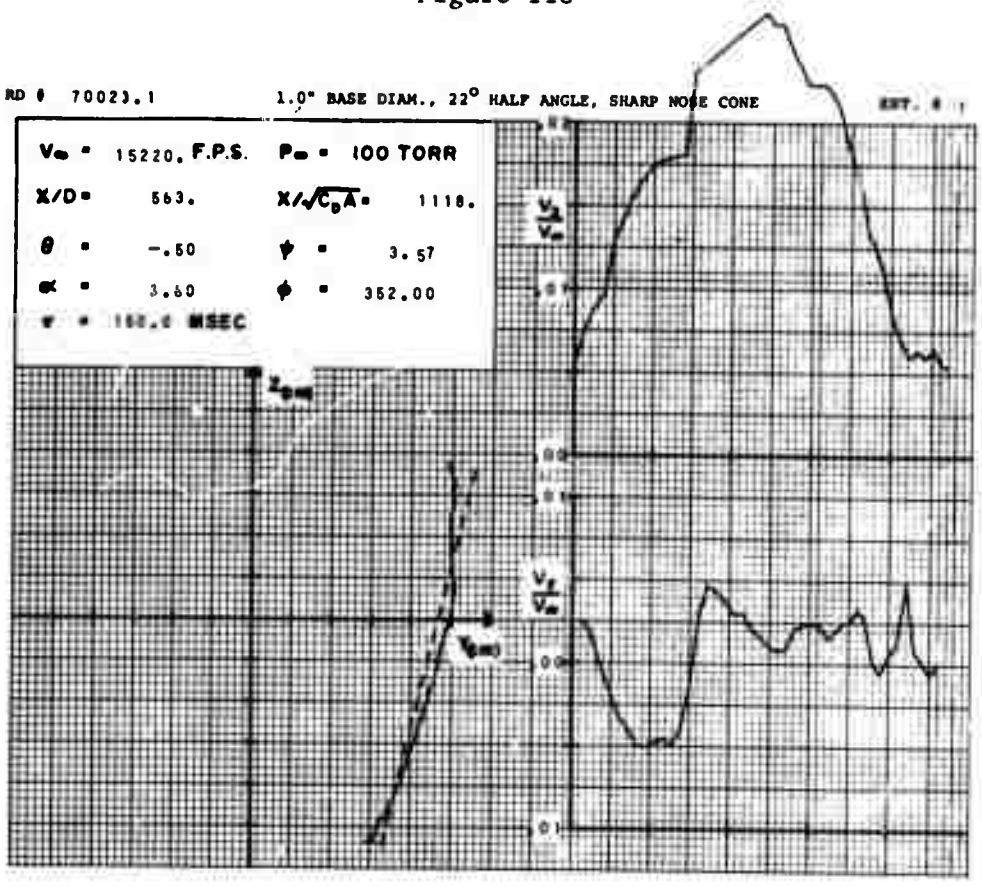

Figure 119

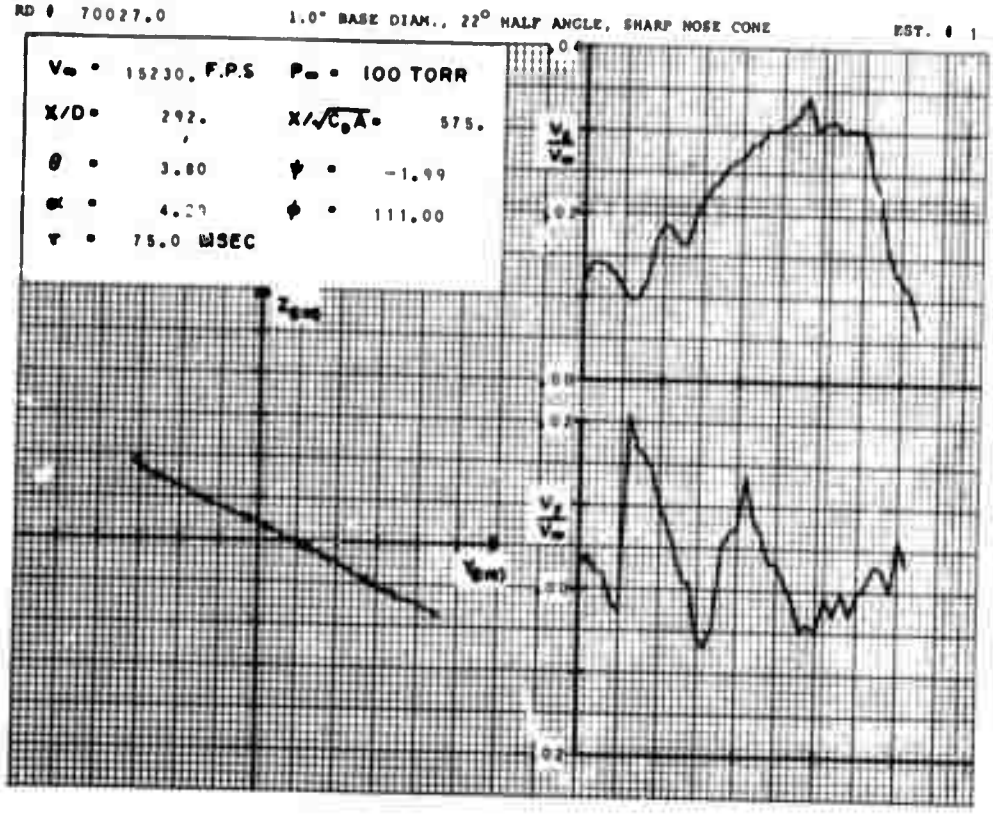

Figure 120

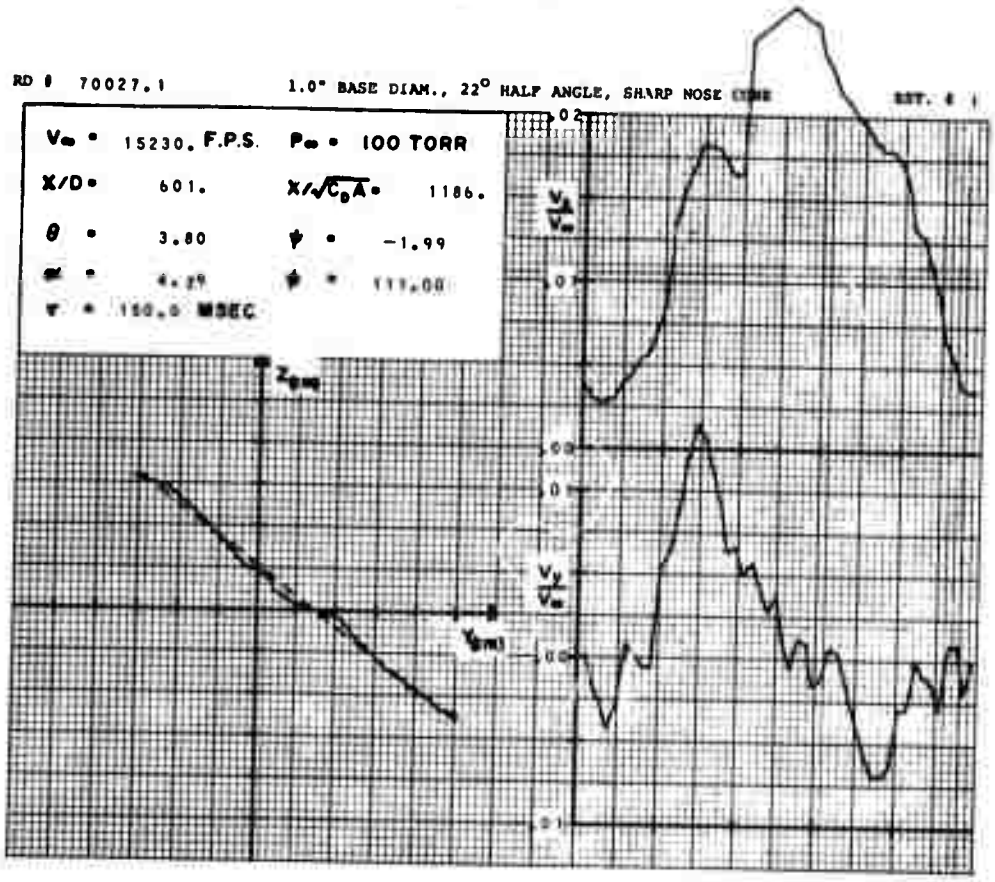

Figure 121